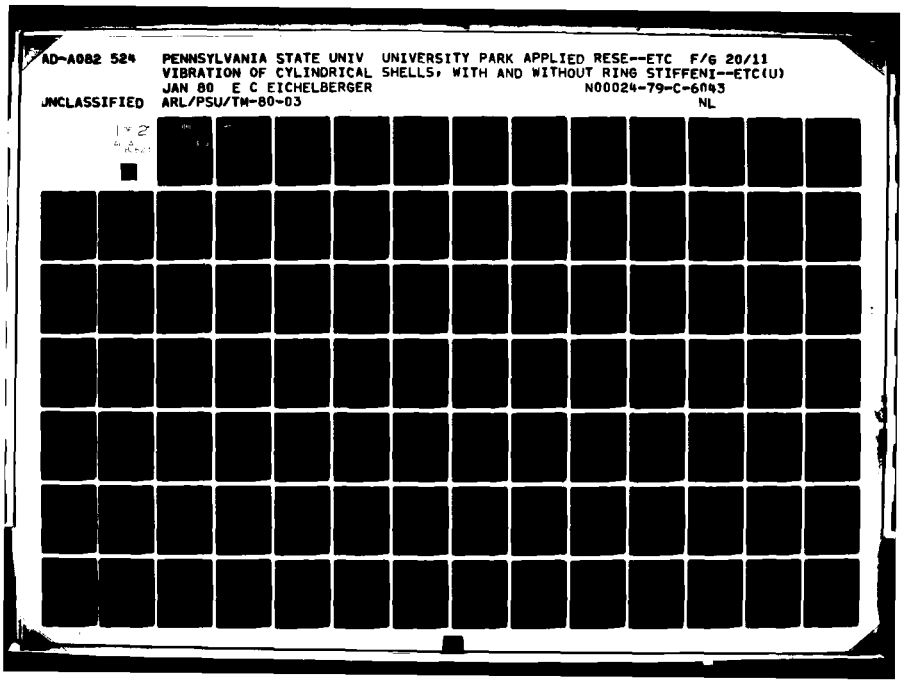
AD-A082 524
PENNSYLVANIA STATE UNIV UNIVERSITY PARK APPLIED RESE--ETC F/G 20/11
VIBRATION OF CYLINDRICAL SHELLS, WITH AND WITHOUT RING STIFFENI--ETC(U)
JAN 80 E C EICHELBERGER
N00024-79-C-6043
UNCLASSIFIED
ARL/PSU/TM-80-03
NL

LEVEL II

VIBRATION OF CYLINDRICAL SHELLS, WITH AND WITHOUT RING STIFFENING

Eugene C. Eichelberger, Jr.

Technical Memorandum
File No. TM 80-03
January 11, 1980
Contract No. N00024-79-C-6043

Copy No. 5

The Pennsylvania State University
Institute for Science and Engineering
APPLIED RESEARCH LABORATORY
Post Office Box 30
State College, PA 16801

NAVY DEPARTMENT

NAVAL SEA SYSTEMS COMMAND

UNCLASSIFIED

SECURITY CLASSIFICATION OF THIS PAGE *(When Data Entered)*

REPORT DOCUMENTATION PAGE

READ INSTRUCTIONS BEFORE COMPLETING FORM

1. REPORT NUMBER TM 80-03	2. GOVT ACCESSION NO.
3. RECIPIENT'S CATALOG NUMBER	
4. TITLE (and Subtitle) VIBRATION OF CYLINDRICAL SHELLS, WITH AND WITHOUT RING STIFFENING	5. TYPE OF REPORT & PERIOD COVERED M.S. Thesis, March 1980
	6. PERFORMING ORG. REPORT NUMBER TM 80-03
7. AUTHOR(s) Eugene C. Eichelberger, Jr	8. CONTRACT OR GRANT NUMBER(s) N00024-79-C-6043
9. PERFORMING ORGANIZATION NAME AND ADDRESS The Pennsylvania State University Applied Research Laboratory/ P. O. Box 30, State College, PA 16801	10. PROGRAM ELEMENT, PROJECT, TASK AREA & WORK UNIT NUMBERS
11. CONTROLLING OFFICE NAME AND ADDRESS Naval Sea Systems Command Department of the Navy Washington, D.C. 20362	12. REPORT DATE Jan[illegible] 1980 13. NUMBER OF PAGES 139 pages & figures
14. MONITORING AGENCY NAME & ADDRESS *(if different from Controlling Office)* 9 Technical memo.	15. SECURITY CLASS. *(of this report)* Unclassified, Unlimited 15a. DECLASSIFICATION/DOWNGRADING SCHEDULE

16. DISTRIBUTION STATEMENT *(of this Report)*

Approved for public release, distribution unlimited, per NSSC (Naval Sea Systems Command), 2/1/80

12 141

17. DISTRIBUTION STATEMENT *(of the abstract entered in Block 20, if different from Report)*

11 ARL/P-4/TM-80-13

18. SUPPLEMENTARY NOTES

19. KEY WORDS *(Continue on reverse side if necessary and identify by block number)*

dynamical, response, cylindrical, shells, mean-value, admittance, vibration,

20. ABSTRACT *(Continue on reverse side if necessary and identify by block number)*

The dynamical response of two cylindrical shells, one with and one without ring-stiffening, was investigated. The driving-point admittance was measured and compared with predictions using the Mean-Value Admittance Method. This method predicts the geometric mean of the response of a vibrator with respect to frequency and is useful in understanding the behavior of many complex structures. The basic computations involve the mode functions, mode masses, and the mode density. The measurements were in good agreement with the theory, and

DD FORM 1 JAN 73 1473 EDITION OF 1 NOV 65 IS OBSOLETE

391007

UNCLASSIFIED

SECURITY CLASSIFICATION OF THIS PAGE *(When Data Entered)*

20. ABSTRACT (continued)

demonstrate that the Mean-Value Admittance Method is a practical means of predicting the vibrational response of shell structures to point excitation.

ABSTRACT

The dynamical response of two cylindrical shells, one with and one without ring-stiffening, was investigated. The driving-point admittance was measured and compared with predictions using the Mean-Value Admittance Method. This method predicts the geometric mean of the response of a vibrator with respect to frequency and is useful in understanding the behavior of many complex structures. The basic computations involve the mode functions, mode masses, and the mode density. The measurements were in good agreement with the theory, and demonstrate that the Mean-Value Admittance Method is a practical means of predicting the vibrational response of shell structures to point excitation.

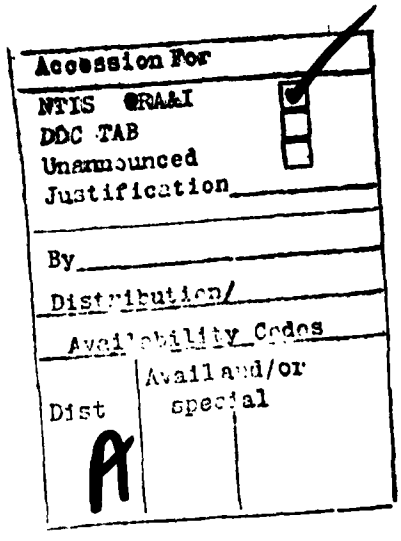

TABLE OF CONTENTS

LIST OF FIGURES

LIST OF TABLES

LIST OF SYMBOLS

Letter Symbols

a	nominal radius of cylindrical shell
a_h	acceleration of impedance head
a_s	acceleration of test specimen
b	thickness of ring
B_o	imaginary part of the driving-point admittance
c	velocity of sound
$c_{p\ell}$	velocity of a longitudinal wave in a plate, $\sqrt{E'/\rho}$
c_E	Velocity of a longitudinal wave in a bar, $\sqrt{E/\rho}$
C	compliance
C_ν	compliance of νth mode
e	base of the natural logarithm
E	Young's elastic modulus
E'	$E/(1-\mu^2)$
f	frequency in Hz
f_o	radial resonance frequency of cylindrical shell, $c_{p\ell}/2\pi a$
F	general forcing function
F_o	total force, or point force
G_o	real part of the driving-point admittance
h	thickness
h_r	thickness of ring
h_s	thickness of shell
j	imaginary number, $\sqrt{-1}$
k	wavenumber, ω/c
k_m	wavenumber in the axial direction

LIST OF SYMBOLS

Letter Symbols

a	nominal radius of cylindrical shell
a_h	acceleration of impedance head
a_s	acceleration of test specimen
b	thickness of ring
B_o	imaginary part of the driving-point admittance
c	velocity of sound
$c_{p\ell}$	velocity of a longitudinal wave in a plate, $\sqrt{E'/\rho}$
c_E	Velocity of a longitudinal wave in a bar, $\sqrt{E/\rho}$
C	compliance
C_ν	compliance of νth mode
e	base of the natural logarithm
E	Young's elastic modulus
E'	$E/(1-\mu^2)$
f	frequency in Hz
f_o	radial resonance frequency of cylindrical shell, $c_{p\ell}/2\pi a$
F	general forcing function
F_o	total force, or point force
G_o	real part of the driving-point admittance
h	thickness
h_r	thickness of ring
h_s	thickness of shell
j	imaginary number, $\sqrt{-1}$
k	wavenumber, ω/c
k_m	wavenumber in the axial direction

ℓ length of cylindrical shell

m axial mode number of cylindrical shell (equal to the number of axial half-waves in the vibration pattern)

m specific mass of a vibrator

m_r mass per unit circumferential length of ring

m_s mass per unit area of shell

m_s' mass per unit circumferential length of shell

m_s'' mass per unit axial length of shell

M total mass of vibrator

M_ν point mode mass of the νth mode

n circumferential mode number of cylindrical shell (equal to the number of circumferential waves in the vibration pattern)

N number of resonances

r nominal radius of ring

r polar coordinate of shell wavenumber space

R resistance

R_ν resistance of the νth mode, $\frac{\omega_\nu^2}{\omega} \eta_\nu M_\nu$

S surface area of vibrator

t time variable

u mode number of ring (equal to the number of circumferential waves in the vibration pattern)

v velocity at the point of observation

v_r velocity on the inside of the ring

v_s velocity on the outside of the shell

Y admittance, v/F

Y_o driving-point admittance

z shell coordinate in the axial direction

Z impedance, F/v

Z_o driving-point impedance

Greek Symbols

α^2 stiffness constant, $c\ h/\sqrt{12}$

α_r^2 ring stiffness constant, $c_E\ h_r/\sqrt{12}$

α_s^2 shell stiffness constant, $c_{p\ell}\ h_s/\sqrt{12}$

β shift in ring resonance frequencies due to the shell mass loading, $\left[\frac{M_r/2}{M_r/2 + M_s/4}\right]^{\frac{1}{2}}$

γ thickness to radius parameter, $h/\sqrt{12}\ a$

δ_s change in effective bending stiffness

δ_m change in effective mass

Δx change in x

ε_ν frequency spacing between successive resonances of a general vibrator (inverse of the density of resonances)

θ shell coordinate in circumferential direction

ϕ polar coordinate in shell wavenumber space

η_ν loss factor of νth mode

κ_ν excitation constant, [see Equation (2.5)]

λ wavelength

μ Poisson's ratio

ν general mode number

ξ displacement in the radial direction

ξ_ν displacement of the νth mode (mode function)

$\hat{\xi}$ displacement amplitude

$\langle\xi_\nu^2\rangle$ spacial average of the square of the mode function

π 3.1416...

ρ mass density

σ parameter that is proportional to the axial mode number, $\frac{m\pi a}{\ell}$

Σ sum

ω angular frequency

ω_o radial resonance frequency, $c_{p\ell}/a$

ω_ν resonance frequency of the νth mode

Ω normalized angular frequency, ω/ω_o

ACKNOWLEDGEMENTS

The author is grateful to Dr. Eugen J. Skudrzyk for his guidance and enthusiastic encouragement during the course of this study. A special acknowledgement goes to Dr. Earl Williams for his many helpful discussions and for assistance in the conduct of the experimental measurements.

Also, the comments and suggestions of the faculty readers, Professor Sabih I. Hayek and Professor Gerhard Reethof, added much to the accuracy and organization of this thesis.

This work was performed at the Physics Department of The Pennsylvania State University and was supported by the Office of Naval Research under Contract Number 474.

CHAPTER I

INTRODUCTION

1.1 Background

There is a strong motivation for the study of the vibrations of cylindrical shells. They are the prototypes of such practical structures as pipelines, containment vessels, undersea vehicles, aircraft, and machine housings. Insight into the dynamical response of cylindrical shells to various exciting forces is essential to the understanding of the sound radiation from, or the vibration isolation between components of many practical structures.

Compared to structural elements such as beams and plates, the shell vibrates in an extremely complex manner. Because of the shell's curvature, it is impossible to separate the extensional or membrane-like motion from the bending or plate-like motion. With coupling between extension and bending, the development of an equation of motion is a formidable task. Of all the possible shell structures, only the circular cylindrical and spherical shell are mathematically tractable. An excellent and self-contained derivation of the equations governing the vibration of shells is presented in Reference [1].

Much of the early literature on cylindrical shells was directed toward the development and solution of various shell equations of motion to determine natural frequencies and mode shapes for various boundary conditions. The development of shell theories and their

CHAPTER I

INTRODUCTION

1.1 Background

There is a strong motivation for the study of the vibrations of cylindrical shells. They are the prototypes of such practical structures as pipelines, containment vessels, undersea vehicles, aircraft, and machine housings. Insight into the dynamical response of cylindrical shells to various exciting forces is essential to the understanding of the sound radiation from, or the vibration isolation between components of many practical structures.

Compared to structural elements such as beams and plates, the shell vibrates in an extremely complex manner. Because of the shell's curvature, it is impossible to separate the extensional or membrane-like motion from the bending or plate-like motion. With coupling between extension and bending, the development of an equation of motion is a formidable task. Of all the possible shell structures, only the circular cylindrical and spherical shell are mathematically tractable. An excellent and self-contained derivation of the equations governing the vibration of shells is presented in Reference [1].

Much of the early literature on cylindrical shells was directed toward the development and solution of various shell equations of motion to determine natural frequencies and mode shapes for various boundary conditions. The development of shell theories and their

associated equations of motion reached a high degree of accuracy (and complexity) by the late 1950's. Reference [2] provides an excellent overview of the historical development of various thin shell theories. Of particular importance in the development of modern shell equations of motion is the paper by Arnold and Warburton [3]. This paper quantified the relationship between bending and extensional energies of vibration for the cylindrical shell.

The profusion of thin shell theories led Greenspon [4] to evaluate the range of applicability of these theories in comparison with exact thick shell theories. Greenspon concluded that the membrane theory of shells is accurate for predicting frequencies and displacement ratios of cylinders with appreciable thickness.

An excellent reference for the researcher and engineer is the monograph prepared by Leissa [5]. This monograph summarizes over 500 papers, published before 1977, on cylindrical shells. Chapter I provides a very detailed discussion of the differences between the various shell theories. One can generally conclude that the differences between the shell equations arises from small differences in the strain-displacement relationships, and these differences have little significance in most practical applications.

The development of the shell theories has produced a good understanding of the behavior of vibrating shells. When it comes to practical applications, however, these methods do not go very far. In practice, we are usually concerned with the response of a vibrating system to a given excitation as a function of frequency. Specifically, we are interested in the resulting velocity on the surface of a vibrator for a

given force distribution. This information is embodied in the mechanical impedance, or its reciprocal, the admittance. The simplest force distribution is a point force. Because the response due to an arbitrary forcing function can be generalized from that of a point force, we are most interested in the response to point excitation.

Although there is a wealth of literature available concerning the shell equations, resonance frequencies, and mode shapes, there are relatively few papers which address the mechanical impedance of cylindrical shells.

Franken [6] developed an expression for the impedance of non-axisymmetric modes to point excitation below the radial resonance frequency. The ring-stiffened shell problem was set up conceptually, but was not solved analytically. The models developed in this thesis bear a strong resemblance to the circuit representation in Franken's paper. The model suggested by Franken provides a good estimate of the ring-shell response at low frequencies, but at high frequencies the model must be modified.

Based on approximate shell equations, Heckl [7] developed simple formulas for the resonance frequencies, modal densities, and driving-point impedance of cylindrical shells. Although his results are based on many simplifications, Heckl clearly demonstrates that the simplifications are more than accurate enough for practical vibration control work. The simplified frequency equations which Heckl presents are used in this thesis in deriving the density of resonances for a cylindrical shell.

Palladino and Neubert [8] demonstrated the use of mode-sum techniques for the prediction of the admittance of long pipe-like cylindrical shells to point excitation. Their paper also provides a good discussion of the anomalies that occur in transfer admittance data.

Because of the complex nature of vibrating structures, it is desirable to develop simplified methods for the estimation of gross response. In practice, we are usually concerned with only the mean response over some frequency band. Quite often the excitation can only be described in terms of broad frequency spectra, and in general, one would be interested in only the broad frequency response.

Skudrzyk [9, 10, 11] has developed expressions for the geometric mean of the admittance of the most important vibrators: rods, beams, rings, plates, shells, and membranes. Skudrzyk's Mean-Value Admittance Method predicts the mean line through the logarithmically recorded frequency response curve of a complex vibrator, the height of the resonance peaks, and the depth of the antiresonances. The results obtained using this method provide a good approximation with which to evaluate the design of many complex structures consisting of the fundamental components of plates, shells, beams, and rings. One of the most important features of this method is that, in contrast to other methods such as Statistical Energy Analysis and Finite Element Analysis, the Mean-Value Admittance Method is applicable at low, as well as high frequencies.

1.2 Purpose

The purpose of this thesis is to demonstrate a practical method of predicting the vibrational response of cylindrical shells to

point excitation. The measured driving point admittance is compared with predictions using the Mean-Value Admittance Method.

The scope of this investigation is limited to circular cylindrical shells, although many of the methods used, and the results obtained, can be extended to plates and shells of other shapes. The shells that are studied may be classified as thin; that is to say that the stress distribution can be taken as linear through the thickness. The shells are homogeneous and isotropic. The special case of anisotrophy, orthotrophy, is also investigated. Complicating effects which are not addressed are: initial stresses, variable thickness, large deflections (nonlinear behavior), and the surrounding acoustic media. The effects of shear deformation and rotary inertia are neglected.

Quite often a ring is added to a cylinder to stiffen the shell at a point of excitation, thereby reducing the vibrational energy that is transmitted to the shell structure. A radial point force in the plane of the ring will excite one-dimensional modes in the ring which will then couple with two-dimensional modes in the shell. Analytical models are evaluated that describe in a simplified manner the coupling between shell and ring modes, while retaining the important features of the vibrational response. Methods are presented for the prediction of the mean-value of the driving-point admittance of shells, both with and without stiffening rings. Although not specifically discussed, the results of these investigations can also be extended to the use of stringers to stiffen the shell in the axial direction.

During the course of this investigation numerous driving-point and transfer admittances were measured on two cylindrical shells,

one with and one without ring-stiffening. In order to provide a complete analytical treatment, it was later decided to limit the scope of investigations principally to driving-point admittances. The extension of the mean-value theory to the calculation of transfer admittances is introduced but not pursued.

CHAPTER II

THEORY

2.1 Classical Mode-Sum

Fundamental to most vibrational theories is the concept that the response of any closed system to an arbirtary excitation can be represented by the superposition of the system's natural modes:

$$\xi = \sum_{\nu} \xi_{\nu}(x,y,z)\ e^{j\omega t} \quad . \tag{2.1}$$

Here, ξ represents the scalar displacement on the surface of the vibrator, and ξ_{ν} are the mode functions. The harmonic time dependence of $e^{j\omega t}$ is assumed for all the excitation and response functions and will hereafter be omitted. The mode functions or eigenfunctions of a system represent natural states in which the system prefers to vibrate, independent of the forcing frequency. Along with satisfying the boundary conditions of the system, the mode functions must obey the property of orthogonality. It will suffice to say that the property of orthogonality cannot be satisfied unless the system is closed; by this we mean that it is reasonably isolated from its surroundings such that vibrational energy is not lost or gained in an unpredictable manner.

By representing the system in terms of mode functions, the response of any homogeneous system can be reduced to a set of one-degree of freedom oscillator equations, one equation for each mode. This is accomplished by incorporating into the elements of the one-degree of freedom oscillator information concerning the forcing function and the point of

observation on the surface of the vibrator. Rather than writing out the oscillator equations, it is more convenient to use the symbolic notation of electrical network theory to represent the vibrating system. The circuit representation of a homogeneous vibrating system is illustrated in Figure 1. By representing the vibrator by its electrical equivalent, we can make use of the powerful theorems developed for electrical networks and transmission lines [11].

The circuit shown in Figure 1 is called a canonic circuit, and consists of the parallel connection of an infinite number of series-resonant circuits, one for each mode. Each series circuit is composed of a mode mass (M_ν), compliance (C_ν), and resistance (R_ν). At very low frequencies, the system usually behaves like an inductance (M_0), which represents the rigid body translation of the vibrator. At very high frequencies, the system is usually shunted by a capacitance (C_0) which represents the compliance at the interface between the driver and vibrator, or the local deformation of the vibrator material in the vicinity of the driver.

Given the resonance frequencies, ω_ν, and the modal loss factors, η_ν, the mode compliance and resistance can be expressed in terms of the mode mass:

$$C_\nu = \frac{1}{\omega_\nu^2 M_\nu} \tag{2.2}$$

and

$$R_\nu = \frac{\omega_\nu^2}{\omega} \eta_\nu M_\nu \quad . \tag{2.3}$$

The general expression for the mode mass is:

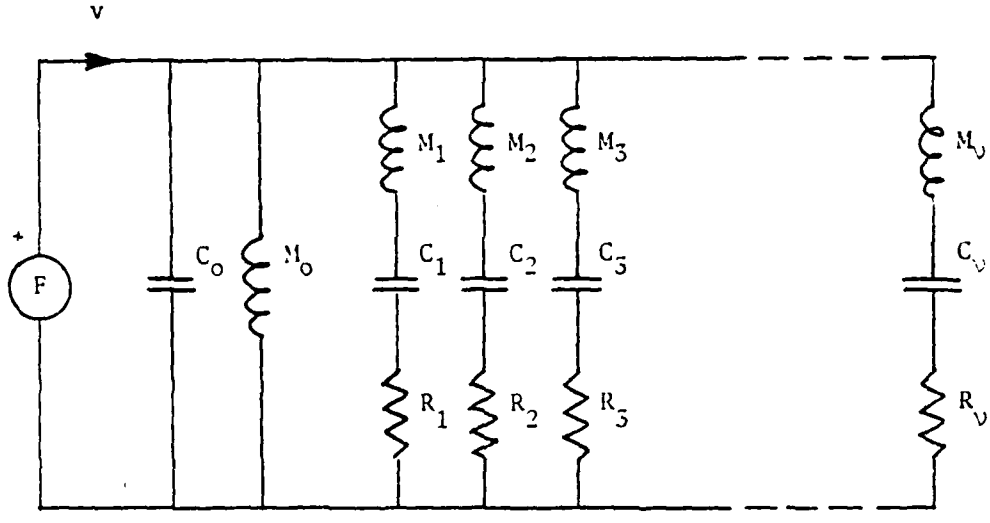

Figure 1 Canonic Circuit Representation of a Homogeneous Vibrating System (*from* Skudrzyk, Reference 11).

$$M_\nu = \frac{1}{\kappa_\nu \xi_\nu^2(A)} \int_S m \xi_\nu^2 \, dS = \frac{M\langle\xi_\nu^2\rangle}{\kappa_\nu \xi_\nu^2(A)} \quad . \tag{2.4}$$

Here, we are assuming that the surface mass density (m) is constant over the surface area (S). The total mass (M) is then: M = mS. The quantity $\langle\xi_\nu^2\rangle$ is the average of the square of the νth mode function over the surface area. The quantity κ_ν is the excitation constant, and is defined by:

$$\kappa_\nu = \frac{1}{F_o} \int_S \frac{F \xi_\nu}{\xi_\nu(A)} \, dS \quad , \qquad F_o = \int_S F \, dS \quad . \tag{2.5}$$

The excitation constant states how much of the total force (F_o) is available to excite a particular mode (ξ_ν). Term A symbolically denotes the point of observation.

For a point force the excitation constant becomes:

$$\kappa_\nu = \frac{\xi_\nu(F)}{\xi_\nu(A)} = 1 \quad , \tag{2.6}$$

where F denotes the coordinates of the point force. Thus, the point mode mass becomes:

$$M_\nu = \frac{M \langle\xi_\nu^2\rangle}{\xi_\nu(F)\xi_\nu(A)} \quad . \tag{2.7}$$

It can easily be shown by integrating the square of the mode function over the surface of a vibrator of total mass M that $M_\nu = \frac{M}{2}$ for one-dimensional vibrators such as beams and rings, and that $M_\nu = \frac{M}{4}$ for two-dimensional vibrators such as plates and shells. Here we are assuming that the mode functions are sinusoidal, and that the distortion of the mode function at the edge of the vibrator may be neglected.

The admittance of the system can now be expressed as the sum of the individual mode admittances (neglecting M_o and C_o):

$$Y = \frac{v}{F} = \sum_{\nu=0}^{\infty} Y_\nu = \sum_{\nu=0}^{\infty} \frac{1}{R_\nu + j\omega M_\nu + \frac{1}{j\omega C_\nu}}$$

$$= \sum_{\nu=0}^{\infty} \frac{\omega}{M_\nu [\omega_\nu^2 \eta_\nu + j(\omega^2 - \omega_\nu^2)]} \quad . \tag{2.8}$$

The admittance is simply the resulting velocity of the system for a given force distribution.

For the driving-point admittance (driver and receiver coincident), all of the modes are excited with the same phase as the driver, and all the circuit elements are positive. Therefore, resonances and antiresonances alternate with increasing frequency as predicted by Fosters Theorem. At a resonance the admittance is a maximum, and at an antiresonance the admittance is at a minimum.

For the transfer admittance (driver and receiver separated), the circuit elements no longer need be positive. The circuit elements, M_ν, will be negative if the point of observation is vibrating in antiphase with the driven point. If the elements of two successive resonant circuits have opposite signs, their contributions add in the frequency region between the resonance frequencies. The result is plotted as a shallow trough, similar to the trough in the transmission curve of a band-pass filter.

The mode-sum procedure offers a straightforward and universal approach to the description of vibrating systems. Yet, it has limited applications for most of the complex structural systems in use today. The mode functions and resonance frequencies are usually too difficult to predict, or if predictable, may be too numerous and calculations become tedious. If only a few resonance frequencies are of interest, a prudent approach for complex systems is to experimentally measure the resonance frequencies, either on the actual system, or if not feasible, on a scale model of the system. The procedure is further limited by the fact that there are no closed systems in practice. The best we can hope for is that the system is only loosely coupled to its surroundings, or that the exchange of vibrational energy to the system's surroundings is somewhat tractable. Finally, the mode-sum procedure may provide more information than is of interest. In fact, the detailed information provided by the procedure may lead us toward a false sense of accuracy. In many practical structures, the resonances are so dense or overlapping because of damping that the identification of individual modal responses would be of little value. Instead, we are interested in the gross response over some frequency band that may contain many overlapping modal responses. A suitable measure of this gross response would be the geometric mean of the admittance over some frequency interval. This measure is the topic of the next section.

2.2 Mean-Value Driving-Point Admittance

If the velocity amplitude of a vibrating system is plotted on a logarithmic scale, the resonance maxima extend above the mean line through the frequency-response curve as much as the minima extend below

it. As the damping increases, the maxima and the minima coalesce to the same geometric-mean response curve. The mean line can be considered to represent the characteristic wave field that would be generated by the driver if the vibrator were sufficiently large or sufficiently damped so that reflections from the boundaries do not contribute significantly to the response at the driving point.

By integrating the modal responses over a unit frequency interval, Skudrzyk [9, 10, 11] has shown that the geometric mean of the driving-point admittance of any homogeneous vibrator is described by:

$$Y_o = G_o + jB_o = \frac{\pi}{2\varepsilon_\nu M_\nu} + jB_o \quad , \tag{2.9}$$

where ε_ν is the frequency difference between successive resonances (inverse of the density of resonances) and M_ν is the point mode mass. The real part of the admittance describes an energy carrying wave that propagates away from the driving point (characteristic wave), and the imaginary part represents a wattless field that is observed near the driver.

For vibrators with constant $\varepsilon_\nu M_\nu$, the imaginary part of the admittance is zero. This result follows from the fact that the contributions to B_o from the modes whose resonances are above the forcing frequency cancel the contributions of the modes whose resonances are below the forcing frequency. This applies to most of the important vibrators, such as rods, plates, and shells (above the radial resonance frequency). The exception is the beam or ring, where $\varepsilon_\nu M_\nu$ is proportional to $\sqrt{\omega}$. For these types of vibrators, B_o is a negative mass admittance and is equal to the real part.

For most vibrators, the task of determining the driving-point admittance essentially reduces to that of determining the density of resonances.

CHAPTER III

CYLINDRICAL SHELL

In this chapter, simple expressions are derived for the prediction of the mean-value of the driving-point admittance of a circular cylindrical shell. The task of determing the driving-point admittance essentially reduces to that of determining the density of resonances. The derivation of the density of resonances is generalized to the case of orthotropy where the bending stiffnesses are not equal along the principal axes of the material. The orthotropic cylindrical shell is a useful model of a cylinder with stiffening rings or stringers. The predicted mean-value admittance of an isotropic shell is compared with experimental measurements, and an interpretation of the data is provided. For details of the experimental investigations, the reader is referred to Appendix A.

3.1 Mode Parameters

3.1.1 Mode Mass

The displacement in the radial direction of the cylindrical shell may be described by the mode functions:

$$\xi_{m,n} = \hat{\xi} \cos n\theta \cos k_m z \quad , \quad n = 0,1,2,3... \quad , \tag{3.1}$$

where: $$k_m = \frac{m\pi}{\ell} = \frac{\sigma}{a} \quad , \quad m = 0,1,2,3... \quad . \tag{3.2}$$

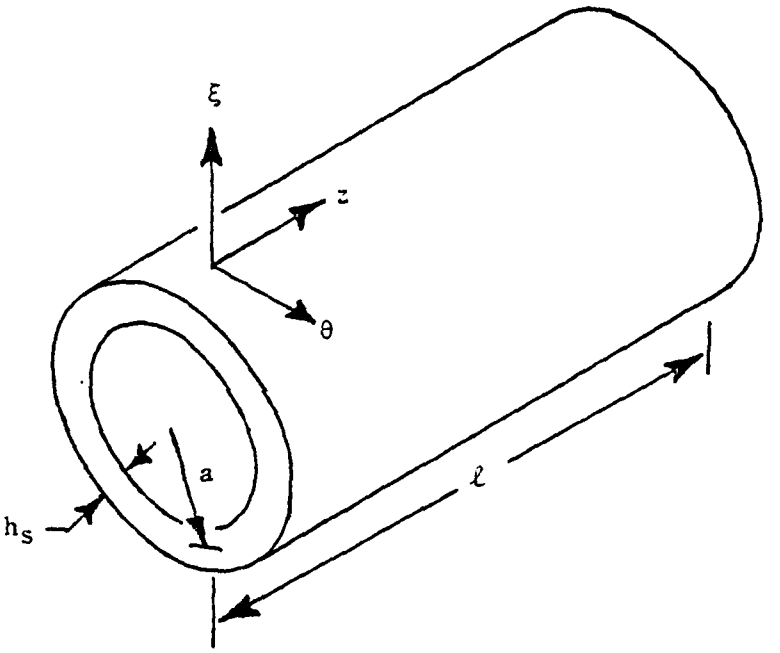

Figure 2 Coordinate System and Dimensions of Circular Cylindrical Shell.

The coordinate system and dimensions of the cylindrical shell are shown in Figure 2. Here, n is the integer number of waves in the circumferential direction, and m is the integer number of half-waves in the axial direction. It is convenient to introduce the normalized wavenumber, σ/a, which will be used in the shell frequency equation.

The spacial average of the square of the mode function is:

$$\langle \xi^2_{m,n} \rangle = \frac{1}{2\pi\ell} \int_0^{2\pi} \int_0^{\ell} \hat{\xi}^2 \cos^2 n\theta \cos^2 \frac{m\pi}{\ell} z \, dz \, d\theta = \frac{\hat{\xi}^2}{4} \quad . \qquad (3.3)$$

For a point force, $\xi_{m,n}(F) = \hat{\xi}$; and if the point of observation coincides with the driving point, $\xi_{m,n}(A) = \hat{\xi}$. Using Equation (2.7), the mode mass then becomes:

$$M_{m,n} = \frac{M}{4} \quad . \qquad (3.4)$$

As one would expect for a two-dimensional vibrator, the point mode mass is one quarter the total mass of the cylinder.

3.1.2 Density of Resonances

The density of resonances (or mode density) for the cylindrical shell has been derived by Heckl [7] and Skudrzyk [11]. Heckl based his analysis on a simplified equation for the natural frequencies. Skudrzyk, using a less simplified form of Heckl's equation and a unique approach, obtained more accurate results. Skudrzyk's derivation can, however, be improved in the region about the radial resonance frequency of the cylinder. The following derivation uses Skudrzyk's approach, but improves the accuracy of the results near the radial resonance frequency.

It also generalizes to the case of orthotrophy where the bending stiffnesses are not equal along the principal axis of the material.

The resonance frequencies of a simply supported finite cylinder of length ℓ, radius a, and thickness h are given by:

$$\Omega^2 = \frac{(1-\mu^2)\sigma^4}{(n^2+\sigma^2)^2} + \gamma^2\left[(n^2+\sigma^2)^2 - \frac{n^2(4-\mu)-2-\mu}{2(1-\mu)}\right] \quad , \qquad (3.5)$$

where $\gamma = h/\sqrt{12}a$ is the thickness-to-radius parameter, μ is Poisson's ratio, and $\Omega = \omega/\omega_o$. The frequency is normalized to the radial resonance frequency $\omega_o = c_{p\ell}/a$, where $c_{p\ell}$ is the velocity of a longitudinal wave in a plate. Heckl shows that this equation is in good agreement with measurements performed by Arnold and Warburton [2]. By using $\mu = 0.3$ this equation reduces to:

$$\Omega^2 = \frac{0.19\,\sigma^4}{(n^2+\sigma^2)^2} + \gamma^2\,[(n^2+\sigma^2)^2 - 2.6\,n^2 + 1.6\,] \quad . \qquad (3.6)$$

In order to calculate the density of resonances, Heckl approximated this frequency equation by:

$$\Omega^2 = \left[\frac{\sigma^2}{(n^2+\sigma^2)} + \gamma(n^2+\sigma^2)\right]^2 \quad , \qquad (3.7)$$

while Skudrzyk used the following form:

$$\Omega^2 = \frac{\sigma^4}{(n^2+\sigma^2)^2} + \gamma^2(n^2+\sigma^2)^2 \quad . \qquad (3.8)$$

Equations (3.6) through (3.8) are plotted in Figures 3 through 5, respectively, for $\gamma = 0.01$. These figures display the contours of constant frequency in wavenumber space, and are shown as continuous functions for convenience only. As shown in these figures, Equation (3.8) is a much better approximation of the frequency equation than is

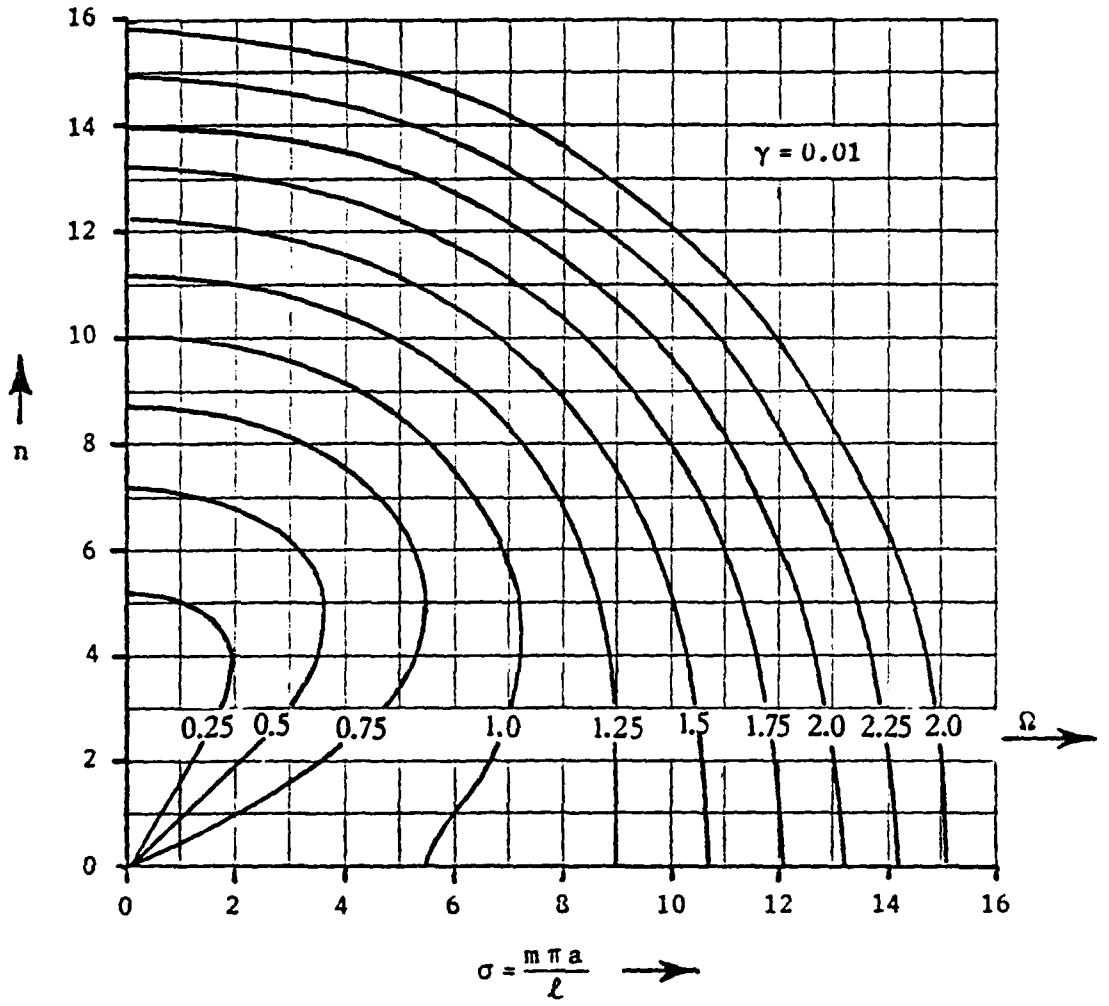

Figure 3 Contours of Constant Frequency in Wavenumber Space for Equation (3.6) .

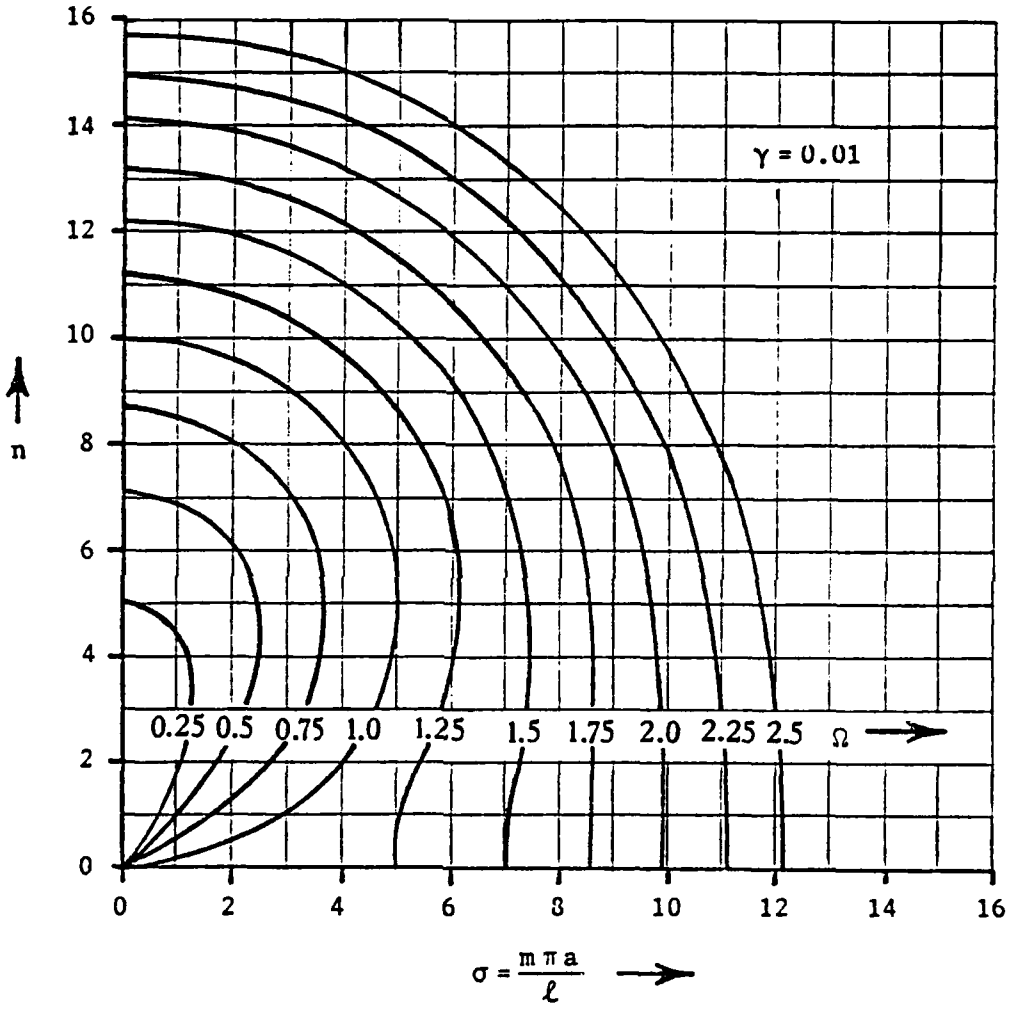

Figure 4 Contours of Constant Frequency in Wavenumber Space for Equation (3.7) .

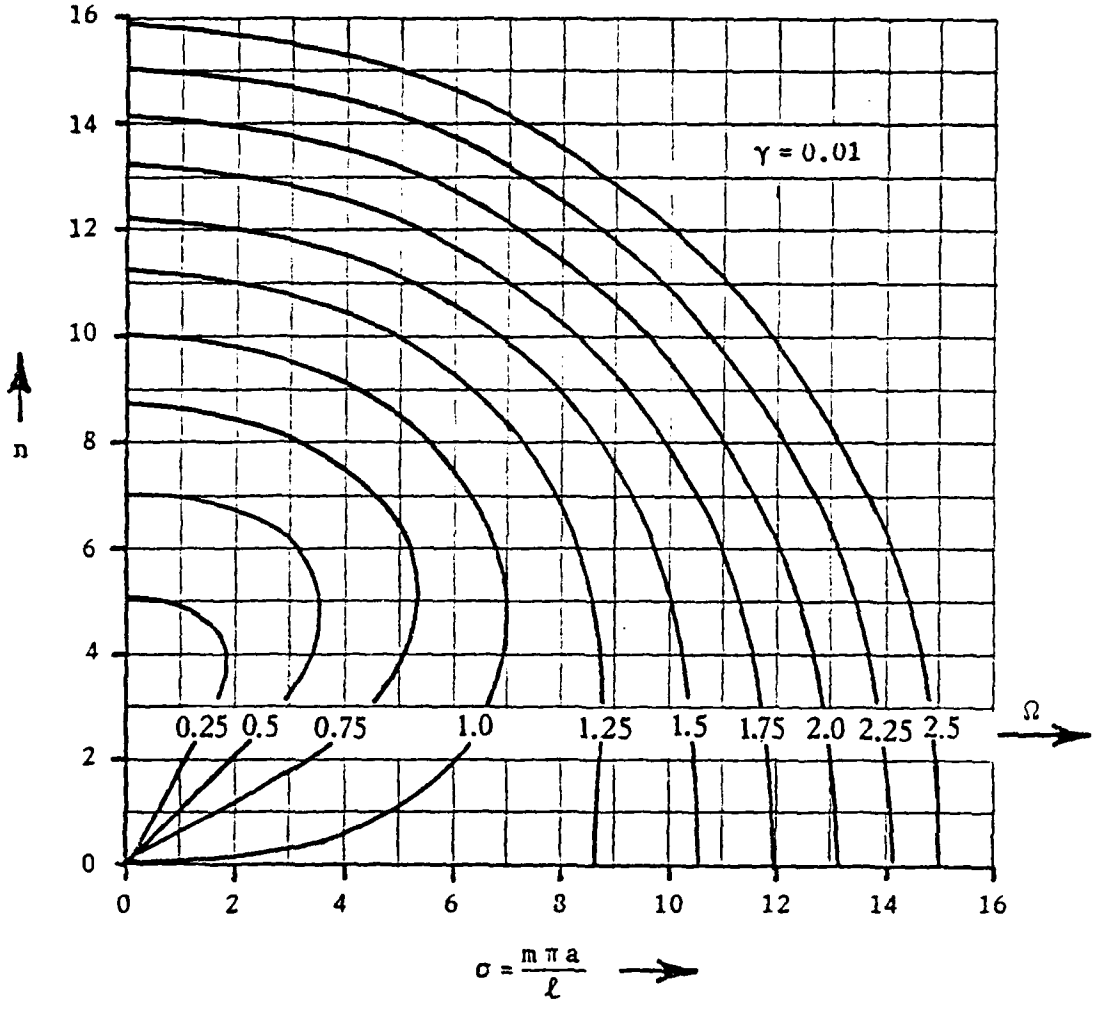

Figure 5 Contours of Constant Frequency in Wavenumber Space for Equation (3.8) .

Equation (3.7), particularly for $\Omega<1$. However, neither approximation is good in the vicinity of $\Omega = 1$. We shall use Equation (3.8) in our calculations, but we must exercise caution in the vicinity of $\Omega = 1$ to assure a valid result.

Recognizing that the bending stiffness is proportional to thickness, and thus γ, we can introduce different bending stiffnesses along the θ and z axes by introducing different γ's for each modenumber:

$$\gamma_1 = h_1/\sqrt{12}\,a \qquad \text{and} \qquad \gamma_2 = h_2/\sqrt{12}\,a \quad . \tag{3.9}$$

Here, γ_1 is the thickness-to-radius parameter in the circumferential direction, and γ_2 is the thickness-to-radius parameters in the axial direction. Equation (3.8) now becomes:

$$\Omega^2 = \frac{\sigma^4}{(n^2+\sigma^2)^2} + (\gamma_1 n^2 + \gamma_2 \sigma^2)^2 \quad . \tag{3.10}$$

Equation (3.10) can be simplified by introducing the polar coordinates:

$$r^2 = n^2 + \sigma^2 \qquad \text{and} \qquad \cos^2\phi = \frac{\sigma^2}{r^2} \quad . \tag{3.11}$$

Thus:

$$\begin{aligned}\Omega^2 &= \cos^2\phi + r^4(\gamma_1 \sin^2\phi + \gamma_2 \cos^2\phi)^2 \\ &= \cos^2\phi + r^4 B^2(\phi) \quad .\end{aligned} \tag{3.12}$$

The relationship of these parameters to the wavenumbers is displayed in Figure 6. Assuming that ϕ is constant, the change in r with respect to frequency is:

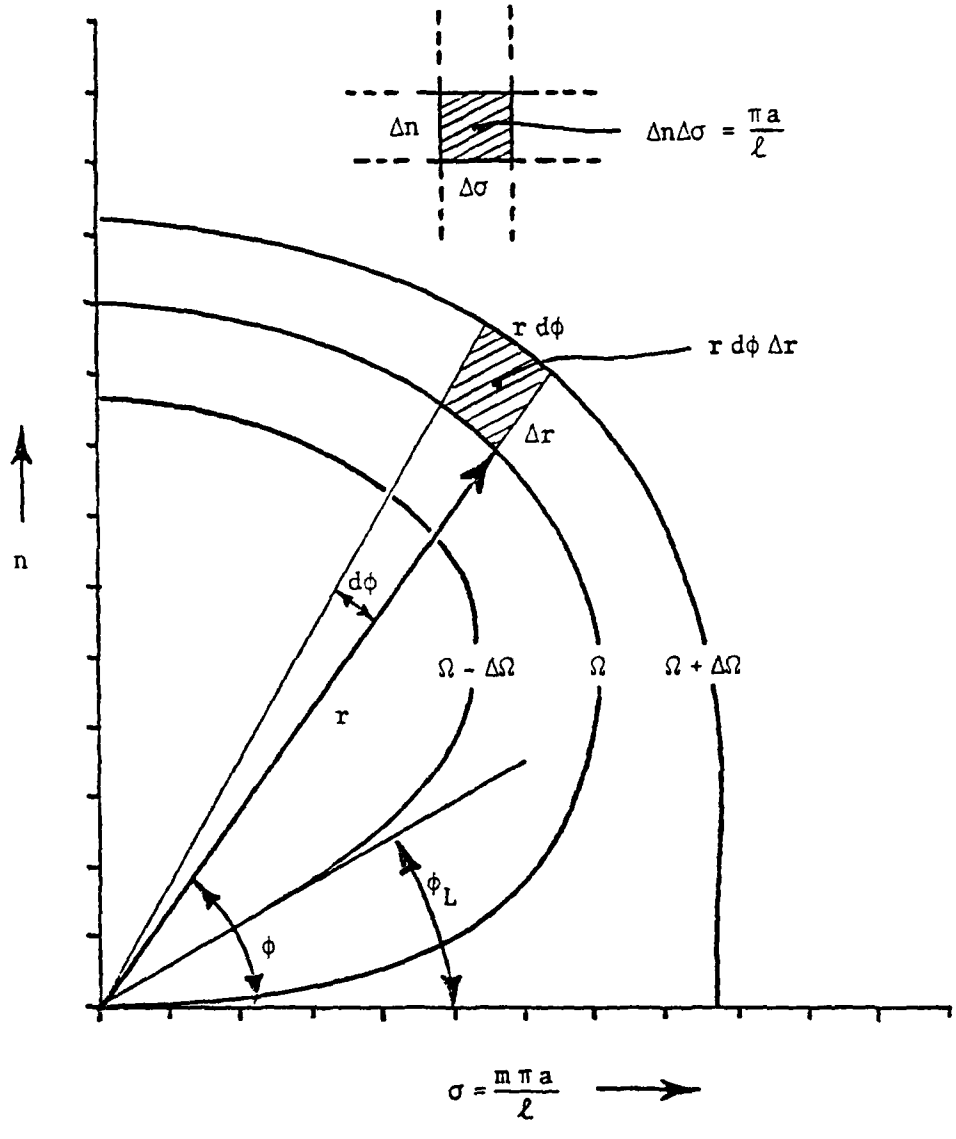

Figure 6 Parameters for the Calculation of the Shell Density of Resonances.

$$2\Omega \frac{\partial \Omega}{\partial \Omega} = 4r^3 B^2(\phi) \frac{\partial r}{\partial \Omega}$$

and

$$\Delta r \Big|_{\phi=\text{const.}} = \frac{\Delta\Omega}{2r} \frac{\Omega}{r^2 B^2(\phi)} = \frac{\Delta\Omega}{2r} \frac{\Omega}{B(\phi)\sqrt{\Omega^2 - \cos^4\phi}} = \frac{\Delta\Omega}{2rB(\phi)\sqrt{1 - \frac{\cos^4\phi}{\Omega^2}}} \quad (3.13)$$

The area between the curves Ω = constant and $\Omega + \Delta\Omega$ = constant is given by:

$$A = \int_{\phi_L}^{\pi/2} \dot{r}\, \Delta r\, d\phi = \frac{\Delta\Omega}{2} \int_{\phi_L}^{\pi/2} \frac{d\phi}{(\gamma_1 \sin^2\phi + \gamma_2 \cos^2\phi)\sqrt{1 - \frac{\cos^4\phi}{\Omega^2}}} \quad . \quad (3.14)$$

The lower limit of integration ϕ_L depends on the value of n. For n = 0, the frequency equation becomes:

$$\Omega^2 = 1 + \gamma_2^2 \sigma^4 \quad . \quad (3.15)$$

The lowest frequency that is possible is $\Omega = 1$, which corresponds to $\sigma = 0$; this means that the cylinder is infinitely long. Therefore, for $\Omega >> 1$ we must use $n = 0$ and $\phi_L = 0$. For $\Omega << 1$, the lowest value of ϕ occurs for n = 1 (see Figure 5), and the frequency equation becomes:

$$\Omega^2 = \frac{\sigma^4}{(1+\sigma^2)^2} + (\gamma_1 + \gamma_2 \sigma^2)^2 \quad . \quad (3.16)$$

Unless σ is very small, the membrane term $\sigma^4/(1+\sigma^2)^2 = 1$, and Ω would be beyond the frequency region of interest. We can thus neglect $\gamma_2 \sigma^2$ Compared to γ_1 . If this were not true, that is if $\gamma_2 \sigma^2$ was the dominant term, Equation (3.16) would reduce to the frequency equation of a beam along the z-axis. Rewriting Equation (3.16) we have:

$$\Omega^2 = \cos^4\phi_L + \gamma_1^2$$

and

$$\phi_L = \cos^{-1}\sqrt[4]{\Omega^2 - \gamma_1^2} = \cos^{-1}\sqrt[4]{(\omega^2-\omega_1^2)/\omega_o^2}$$

$$\simeq \sqrt{\Omega} \quad . \tag{3.17}$$

Here, ω_1 is the first pure circumferential resonance ($n = 1$, $\sigma = 0$). Note that if ω is less than ω_1, sometimes called the cut-off frequency, the limiting angle becomes imaginary. The error in the approximation above is negligible as long as $\omega << \omega_o$ but not so low that $\omega \simeq \omega_1$. As the frequency increases such that Ω approaches 1, the error becomes larger, particularly if the shell is thick or short. For $\Omega = 1$, we use $n = 1$ in an approximate form of Equation (3.6):

$$\Omega^2 = 1 \simeq 0.91\cos^4\phi_L + r^4(\gamma_1\sin^2\phi_L + \gamma_2\cos^2\phi_L)^2$$

$$\simeq 0.91\cos^4\phi_L + \frac{1}{\sin^4\phi_L}(\gamma_1\sin^2\phi_L + \gamma_2\cos^2\phi_L)^2 \quad .$$

Since ϕ_L is small, $\cos\phi_L \simeq 1$ and $\sin\phi_L \simeq \phi_L$; and we have:

$$1 \simeq 0.91 + \frac{1}{\phi_L^4}(\gamma_1\phi_L^2 + \gamma_2)^2 \simeq 0.91 + \frac{\gamma_2^2}{\phi_L^4}$$

and

$$\phi_L \simeq 2\sqrt{\gamma_2} \quad . \tag{3.18}$$

The area in the r,ϕ plane that corresponds to one resonance is $\Delta n\Delta\sigma = \pi a/\ell$, and the number of modes per unit frequency interval is given by:

$$\frac{\Delta N}{\Delta\Omega} = \frac{\frac{A}{\Delta n\Delta\sigma}}{\Delta\Omega} = \frac{\ell}{2\pi a}\int_{\phi_L}^{\pi/2} \frac{d\phi}{(\gamma_1\sin^2\phi + \gamma_2\cos^2\phi)\sqrt{1 - \frac{\cos^4\phi}{\Omega^2}}} \quad . \tag{3.19}$$

For $\Omega >> 1$, $\sqrt{1 - \frac{\cos^4\phi}{\Omega^2}} \simeq 1$, and the density of resonances is:

$$\frac{\Delta N}{\Delta\Omega} = \frac{\ell}{2\pi a}\int_0^{\pi/2} \frac{d\phi}{\gamma_1 \sin^2\phi + \gamma_2 \cos^2\phi} = \frac{\ell}{2\pi a}\,\frac{\pi}{2\sqrt{\gamma_1\gamma_2}} = \frac{\ell}{4a\sqrt{\gamma_1\gamma_2}}$$

$$= \frac{\sqrt{3}\,\ell}{2\sqrt{h_1 h_2}} \quad . \tag{3.20}$$

Thus, at high frequencies, the mode density is inversely proportional to the geometric mean of the axial and circumferential thicknesses. If $h_1 = h_2 = h$, the mode density reduces to $\sqrt{3}\,\ell/2h$, which is the same as that of a plate.

At frequencies in the vicinity of the radial resonance frequency ($\Omega = 1$), the density of resonances becomes:

$$\frac{\Delta N}{\Delta\Omega} = \frac{\ell}{2\pi a}\int_{2\sqrt{\gamma_2}}^{\pi/2} \frac{d\phi}{(\gamma_1 \sin^2\phi + \gamma_2 \cos^2\phi)\sqrt{1 - \cos^4\phi}}$$

$$= \frac{\ell}{2\pi a}\int_{4\gamma_2}^{+1} \frac{dx}{[(\gamma_1 - \gamma_2)x + \gamma_2]\,2x\sqrt{2 - 3x + x^2}}$$

Neglecting $(\gamma_1 - \gamma_2)x$ compared to γ_2 we have:

$$\frac{\Delta N}{\Delta \Omega} \simeq \frac{\ell}{2\pi a} \frac{1}{2\sqrt{2}\gamma_2} \ln(2/\gamma_2) = \frac{\sqrt{3}\,\ell}{2\sqrt{2}\,\pi\, h_2} \ln(2/\gamma_2)$$

$$= 0.195 \frac{\ell}{h_2} \ln(2/\gamma_2) \quad . \tag{3.21}$$

Thus, at frequencies in the vicinity of the radial resonance frequency, the mode density for most practical purposes depends only on the bending stiffness in the axial direction. This is not surprising since a great many axial modes (n = 0) occur in the vicinity of ω_o.

At very low frequencies ($\Omega << 1$), the angle ϕ approaches $\pi/2$ and we can write $\phi = \frac{\pi}{2} - \varepsilon$. Substituting this ϕ into Equation (3.19), the density of resonances becomes:

$$\frac{\Delta N}{\Delta \Omega} = \frac{\ell}{2\pi a} \int_0^{\sqrt{\Omega}} \frac{d\varepsilon}{(\gamma_1 + \gamma_2 \varepsilon^2)\sqrt{1 - \frac{\varepsilon^4}{\Omega^2}}} \simeq \frac{\ell}{2\pi a \gamma_1} \int_0^{\sqrt{\Omega}} \frac{d\varepsilon}{\sqrt{1 - \frac{\varepsilon^4}{\Omega^2}}}$$

$$= \frac{\ell\sqrt{\Omega}}{2\pi a \gamma_1} \int_0^{+1} \frac{dx}{\sqrt{1 - x^4}} = \frac{\ell\sqrt{\Omega}}{2\pi a \gamma_1} \frac{\pi}{2\sqrt{2}} = 1.1 \frac{\ell\sqrt{\Omega}}{2\pi a \gamma_1}$$

$$= \frac{\sqrt{3}\,\ell}{2\sqrt{2}\,h_1} \sqrt{\Omega} \quad . \tag{3.22}$$

This result was obtained by Skudrzyk. By noting that ϕ approaches $\pi/2$ as the frequency decreases, one is tempted to assume that $\cos^4\phi \simeq 0$ and that Equation (3.19) becomes:

$$\frac{\Delta N}{\Delta \Omega} = \frac{\ell}{2\pi a} \int_{\cos^{-1}\sqrt{\Omega}}^{\pi/2} \frac{d\phi}{(\gamma_1 \sin^2\phi + \gamma_2 \cos^2\phi)\sqrt{1 - \frac{\cos^4\phi}{\Omega^2}}} \simeq \frac{\ell}{2\pi a \gamma_1} \int_{\cos^{-1}\sqrt{\Omega}}^{\pi/2} d\phi$$

$$= \frac{\ell}{2\pi a \gamma_1} (\pi/2 - \cos^{-1}\sqrt{\Omega}) = \frac{\ell}{2\pi a \gamma_1} \sin^{-1}\sqrt{\Omega} \simeq \frac{\ell\sqrt{\Omega}}{2\pi a \gamma_1} \quad . \qquad (3.23)$$

This is the underlying assumption in Heckl's calculations. However, the ratio $\frac{\cos^4\phi}{\Omega^2}$ cannot be considered zero within the lower range of ϕ. Heckl noted that his experimental data was a factor 1.1 greater than his theory. Thus, Equation (3.22) would show excellent agreement with Heckl's experimental data.

The density of resonances at low frequencies depends primarily on the bending stiffness in the circumferential direction. This is in contrast to the situation at high frequencies where the density of resonances depends on the geometric mean of the stiffnesses in the axial and circumferential direction.

In summary, the density of resonances $(1/\varepsilon_{m,n})$ for the orthotropic cylindrical shell may be approximated by:

$$\frac{\Delta N}{\Delta \omega} = \frac{\Delta N}{\Delta \Omega} \frac{1}{\omega_o} = \left\{ \begin{array}{ll} \dfrac{a\ell}{4\alpha_1\alpha_2} & , \quad \omega > \omega_o \\ \dfrac{a\ell}{4\sqrt{2}\,\pi\,\alpha_2^2} \ln(2/\gamma_2) & , \quad \omega \approx \omega_o \\ \dfrac{a\ell}{4\sqrt{2}\,\alpha_1^2}\sqrt{\Omega} & , \quad \omega < \omega_o \end{array} \right\} . \qquad (3.24)$$

Here, we have introduced the circumferential and axial stiffness constants, defined by:

$$\alpha_1^2 = \frac{c_{p\ell}\, h_1}{\sqrt{12}} \qquad \text{and} \qquad \alpha_2^2 = \frac{c_{p\ell}\, h_2}{\sqrt{12}} \qquad . \qquad (3.25)$$

The density of resonances for the orthotropic cylindrical shell is illustrated in Figure 7, for various values of α_1 and α_2. The curves in this figure were computed numerically using Equation (3.10) and normalized to the high frequency mode density of an isotropic shell with stiffness constant α_s^2 . At low frequencies the density of resonances for the most part is inversely proportional to the stiffness in the circumferential direction. If this stiffness is reduced by ½ the density is doubled. At high frequencies the density of resonances is inversely proportional to the geometric mean of the circumferential and axial stiffnesses. If either one of these stiffnesses is reduced by ½ the density is increased by a factor of $\sqrt{2}$. If both of these stiffnesses are reduced by ½ the density of resonances is doubled.

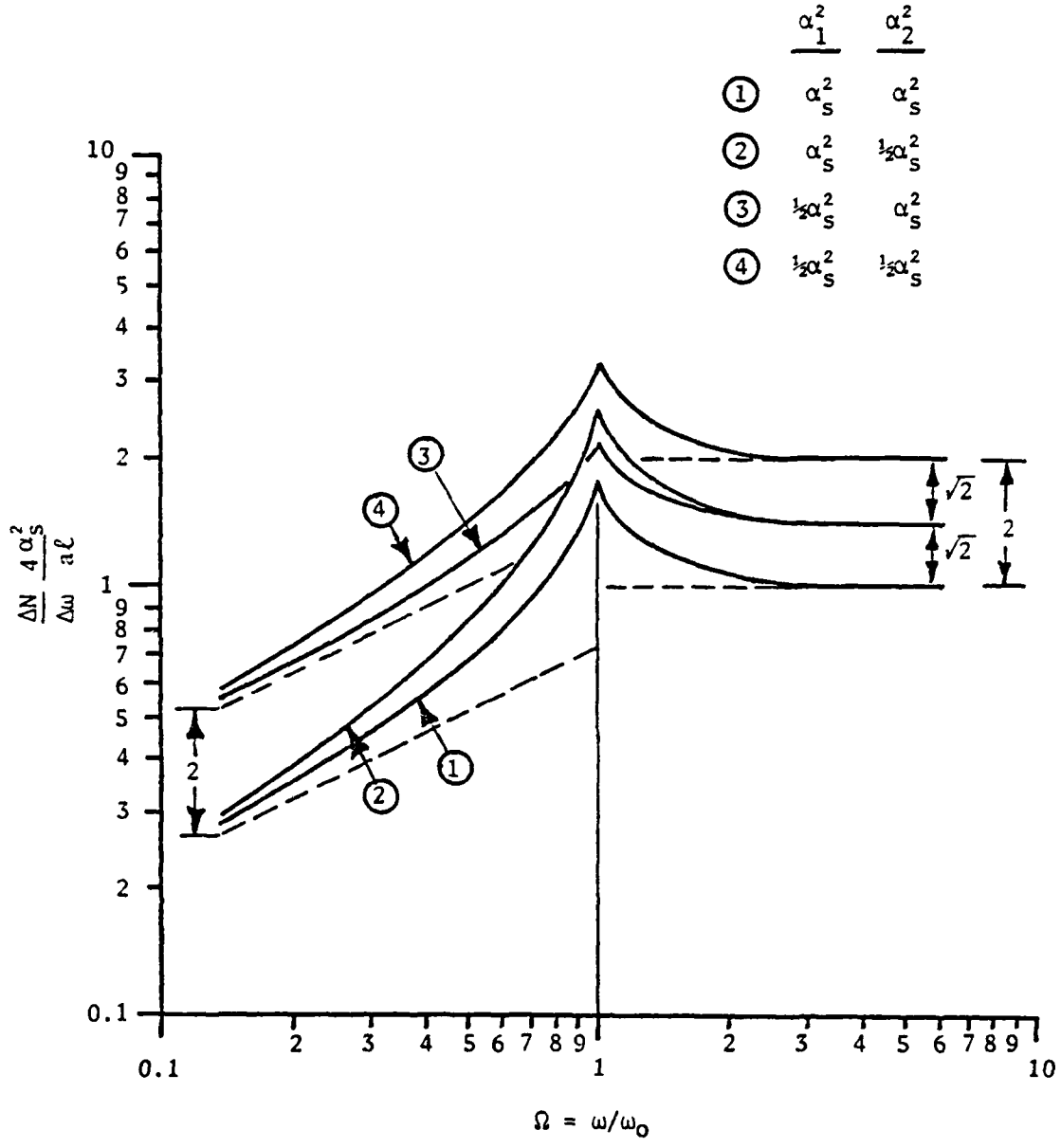

Figure 7 Variation of the Density of Resonances for an Orthotropic Cylindrical Shell with the Variation of the Circumferential and Axial Stiffness Constants.

For the isotropic shell, $\alpha_1 = \alpha_2 = \alpha_s$. The density of resonances for the isotropic shell is illustrated in Figure 8. This figure is normalized to the high frequency asymptotic value. At low frequencies the mode density increases proportional to the square-root of frequency, just as a membrane where extensional modes are predominant. In the vicinity of the radial resonance frequency, the mode density attains a value that varies inversely with the thickness to radius parameter, γ . The density peaks at a value that is greater than the high frequency mode density. At high frequencies the shell behaves as a plate with a constant mode density of $(a\ell/4\alpha_s^2)$. As shown in Figure 3, the contours of equal frequency approach that of a quarter circle with its center at the origin, the same as a plate. The density of resonances for the shell is, however, twice as great as that of a rectangular plate of the same surface area and thickness. This is a consequence of the degeneracy of the circumferential modes which need only satisfy the condition of periodicity about the circumference.

Strictly speaking, the density of resonances derived in this section is valid only for simply supported cylinders. But, these results can be applied to any cylinder with nondissipative boundaries. This is because the resonance frequencies of a simply supported cylinder are identical to those of a cylinder with nondissipative boundaries whose length has been slightly adjusted to match the nodal lines closest to the boundary. As long as the axial wavelength is small compared to the length of the cylinder [an assumption made in deriving Equation (3.6)], the error is negligible.

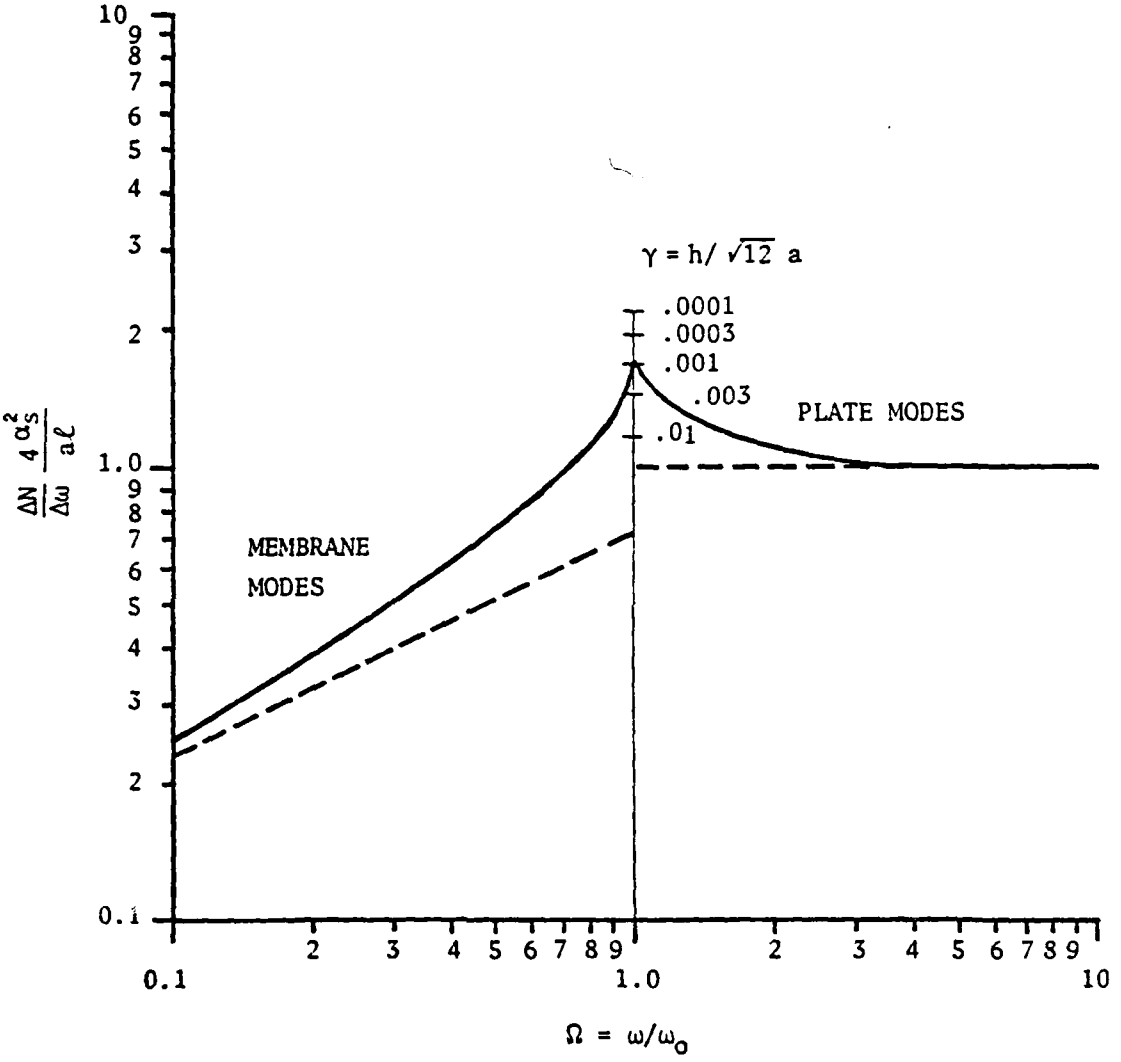

Figure 8 Normalized Density of Resonances for an Isotropic Cylindrical Shell.

3.2 Mean-Value Driving-Point Admittance

Using Equations (2.9) and (3.24), the real part of the driving-point admittance of an isotropic cylindrical shell, excited by a radial force at an internal point is given by:

$$G_s = \frac{1}{2(2\,\varepsilon_{m,n})\frac{M_s}{4}} = \left\{ \begin{array}{ll} \dfrac{1}{8m_s\alpha_s^2} & , \quad \omega > \omega_o \\ \dfrac{1}{8m_s\alpha_s^2}\,\dfrac{\ln(2/\gamma_2)}{\sqrt{2}\,\pi} & , \quad \omega \simeq \omega_o \\ \dfrac{1}{8m_s\alpha_s^2}\,\dfrac{\sqrt{\Omega}}{\sqrt{2}} & , \quad \omega < \omega_o \end{array} \right\} \quad . \qquad (3.26)$$

where m_s is the mass per unit surface area of the shell.

The density of resonances derived in the previous section is for axial modes of the form $\cos \frac{m\pi}{\ell} z$. All of these modes are fully excited when the driver is located on the edge of the shell. However, when the driver is moved to an internal point on the shell, not all modes are fully excited. For an internal driving point, it is convenient to assume the driver is at the center of the shell. In this position the odd order modes (m = 1,3,5 ...) are fully excited, and the even modes (m = 2,4,6 ...) are not excited at all. Thus, the density of resonances ($1/\varepsilon_\nu$) at an internal point on the shell is half the density if the driver were at the edge of the shell. It follows, then, that the driving-point admittance at an internal point on the shell is half the driving-point admittance at the edge of the shell. From a physical point of view, driving at an internal point on the shell means that the characteristic wave is radiating into a full-plane; and we can expect

that the velocity and admittance would be half that of the velocity and admittance if driving at the edge, where the characteristic wave radiates into a half-plane.

The imaginary part of the driving-point admittance, B_s, is equal to the real part, G_s, if $\omega<\omega_o$, and is approximately zero if $\omega>\omega_o$. The magnitude of the driving point admittance is then:

$$|Y_s| = \sqrt{G_s^2 + B_s^2} = \left\{ \begin{array}{ll} \dfrac{1}{8m_s\alpha_s^2} & , \quad \omega > \omega_o \\ \\ \dfrac{\sqrt{\Omega}}{8m_s\alpha_s^2} & , \quad \omega < \omega_o \end{array} \right\} . \qquad (3.27)$$

For most engineering applications it is sufficient to calculate the high frequency admittance, $20 \log |Y_s| = -20 \log (8m_s\alpha_s^2)$, and the radial resonance frequency, $f_o = c_{p\ell}/2\pi a$. The low frequency asymptote of $20 \log |Y_s|$ is then obtained by plotting a line with a +3 dB per octave slope that intersects the high frequency admittance at f_o . In most cases the increase above the high frequency admittance at f_o can be neglected.

Experimental verification of the foregoing mean-value theory was conducted using an aluminum cylindrical shell. The dimensions and physical properties of the shell are provided in Appendix A. The surface mass of the shell is $m_s = \rho h_s = 21.6$ kg/m^2 , the stiffness constant is $\alpha_s^2 = c_{p\ell} h_s / \sqrt{12} = 12.5$ m^2/sec , and the radial resonance frequency is $f_o = c_{p\ell}/2\pi a = 3300$ Hz . Using Equation (3.27), the high frequency mean-value driving-point admittance in decibels is:

$$20 \log |Y_s| = -20 \log (8m_s\alpha_s^2) = -66.7 \text{ dB re sec/kg} .$$

The thickness to radius parameter is $\gamma = h_s/a\sqrt{12} = 0.009$, and the increase over the high frequency admittance at f_o is:

$$20 \log \frac{\ln(2/\gamma)}{\sqrt{2}\,\pi} = +1.7 \text{ dB re sec/kg} .$$

For most engineering applications the increase of 1.7 dB can be ignored because of the narrow bandwidth in which it occurs. However, in order to illustrate some of the obscure features of vibrating shells, the 1.7 dB increase at the radial resonance frequency will be included in our predictions.

Figure 9 shows the measured driving-point admittance for both undamped and damped cases, and the predicted mean-value driving-point admittance. Here the driver is located at an internal point, approximately 6 cm from the center of the shell. From the undamped curve it may be seen that at low frequencies the density of resonances increases with frequency, and at high frequencies the density is relatively constant. In the vicinity of f_o there are a great many axial modes that occur for the case where no circumferential modes exist (n = 0). The circumferential resonance frequencies can easily be calculated by letting $\sigma = 0$ in the frequency Equation (3.5). These resonances are marked by an asterisk in Figure 9. From the undamped curve we see that the resonances usually occur as groups of axial resonances (m = 1,2,3...) about the dominant circumferential resonances (n = 1,2,3...). Whenever a new value of n is possible, the axial resonances occur very close to one another. It is interesting to note that as the length of the shell is

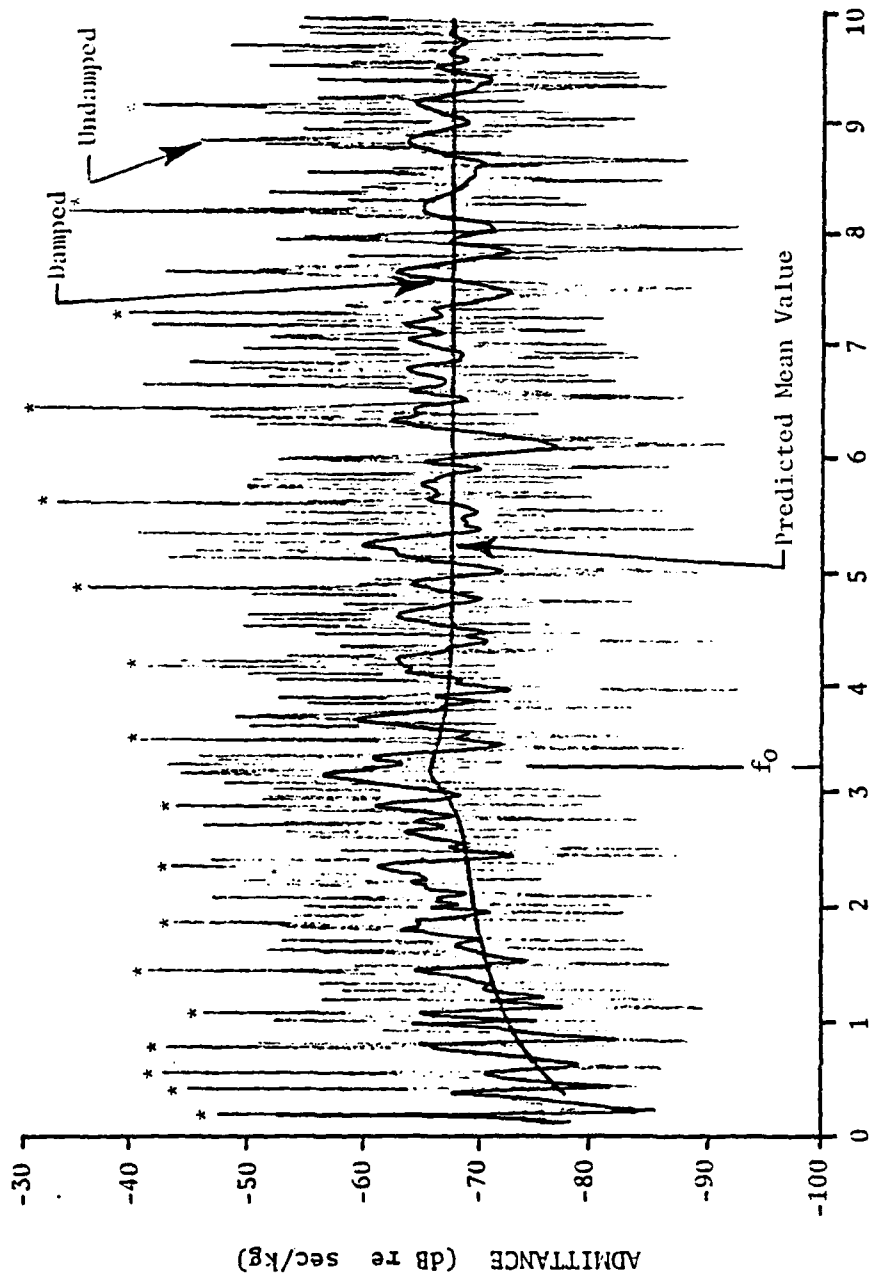

Figure 9 Predicted Mean-Value and Measured Driving-Point Admittance of Cylindrical Shell Driven 6 cm from the Axial Center.

increased, the axial resonances would become less pronounced, and the frequency curve would approach a curve resembling only the circumferential resonances. This is because the waves with large axial components must travel farther and are attenuated more than the pure circumferential waves.

As damping is increased many resonances are excited within their bandwidth, and the admittance approaches the predicted mean-value in Figure 9. This is significant because most cylindrical structures will exhibit a response similar to the damped curve in Figure 9. The mean-value admittance theory will then provide a simple but accurate method of predicting the mean response of many practical cylindrical structures.

Figure 10 shows the same data as Figure 9, except that the driving point is located at the exact center of the shell. In this position the driver can only excite the odd-ordered axial modes. These modes are, however, fully excited, and many have resonance peaks that are as strong as the circumferential resonances. As damping is increased the admittance approaches the predicted mean-value.

Figure 10 illustrates a unique exception to the mean-value theory. Because of the unique dimensions of the cylinder, more of the resonances in the vicinity of the radial resonance frequency, f_o, are even-ordered than odd-ordered axial resonances. The result is that 3/5 of the resonances in the vicinity of the radial resonance frequency are even-ordered axial resonances. These even axial modes, however, cannot be excited by driving at the center. Thus, instead of half the mode

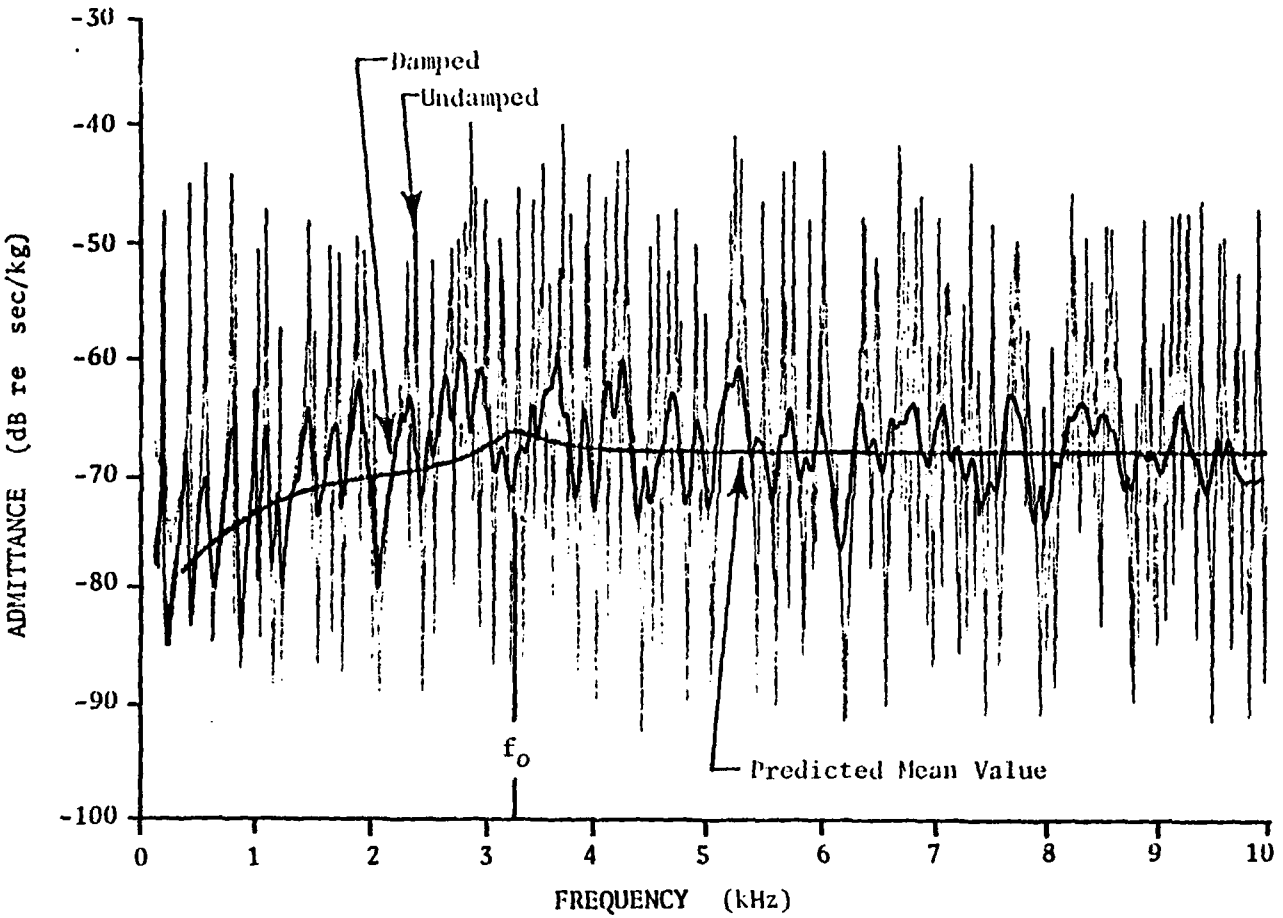

Figure 10 Predicted Mean-Value and Measured Driving-Point Admittance of Cylindrical Shell Driven at Center.

density for the center driven cylinder, we have 2/5 the mode density in the vicinity of f_o. The mean-value characteristic admittance at f_o is then 20 log $\left|\frac{2/5}{1/2}\right|$ = -2 dB less than our initial prediction. If the dimensions of the shell are changed slightly, or if the driver is moved off center, the dip in the vicinity of the radial resonance frequency would disappear.

Figure 11 is the same as the damped curve in Figure 10, except that the frequency is plotted on a logarithmic rather than a linear scale. The $\sqrt{\omega}$ dependence of the admittance below the radial resonance frequency is simply a straight line with a +3 dB per octave slope. The slight rise in the predicted mean-value at f_o is omitted.

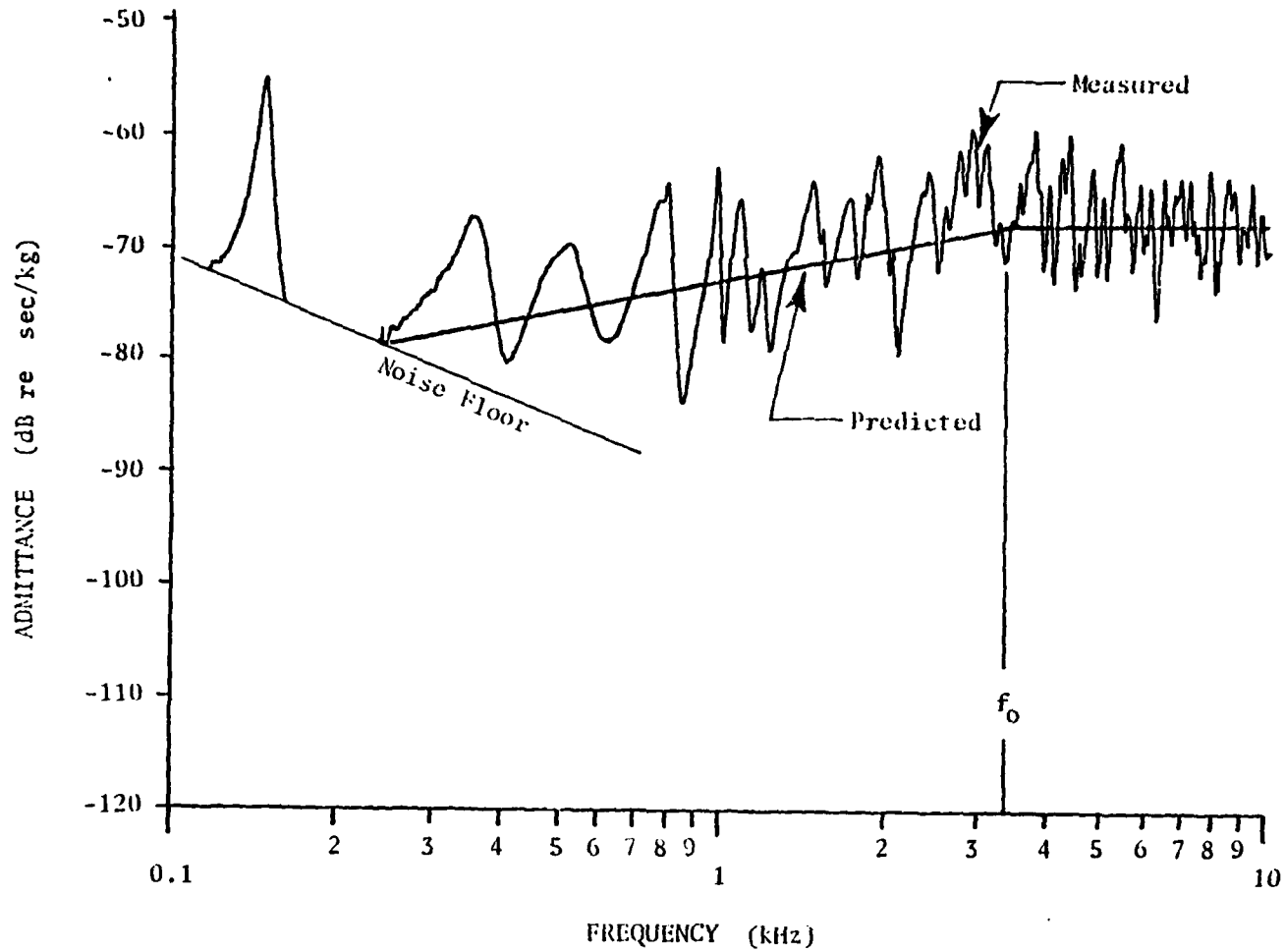

Figure 11 Predicted Mean-Value and Measured Driving-Point Admittance of Cylindrical Shell Driven at Center (Plotted on a Logarithmic Frequency Scale).

CHAPTER IV

RING-STIFFENED CYLINDRICAL SHELL

The vibrational response of a ring-stiffened cylindrical shell to point excitation in the plane of the ring is investigated in this chapter. Several analytical models are developed to describe the behavior of the ring-stiffened shell. Each model varies in its complexity and its accuracy in predicting the driving-point admittance in the plane of the ring. The model selection in an engineering application would depend on what details of the frequency response curve that the designer is interested in. The models presented in Sections 4.2.1 and 4.2.2 differ primarily in the degree of simplification used in describing the coupling between ring and shell modes. Very simplified models can be used if one is interested in either very high or very low frequencies relative to the radial resonance frequency. The high and low frequency models are presented in Section 4.2.3. For thick rings, the high frequency model must be modified to account for the first ring thickness antiresonance. This modification is presented in Section 4.2.4. Finally, the application of ring-stiffening to reduce the vibrational velocity of a cylindrical shell at the point of excitation is discussed in Section 4.3.

Throughout this chapter, experimental measurements are presented to support the various analytical models. For details of the experimental investigations, the reader is referred to Appendix A.

4.1 Mode Parameters

4.1.1 Mode Mass

The displacement in the radial direction of the ring may be described by the mode functions:

$$\xi_u = \hat{\xi} \cos u\theta \quad , \quad u = 1,2,3 \ldots \quad , \tag{4.1}$$

where u is the integer number of waves in the circumferential direction. The mode functions of the cylindrical shell are described by Equation (3.1). The dimensions of the ring-stiffened cylindrical shell are shown in Figure 12. The shell is sectioned axially in this figure to expose the details of the ring.

For a radial point force in the plane of the ring, the general expression for the point mode mass of the ring-shell structure is:

$$M_\nu = \frac{1}{\xi_\nu^2(A)} \int_S m_s \xi_\nu^2 \, dS \quad . \tag{4.2}$$

Here, the excitation constant, κ_ν, is unity for a point force. The surface mass density is a function of the axial coordinate as follows:

$$m_s(z) = \begin{cases} \dfrac{M_s}{2\pi a \ell} & , \quad 0 < z < \ell_1 \\ \dfrac{M_s}{2\pi a \ell} + \dfrac{M_r}{2\pi r b} & , \quad \ell_1 < z < \ell_1 + b \\ \dfrac{M_s}{2\pi a \ell} & , \quad \ell_1 + b < z < \ell \end{cases} \quad . \tag{4.3}$$

Assuming that the mode function, ξ_ν, is fairly constant across the ring width, b:

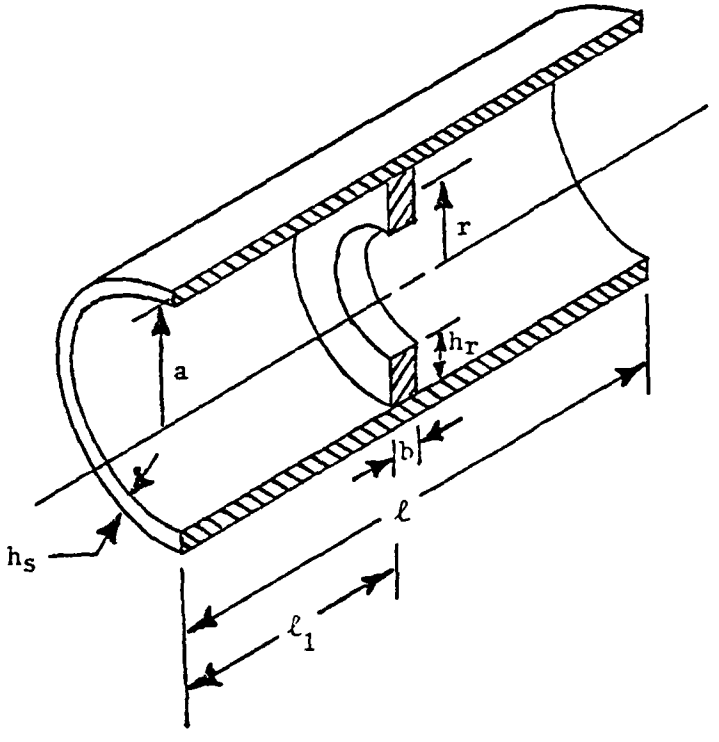

Figure 12 Dimensions of Ring-Stiffened Cylindrical Shell.

$$M_\nu \simeq [m_s''(\ell - b)] \frac{\langle \xi_\nu^2 \rangle}{\xi_\nu^2(A)} + (M_r + m_s'' b) \frac{\langle \xi_\nu^2 \rangle}{\xi_\nu^2(A)}$$

$$= \tfrac{1}{4}[m_s''(\ell - b)] + \tfrac{1}{2}(M_r + m_s'' b)$$

$$= \tfrac{1}{4} m_s''(\ell + b) + \tfrac{1}{2} M_r$$

$$= \tfrac{1}{4} M_s \left(1 + \frac{b}{\ell}\right) + \tfrac{1}{2} M_r$$

$$\simeq \tfrac{1}{4} M_s + \tfrac{1}{2} M_r \quad . \tag{4.4}$$

In the above expression, $m_s'' = M_s/\ell$ is the mass per unit axial length of the shell. The final approximation is valid as long as the width of the ring is much less than the length of the shell.

Equation (4.4) is not surprising, since we would intuitively assume that the point mode mass of the total ring-shell structure would be the sum of the point mode masses of the shell and ring alone. This assumption is valid, however, only if the axial mode function is relatively constant across the width of the ring, and if the length of the shell is much greater than the width of the ring. The first restriction is equivalent to the statement that the ring is a one-dimensional vibrator. The second restriction above is equivalent to the statement that the shell is a two-dimensional vibrator, because if the shell length is reduced to the width of the ring the resulting mode mass would be the same as a one-dimensional vibrator with a total mass of $M_s + M_r$. From this argument, we see that for a very short cylinder the point mode mass of the ring-shell structure would fall somewhere between $\left(\frac{M_s}{4} + \frac{M_r}{2}\right)$ and $\left(\frac{M_s + M_r}{2}\right)$.

4.1.2 Ring Density of Resonances

For bending vibrations in the plane of the ring, the ring resonance frequencies are described by [13]:

$$\omega_u = \frac{(u+1)[(u+1)^2-1]}{\sqrt{(u+1)^2+1}} \frac{\alpha_r^2}{r^2} \quad , \quad u = 1,2,3 \ldots \quad . \quad (4.5)$$

Here, r is the radius of the centerline of the ring and the stiffness constant is: $\alpha_r^2 = c_E h_r/\sqrt{12}$, where c_E is the velocity of sound in a rod.

The ring vibrates similar to a center-driven beam of the same cross section and length $2\pi r$, such that the vibration is symmetric about the driven point. At the fundamental resonance of such a beam, the wave travels down the beam and is reflected back to the driving point in phase ($\lambda = 2\pi r$). The beam resonance frequencies are, therefore, given by:

$$\omega_u = 2\pi u \frac{c_E}{\lambda} = 2\pi u \frac{\alpha_r \sqrt{\omega_u}}{2\pi r} = u \frac{\alpha_r}{r} \sqrt{\omega_u} = u^2 \frac{\alpha_r^2}{r^2} \quad . \quad (4.6)$$

This is the asymptotic value of Equation (4.5). The curvature of the ring increases the effective stiffness, unless the bending wavelength is much smaller than the ring circumference. The first few resonance frequencies of the ring are, therefore, higher than the frequencies given by Equation (4.6).

If the ring is attached to the shell, we would expect the ring resonances to be different than those given by Equation (4.5). The shell will increase the effective mass and stiffness of the ring at the driven point. Because the ring is much stiffer than the shell, we may neglect the increase in stiffness created by the shell; thus the primary effect of the shell on the ring is to mass load the ring. The increase in

effective mass at the driving point is simply the increase in the point mode mass due to the shell. This increase in effective mass will decrease the ring resonance frequencies by a factor of:

$$\beta = \left[\frac{\frac{1}{2} M_r}{\frac{1}{2} M_r + \frac{1}{4} M_s} \right]^{\frac{1}{2}} \quad . \tag{4.7}$$

Here, $\frac{M_r}{4}$ is the mode mass of the ring, and $\frac{M_s}{4}$ is the mode mass of the shell. The ring resonance frequencies with shell mass loading are, therefore:

$$\omega_u = \frac{(u+1)\left[(u+1)^2 - 1\right]}{\sqrt{(u+1)^2 + 1}} \frac{\alpha_r^2}{r^2} \beta \quad . \tag{4.8}$$

This result is demonstrated more rigorously in Section 4.2.1 by analysis of the modal coupling between ring and shell.

Experimental verification of Equation (4.8) was conducted using a steel ring-stiffened cylindrical shell. Details of this shell may be found in Appendix A. Figure 13 compares the measured ring resonance frequencies with those predicted by Equation (4.8). The agreement between the measured and predicted ring resonance frequencies is good.

Above the first few resonances, the ring resonance frequencies may be approximated by:

$$\omega_u = u^2 \frac{\alpha_r^2}{r^2} \beta \quad . \tag{4.9}$$

The change in frequency between successive resonances (inverse of the density of resonances) is:

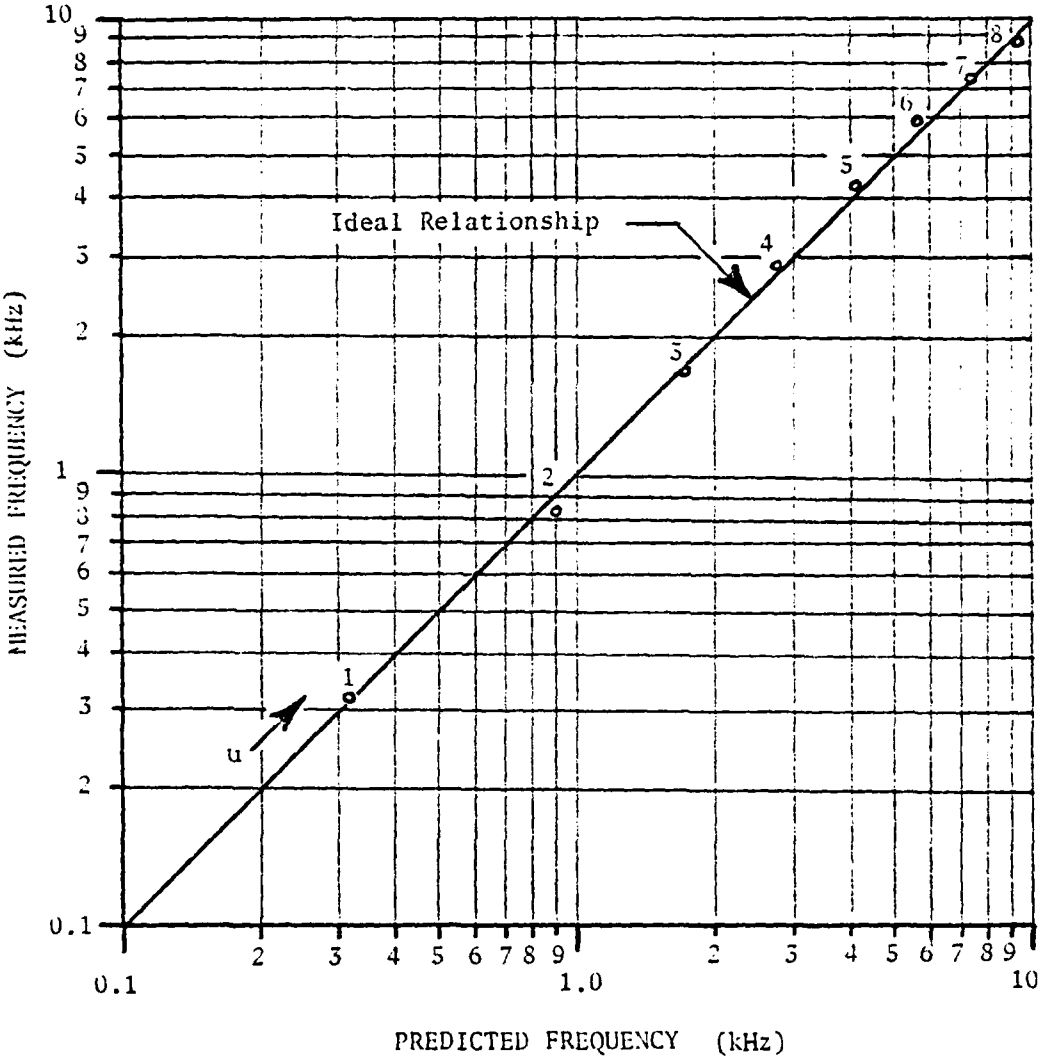

Figure 13 Measured Verses Predicted Ring Resonance Frequencies with Shell Mass Loading.

$$\varepsilon_u = \frac{\partial \omega_u}{\partial u} = 2\beta \frac{\alpha_r^2}{r^2} u = 2\beta \frac{\alpha_r^2}{r^2} \frac{r\sqrt{\omega}}{\alpha_r \sqrt{\beta}} = 2\sqrt{\beta}\, \frac{\alpha_r}{r} \sqrt{\omega} \quad . \qquad (4.10)$$

The mode density of the ring is, therefore, increased by a factor that is proportional to the fourth-root of the added mode mass of the shell.

4.1.3 Shell Density of Resonances

The resonance frequencies of the orthotropic cylindrical shell are given by Equation (3.10). By making the following substitutions:

$$\gamma_1 \simeq \frac{h_r}{\sqrt{12}\, r} \quad , \qquad \gamma_2 = \frac{h_s}{\sqrt{12}\, a} \quad ,$$

$$\alpha_r^2 = \frac{c_E\, h_r}{\sqrt{12}} \quad , \qquad \alpha_s^2 = \frac{c_{p\ell}\, h_s}{\sqrt{12}} \quad ,$$

$$\Omega = \frac{\omega}{\omega_o} \qquad \text{and} \qquad \omega_o = \frac{c_{p\ell}}{a} \simeq \frac{c_E}{r}$$

the shell frequency equation becomes:

$$\omega_{m,n}^2 = \frac{\omega_o^2 \sigma^4}{(n^2 + \sigma^2)^2} + \left(\frac{\alpha_r^2}{r^2} n^2 + \frac{\alpha_s^2}{a^2} \sigma^2 \right)^2 \quad . \qquad (4.11)$$

This is the frequency equation for the orthotropic shell, with the circumferential bending stiffness determined by the stiffness of the ring and the axial bending stiffness determined by that of the shell itself. The membrane term remains essentially unchanged.

Given that Equation (4.11) reduces to $\omega_n = \frac{\alpha_r^2}{r^2} n^2$ for the pure circumferential resonances ($\sigma = 0$) and that the ring resonance frequencies are $\omega_u = \frac{\alpha_r^2}{r^2} u^2 \beta$, one is tempted to assume that the circumferential

bending stiffness term in the shell frequency equation should also be modified by the factor of β. This would assure that the shell's circumferential bending pattern would match that of the rings at the ring resonance frequencies. This boundary condition exists, however, only in the plane of the ring and cannot be applied to the entire shell. The mass loading factor β can be applied to the shell's circumferential stiffness only if the shell is stiffened by consecutive rings closely spaced along the entire shell, or if the shell's response is primarily dictated by circumferential modes which must match the ring resonance frequencies, such as would occur near the circumferential mode cut-off frequencies. These conditions are demonstrated more rigorously in Section 4.2.1, by analysis of the modal coupling between ring and shell.

It was not possible to conclusively verify Equation (4.11) by experimentally measuring the ring-stiffened shell resonance frequencies. The response of the shell is composed of numerous and overlapping resonance maxima which are difficult, if not impossible, to resolve (see Figure 14). Furthermore, it is difficult to identify the mode function associated with a particular resonance maxima. However, since our goal is to estimate the mode density, a more reasonable approach toward verifying Equation (4.11) would be to compare the predicted number of shell resonances within a given frequency interval with the measured number of resonances.

Table I lists the shell resonance frequencies predicted by Equation (4.11). The circumferential resonance frequencies ($\sigma = 0$) do not match the rings and, of course, are not excited. The resonance frequencies in Table I are partitioned according to the ring resonance

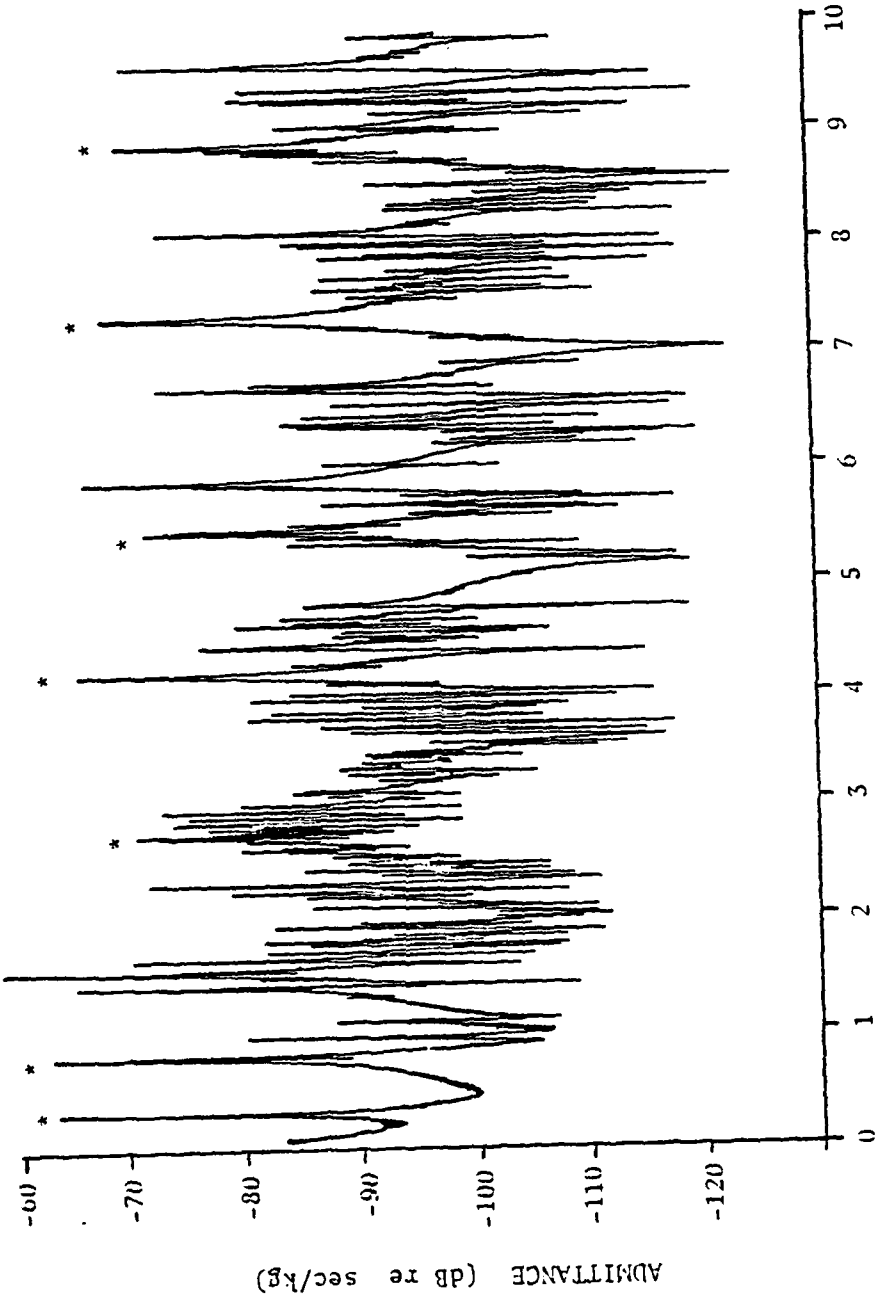

Figure 14 Driving-Point Admittance of Undamped Ring-Stiffened Cylindrical Shell for Driver and Receiver in the Plane of the Ring.

Table I

Predicted Resonance Frequencies (in Hz)
of the Ring-Stiffened Cylindrical Shell
Using Equation (4.11).

σ \ n	0	1	2	3	4	5	6	7
27	9528	9716	10282	11231	12570	14302	16432	18960
26	8892	9079	9642	10586	11920	13648	15774	18300
25	8285	8470	9029	9968	11296	13020	15142	17665
24	7706	7890	8443	9376	10698	12417	14535	17054
23	7157	7338	7886	8812	10126	11839	13953	16469
22	6638	6816	7357	8274	9581	11286	13395	15909
21	6149	6324	6857	7763	9061	10759	12863	15373
20	5691	5863	6385	7280	8567	10257	12355	14861
19	5266	5432	5943	6824	8098	9780	11872	14374
18	4873	5034	5531	6395	7656	9327	11413	13912
17	4513	4668	5148	5994	7239	8899	10978	13475
16	4189	4335	4796	5620	6847	8495	10567	13058
15	3899	4036	4474	5272	6479	8115	10180	12667
14	3644	3770	4182	4951	6136	7758	9815	12299
13	3425	3538	3919	4655	5816	7423	9473	11954
12	3241	3340	3685	4384	5517	7110	9153	11632
11	3089	3172	3478	4135	5239	6817	8854	11332
10	2969	3034	3296	3906	4979	6543	8576	11054
9	2877	2922	3135	3693	4734	6286	8318	10798
8	2808	2832	2991	3493	4502	6045	8079	10565
7	2761	2759	2856	3297	4278	5818	7860	10354
6	2729	2698	2721	3096	4056	5605	7662	10167
5	2710	2638	2568	2875	3834	5408	7486	10007
4	2699	2564	2369	2619	3612	5231	7339	9875
3	2694	2442	2070	2317	3405	5087	7224	9774
2	2692	2167	1585	2002	3247	4988	7146	9704
1	2691	1362	965	1805	3168	4938	7104	9664
0		197	788	1773	3152	4924	7091	9652

frequencies that are marked by an asterisk in Figure 14. As predicted, there are no shell resonances up to the second ring resonance. Between the second and third ring resonance, Equation (4.11) predicts 3 shell resonances; and between the third and fourth ring resonance, 21 shell resonances are predicted. These predictions agree reasonably well with the measured number of shell resonances shown in Figure 14. Above the fourth ring resonance, the measured resonances cannot be resolved because of modal overlap. From this agreement, we can assume that the frequency Equation (4.11) will provide a reasonable estimate of the density of resonances for the ring-stiffened shell.

Using the results of Section 3.1.2 for the orthotropic shell, the frequency spacing between successive resonances (inverse of the density of resonances) may be summarized as follows:

$$\varepsilon_\nu = \frac{\Delta\Omega}{\Delta N}\omega_o = \left\{ \begin{array}{ll} \dfrac{4\alpha_r\alpha_s}{\sqrt{ar}\,\ell} & , \quad \omega >> \omega_o \\ \dfrac{4\sqrt{2}\,\pi\,\alpha_s^2}{a\,\ell\,\ln(2/\gamma_2)} & , \quad \omega \simeq \omega \\ \dfrac{4\sqrt{2}\,\alpha_r^2}{r\,\ell\,\sqrt{\Omega}} & , \quad \omega << \omega_o \end{array} \right\} \quad , \qquad (4.12)$$

where $\omega_o = \dfrac{c_{p\ell}}{a}$ is the radial resonance frequency, α_s is the shell stiffness constant, and α_r is the ring stiffness constant.

4.2 Mean-Value Driving-Point Admittance

The ring-stiffened cylindrical shell may be represented by the general circuit shown in Figure 15. This circuit is a reasonable representation of the mechanical system as long as the velocities at points (1) and (2) are equal in phase and magnitude, or as long as the nondispersive wavelength in the ring is much greater than the thickness of the ring. At very high frequencies the circuit representation must be modified to account for the ring thickness antiresonance.

In Figure 15, Z_r is the impedance of the ring, and Z_s is the impedance of the shell. The impedances must be modified to account for the modal coupling between the ring and shell. The coupling can be described in various degrees of complexity, depending on what features of the vibrational response are considered important.

4.2.1 Hybrid Mode-Sum and Mean-Value Model

Considerable physical insight can be gained by the representation of the ring and shell by their closed system mode-sums, and by considering how these two component systems are coupled to form a new closed system. We can expect that the new system formed by connecting the ring and shell has resonance frequencies that are different than those of the ring and shell alone. The interaction between ring and shell will in general depend on the degree of matching between resonance frequencies, on the degree of similarity of their mode shapes, and on how the damping is distributed between the two components.

The driving-point admittance of the ring and shell may be represented as the parallel combination of the ring modes in series with

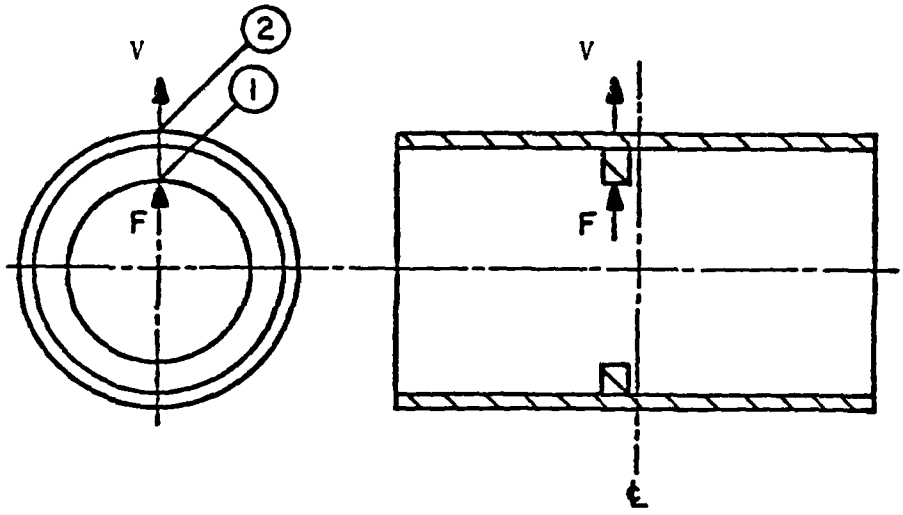

MECHANICAL SYSTEM

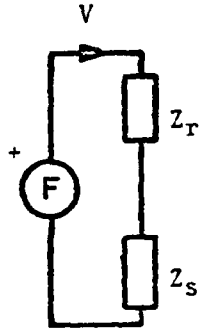

$$Z_T = \frac{F}{V} = Z_r + Z_s$$

CIRCUIT REPRESENTATION

Figure 15 General Series Circuit Representation of Ring-Stiffened Cylindrical Shell for Radial Point Force in the Plane of the Ring.

the parallel combination of shell modes as shown in Figure 16. Here, the driving-point admittance is $Y_o = v/F$, and the mode parameters are defined by:

$$M_u = \frac{M_r}{2} \quad , \qquad M_n = \frac{M_s}{4} \quad , \qquad M_m = \frac{M_s}{4} \quad ,$$

$$C_u = \frac{1}{\omega_u^2 M_u} \quad , \qquad C_n = \frac{1}{\omega_n^2 M_n} \quad , \qquad C_m = \frac{1}{\omega_m^2 M_m} \quad , \tag{4.15}$$

$$R_u = \frac{\omega_u^2}{\omega} \eta_u M_u \quad , \qquad R_n = \frac{\omega_n^2}{\omega} \eta_n M_n \quad , \qquad R_m = \frac{\omega_m^2}{\omega} \eta_m M_m \quad ,$$

where M_r and M_s are the total mass of the ring and shell, respectively, ω_u are the ring resonances, ω_n are the shell's pure circumferential resonances ($\sigma = 0$), and ω_m are the remaining shell resonances ($\sigma \neq 0$).

The circuit representation in Figure 16 is valid only if the ring and shell are attached at a single point; that is, at the driver. However, they are attached along the entire circumference of the ring, and we must modify the mode parameters and the circuit accordingly.

The shell modes in Figure 16 are purposely arranged to illustrate the coupling between the ring and shell. The pure circumferential modes of the shell are shown separate from the remaining shell modes which have some axial component. Because the shell's bending pattern must match the rings bending pattern at the driving point, for every ring mode there is a corresponding shell circumferntial mode. Furthermore, since these corresponding pairs of ring and shell modes have the same bending wavelength, then, $n = u$. The remaining shell modes where $\sigma \neq 0$ represent those modes that will propagate vibrational energy away from the ring.

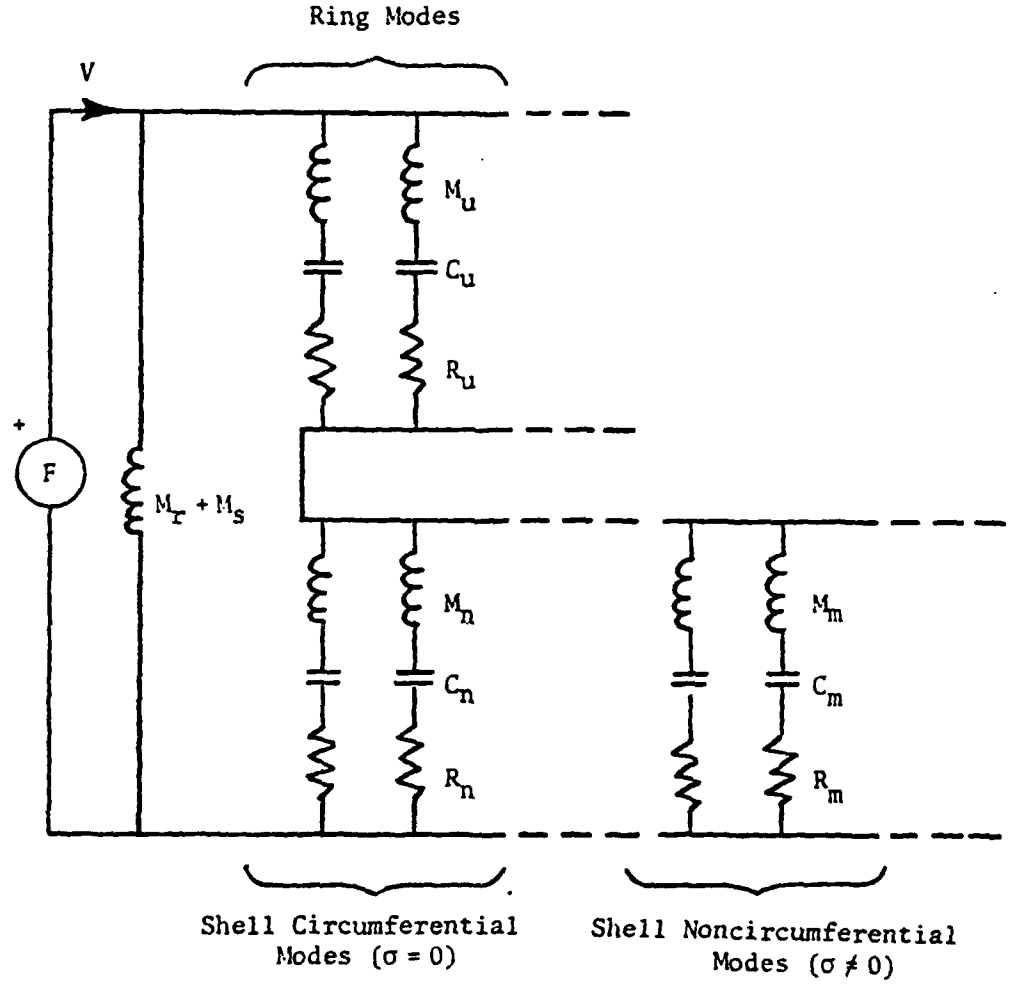

Figure 16 Mode-Sum Representation of Ring and Shell Admittance for Simple Mechanical Connection at the Driving Point.

With the ring and shell attached we can expect the new system to possess resonance frequencies that are different from the ring and shell alone. Consider a single ring mode and a single shell circumferential mode driven at resonance as shown in Figure 17. The resulting simple circuit illustrates how the ring and shell mode parameters combine to form a new mode branch whose resonance frequency is different from either the ring or shell alone. Of particular interest is the effective bending stiffness (or compliance) of the new system:

$$C_{eff} = \frac{1}{\omega_\nu^2 \left(\frac{1}{2} M_r + \frac{1}{4} M_s \right)} = \frac{1}{\omega_u^2 \frac{M_r}{2} + \omega_n^2 \frac{M_s}{4}}$$

$$= \frac{1}{\left(u^2 \frac{\alpha_r^2}{r^2}\right)^2 \frac{M_r}{2} + \left(n^2 \frac{\alpha_s^2}{a^2}\right)^2 \frac{M_s}{4}} \quad . \qquad (4.14)$$

Here, ω_ν is the new circumferential resonance frequency that is created by coupling of the ring and shell. The boundary conditions require that $\nu = u = n$. Or in other words, the modal configuration of both the ring and shell must match the modal configuration of the combined system. The new circumferential resonance frequencies of the combined system are therefore:

$$\omega_\nu^2 \left(\frac{1}{2} M_r + \frac{1}{4} M_s \right) = \nu^4 \left(\frac{\alpha_r^4}{r^4} \frac{M_r}{2} + \frac{\alpha_s^4}{a^4} \frac{M_s}{4} \right) \simeq \nu^4 \frac{\alpha_r^4}{r^4} \frac{M_r}{2}$$

$$\omega_\nu \simeq \nu^2 \frac{\alpha_r^2}{r^2} \left[\frac{\frac{1}{2} M_r}{\frac{1}{2} M_r + \frac{1}{4} M_s} \right]^{\frac{1}{2}} = \nu^2 \frac{\alpha_r^2}{r^2} \beta \quad . \qquad (4.15)$$

This is the same result as presented in Section 4.12. As shown in this section, the resonance frequencies predicted using this equation agree

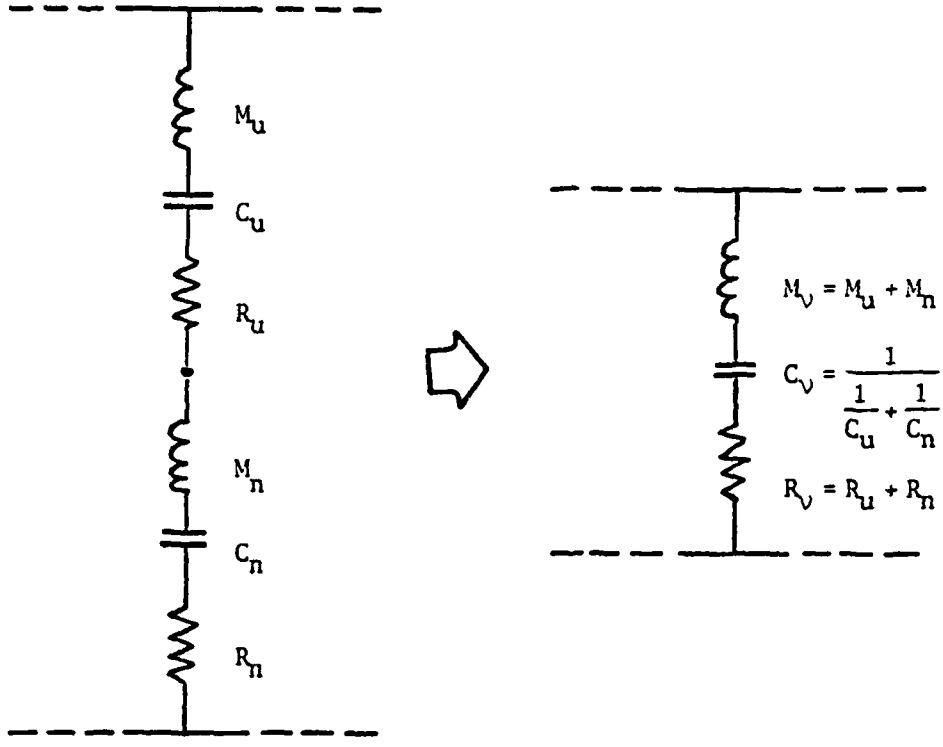

Figure 17 Pair of Ring and Shell Circumferential Modes Driven at Resonance.

well with measured frequencies on a ring-stiffened shell. The approximation in Equation (4.15) is equivalent to neglecting the stiffness of the shell compared to that of the ring. For the shell on which the measurements were performed the ring stiffness term (α_r^4/r^4) is 140 times larger than the shell stiffness term (α_s^4/a^4).

It must be emphasized that the foregoing analysis is only valid for the driver and receiver in the plane of the ring. The shell still possesses resonances that do not match the ring's modal configuration around the circumference. These shell resonances are, however, not effectively excited by the ring, which acts indirectly as a driver. We can detect the shell's own circumferential resonances as the receiver is moved away from the plane of the ring. This is illustrated by Figures 18 and 19. As the receiver is moved away from the ring, weakly excited shell resonances can be observed that are not detected in the plane of the ring. These resonances are simply not excited sufficiently to be observed at the driving-point on the ring. Of particular interest is the frequency region in the vicinity of the second ring resonance (900 Hz). Here, we see that much of the vibrational energy of the second ring resonance (Figure 18) is coupled into other shell resonances (Figure 19) as one moves onto the interior surface of the shell.

This also explains why the mode masses M_n in Figure 17 are equal to $\frac{M_s}{4}$ rather than $\frac{M_s}{2}$ for $\sigma = 0$. The shell cannot be driven at a purely one-demensional vibration unless the ring stiffness term is equal to the shell stiffness term: $\alpha_r/r = \alpha_s/a$. This condition follows from Equation (4.15). For most practical structures, this condition should

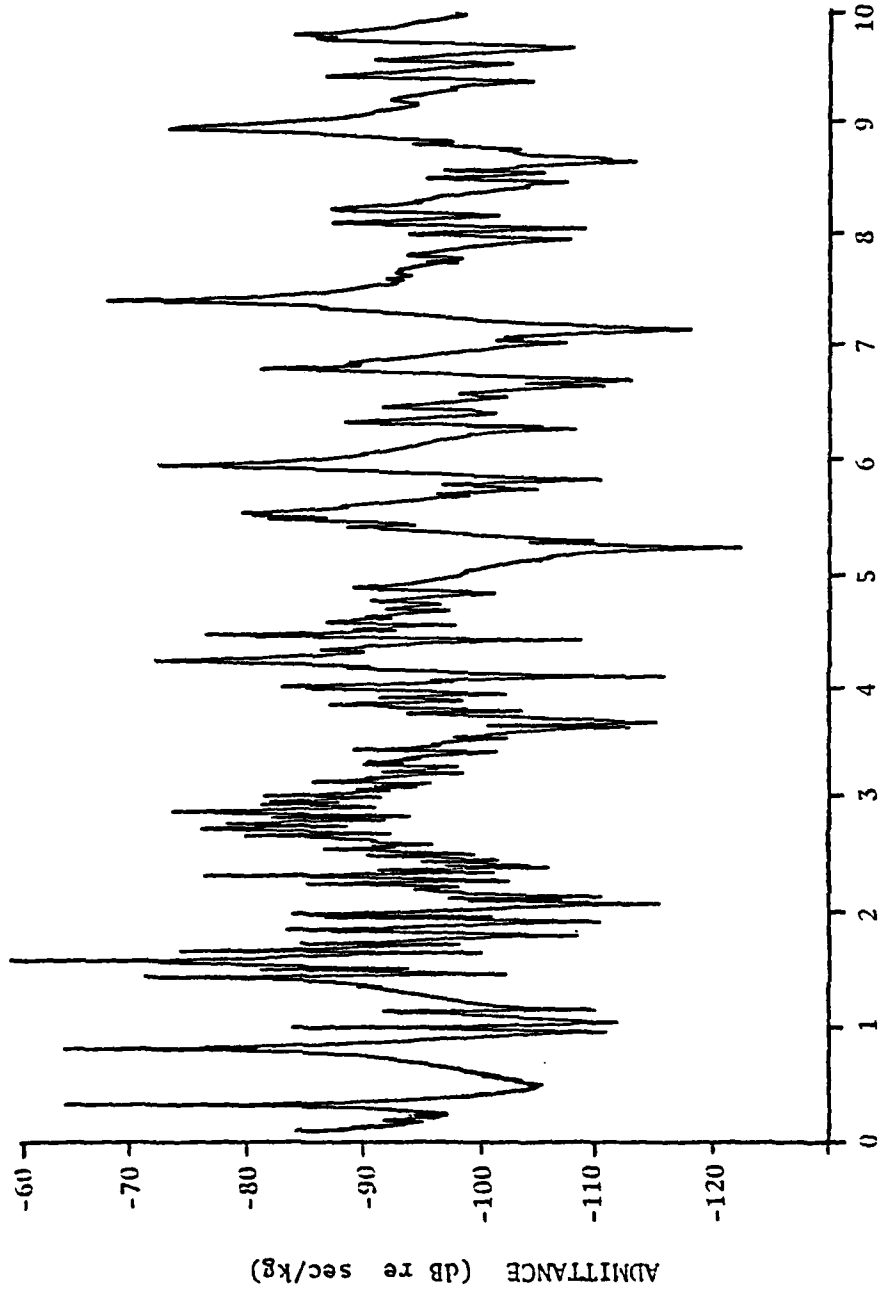

Figure 18 Driving-Point Admittance of Ring-Stiffened Cylindrical Shell, Driver and Receiver in the Plane of the Ring.

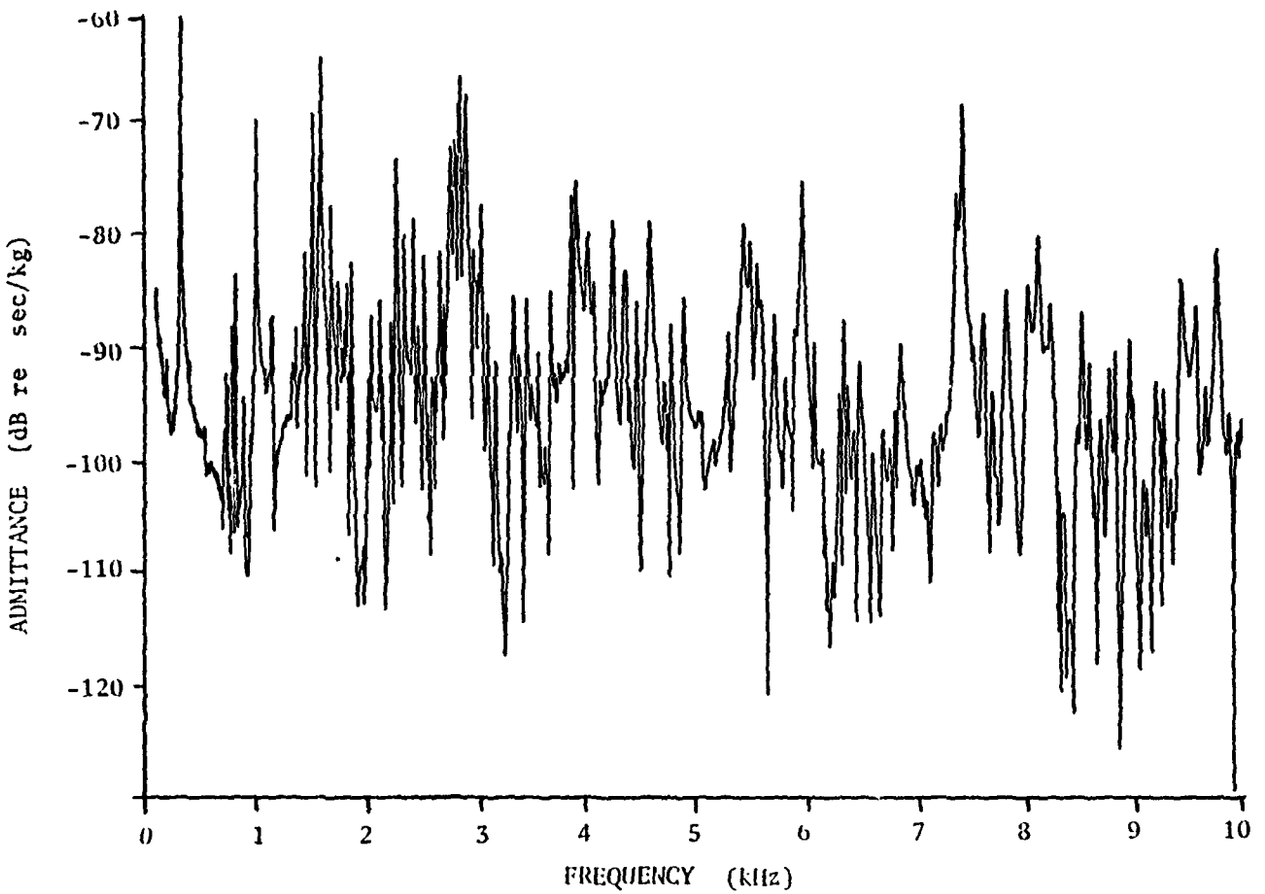

Figure 19 Transfer Admittance of Ring-Stiffened Cylindrical Shell, Driver in the Plane of the Ring and Receiver on the Shell Halfway Between the Plane of the Ring and the Edge of the Shell.

never occur because the ring is usually designed to be much stiffer than the shell.

The shell circumferential modes which match the bending pattern of the ring might be more appropriately named "virtual" modes, since their effects are quantifiable by means of the circuit elements M_n, C_n, and R_n, but their existence is questionable.

In summary, for excitation in the plane of the ring the primary effect of the shell on the ring is to mass load the ring, and the primary effect of the ring on the shell is to stiffen the shell in the circumferential direction. By acting indirectly as a driver, the ring only excites those shell modes that closely match its bending wavelength. All other shell modes will be weakly excited. This phenomenon can be interpreted analytically as an effective increase in the shell's circumferential stiffness, and the general expressions derived in Section 4.1.3 for the orthotropic shell apply.

The hybrid mode-sum, mean-value representation of the ring-stiffened shell is now presented in Figure 20. The driving-point admittance of the new closed system is:

$$Y_o = \frac{1}{j\omega\,(M_s + M_r)} + \sum_{\nu} \frac{1}{Z_r + \dfrac{1}{\dfrac{1}{Z_n} + Y_m}} \quad , \tag{4.16}$$

where:

$$Z_r = R_u + j\omega M_u + \frac{1}{j\omega C_u} = \frac{M_r}{2\omega}\left[\omega_\nu^2 \eta_u + j(\omega^2 - \omega_\nu^2)\right] \tag{4.17}$$

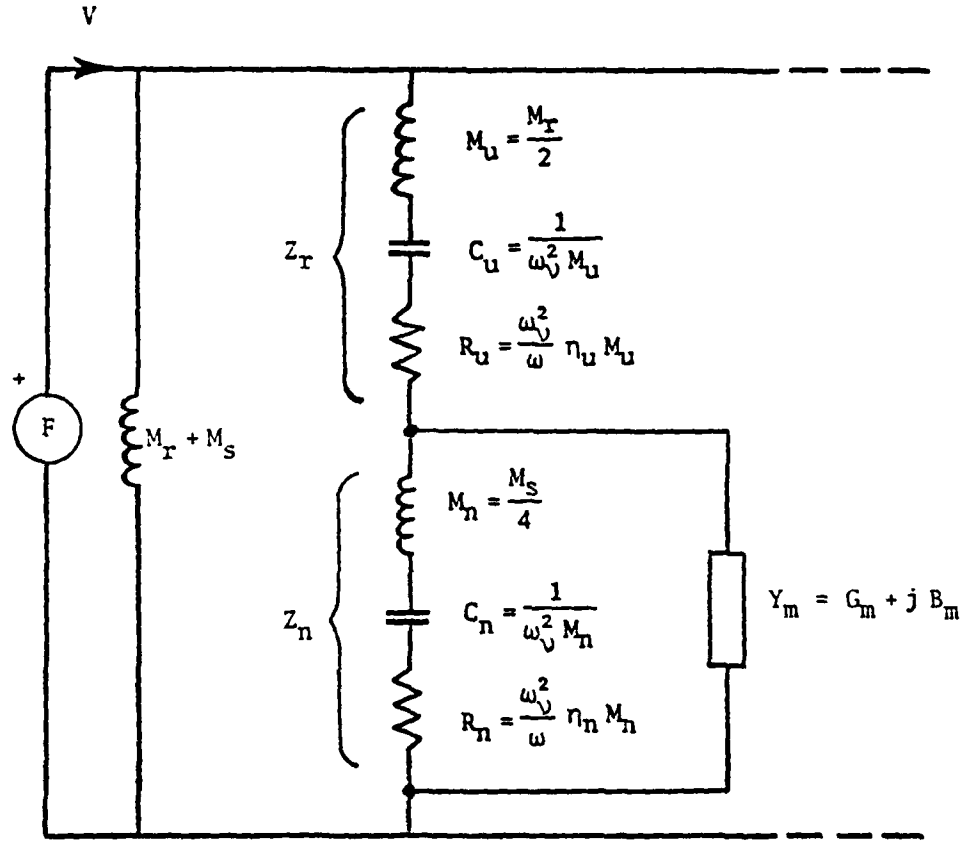

Figure 20 Hybrid Mode-Sum and Mean-Value Model of the Ring-Stiffened Cylindrical Shell for Point Excitation in the Plane of the Ring.

and

$$Z_n = \frac{M_s}{4\omega} [\omega_\nu^2 \eta_n + j(\omega^2 - \omega_\nu^2)] \quad . \tag{4.18}$$

The admittance Y_m is the mean-value admittance of the modes that correspond to a constant circumferential mode number. These axial type modes, along with the virtual circumferential mode represented by Z_n, form a complete mode series for a constant mode number ν.

Figure 20 provides a good picture of the principal loss mechanism at high frequencies. The Y_m can be thought of as a radiation admittance which conducts vibrational energy away from the ring. A detailed knowledge of the ring or shell loss factors is not required as long as the shell is sufficiently large or damped, so that a wave reflected from the shell edges does not significantly contribute to the characteristic wave travelling outward from the driving point.

To compute the value of Y_m we proceed, as before, by driving the density of resonances ε_m (for a constant circumferential mode number) and substituting into the general equation for the mean-value admittance.

Figure 21 illustrates the mode density ($1/\varepsilon_m$) for the experimental ring-stiffened cylindrical shell. This figure was prepared numerically by computing the inverse of the frequency spacing between successive resonances and plotting this against the geometric mean of the resonance frequencies. Equation (4.11) was used for these computations. A closed form solution of these n functions is so complicated that it has no practical use. A more prudent approach is to approximate the desired mode densities within the frequency regions above and below the radial resonance frequency.

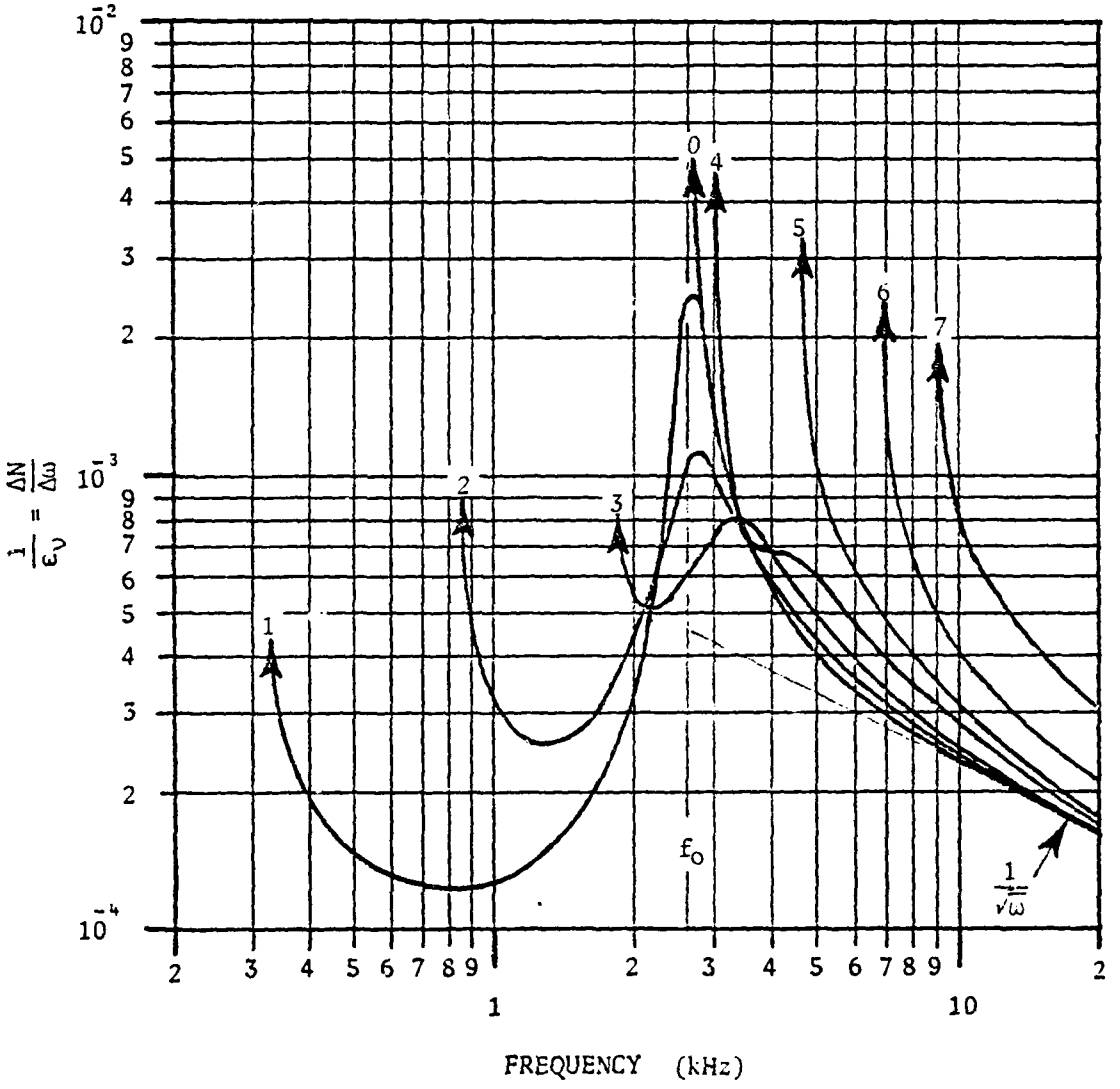

Figure 21 Shell Density of Resonances for Constant Circumferential Mode Number, n , (Curves Were Computed Numerically).

At high frequencies ($\omega > \omega_o$) the shell frequency equation and frequency spacing between resonances can be approximated by:

$$\omega_m \simeq \frac{\alpha_r^2}{r^2} n^2 + \frac{\alpha_s^2}{a^2}\sigma^2 = \omega_n + \frac{\alpha_s^2}{a^2}\sigma^2$$

and

$$\varepsilon_m = \frac{\partial \omega_m}{\partial \sigma} = 2\frac{\alpha_s^2}{a^2}\sigma = 2\frac{\alpha_s}{a}\sqrt{\omega - \omega_n} \quad . \tag{4.19}$$

This approximation is very good for $n \geq 4$. For small values of n the high frequency approximation can be improved by:

$$\omega_m^2 \simeq \omega_o^2 + \left(\frac{\alpha_s^2}{a^2}\sigma^2\right)^2$$

and

$$\varepsilon_m = 2\frac{\alpha_s^2}{a^2}\sigma = 2\frac{\alpha_s}{a}\sqrt[4]{\omega^2 - \omega_o^2} \quad . \tag{4.20}$$

This approximation is very good for $n < 4$. At low frequencies ($\omega < \omega_o$) the shell frequency equation can be approximated by:

$$\omega_m^2 = \left[\frac{\omega_o \sigma^2}{n^2 + \sigma^2}\right]^2 + \omega_n^2$$

which leads to:

$$\varepsilon_m = \frac{2}{n\,\omega\,\omega_o}\left[\mu(\omega_o - \mu)\right]^{3/2} \quad , \tag{4.21}$$

where $\mu^2 = \omega^2 - \omega_n^2$. These approximations are plotted in Figure 22 for the frequency regions in which they apply. The approximate mode densities in Figure 22 show good agreement with the numerically computed mode densities in Figure 21. Note that the mode density for each n approaches infinity at the cut-off frequency, $\omega_n \simeq \omega_v/\beta$. Below the cut-off frequency, the mode density is approximately zero.

Given the foregoing approximations, the mean-value admittance of the shell for a constant circumferential mode number, n, is:

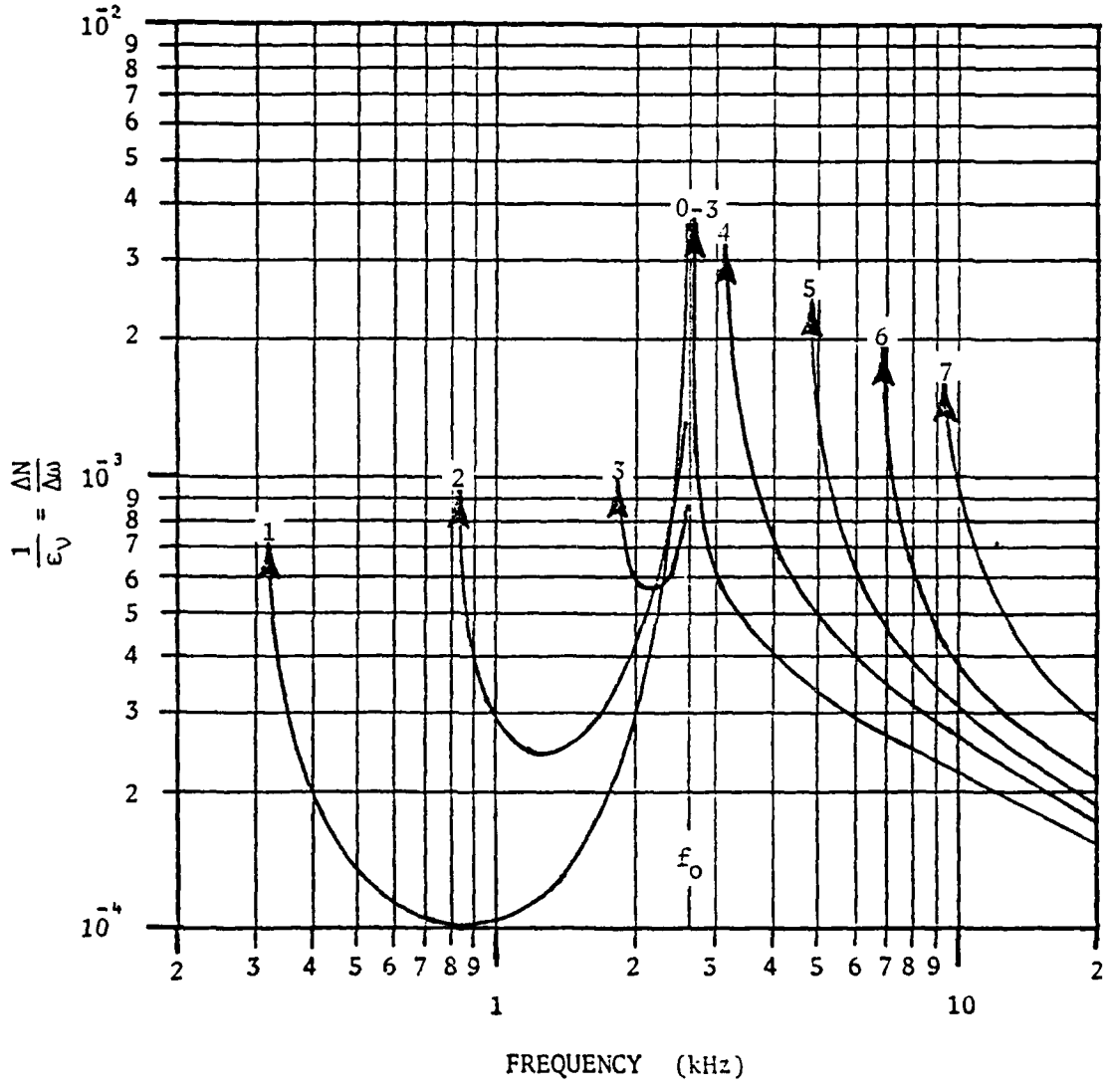

Figure 22 Approximation of Shell Density of Resonances for Constant Circumferential Mode Number, n .

$$Y_m = G_m + j B_m = \frac{\pi}{2(2\varepsilon_m)\,\frac{1}{4}M_s} + j B_m \quad . \qquad (4.22)$$

Above ω_o the mode density is inversely proportional to $\sqrt{\omega}$ as, for example, a beam. Thus, the imaginary part is a mass reactance and is equal in magnitude to the real part: $B_m = -G_m$. Below ω_o the slope of the mode density varies widely, and B_m is not a simple function. Due to the symmetry of the curves, B_m is approximately zero if averaged over the entire low frequency region. Any approximation is, however, acceptable at low frequencies since the imaginary part of the shell impedance is negligible compared to that of the ring impedance.

Below ω_o we are stretching the usefulness of the mean-value theory. The frequency spacing between resonances is so great that the details of individual resonances emerge. In fact, the increase in mode density in the vicinity of the ring resonance frequencies can be interpreted as a resonance rise. By equating the n_{th} mode impedance in Equation (4.18) to the mean-value impedance [inverse of Equation (4.22)], we can compute an equivalent $(\frac{1}{\varepsilon})$ for the single circumferential mode. The $(\frac{1}{\varepsilon})$ for the first three circumferential modes ($\sigma = 0$) are shown superimposed on the mode density for a constant mode number, n, in Figure 23.

In the circuit representation of Figure 20, the circumferential modes are included separately, and we must therefore terminate the axial density of resonances at the $\sigma = 1$ mode as shown in Figure 23. Below this first axial resonance, $\frac{1}{\varepsilon_m}$ is zero and the impedance of the axial branch approaches infinity, thus, leaving only the impedance of the circumferential branch.

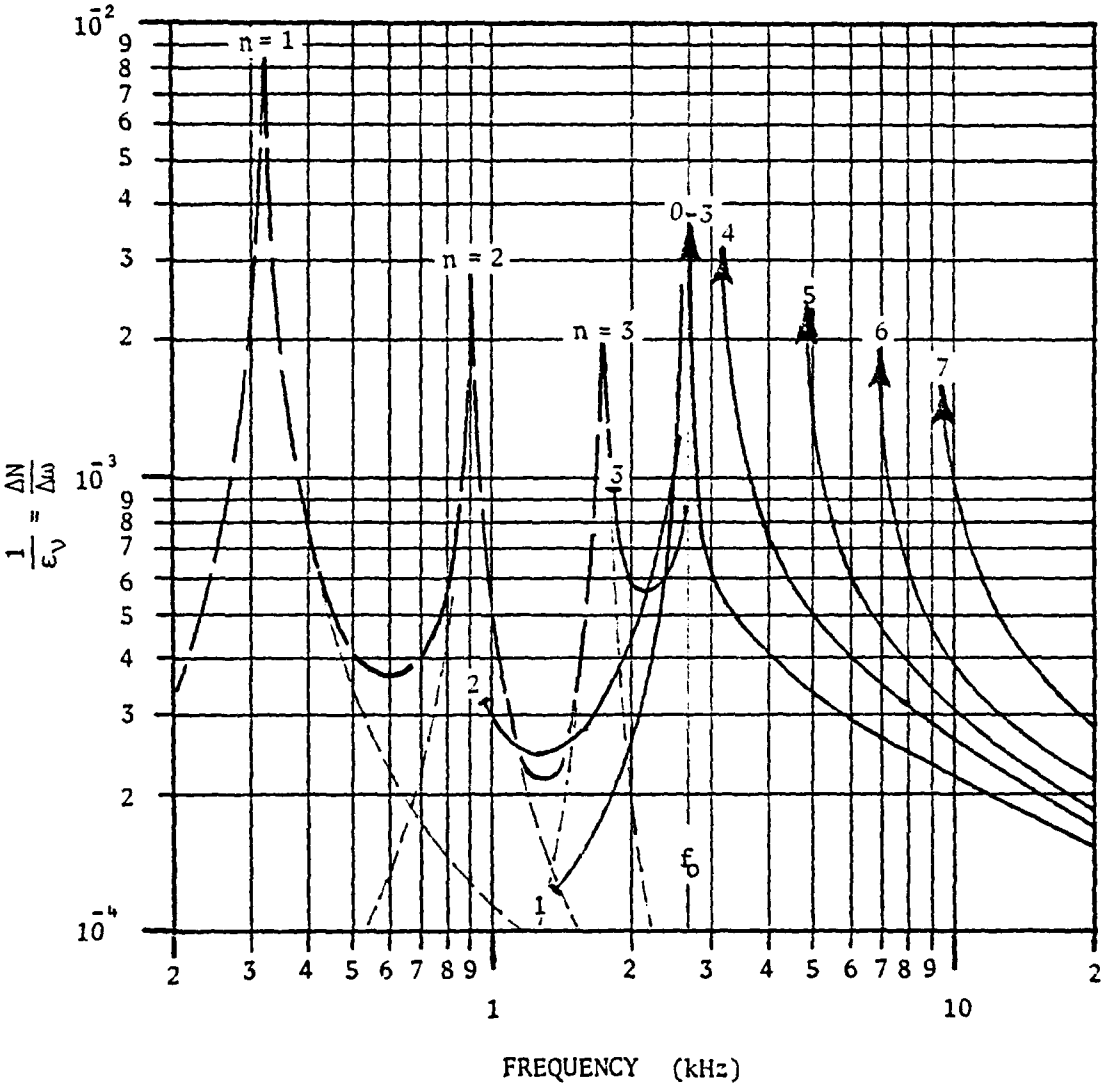

Figure 23 Equivalent Mode Density of the First Three Circumferential Modes (n = 1,2 and 3) Superimposed on the Shell Density of Resonances for a Constant Circumferential Mode Number, n , (Mode Densities $1/\varepsilon_m$ are cut-off at $\sigma = 1$).

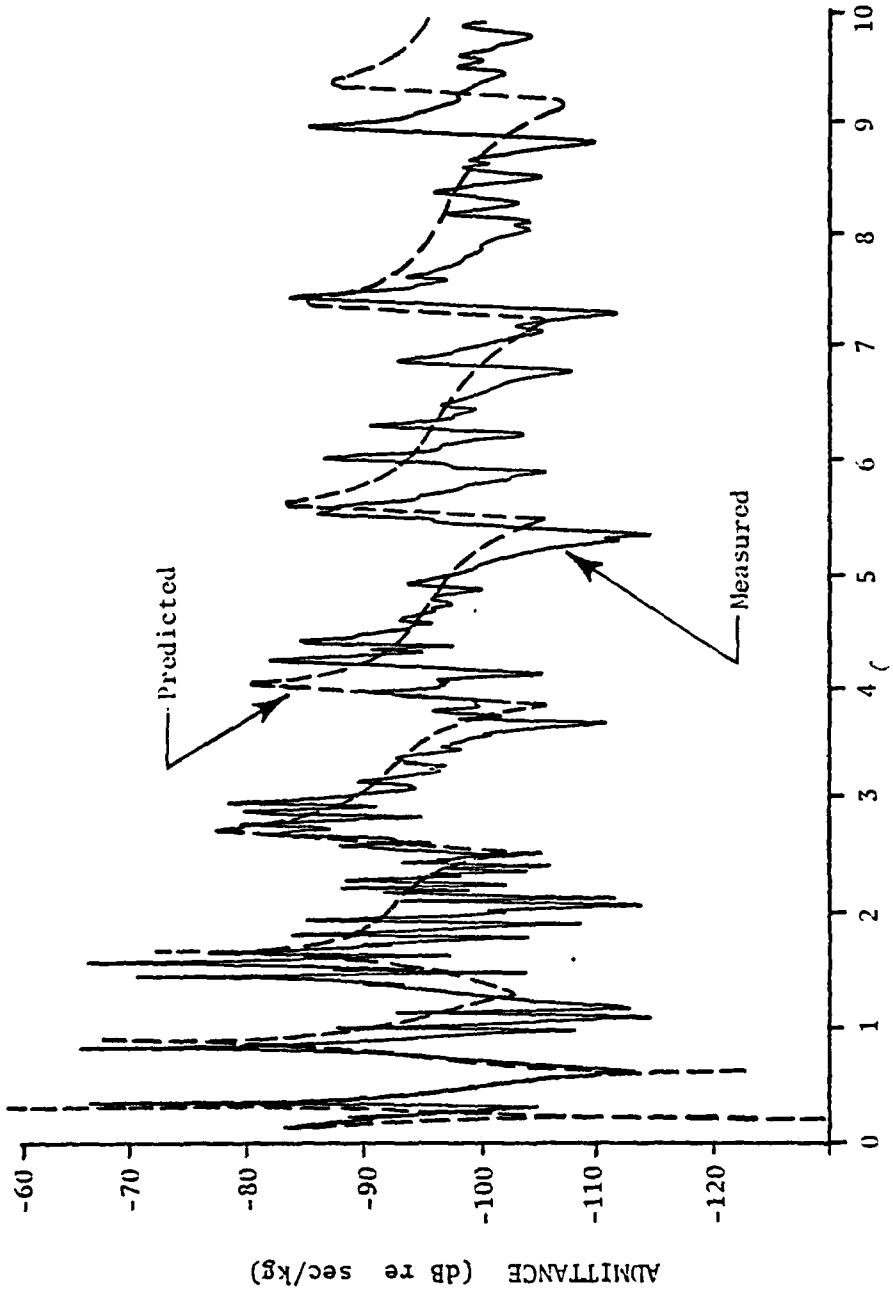

Figure 24 Hybrid Mode-Sum and Mean-Value Prediction, and Measured Driving-Point Admittance of Ring-Stiffened Cylindrical Shell.

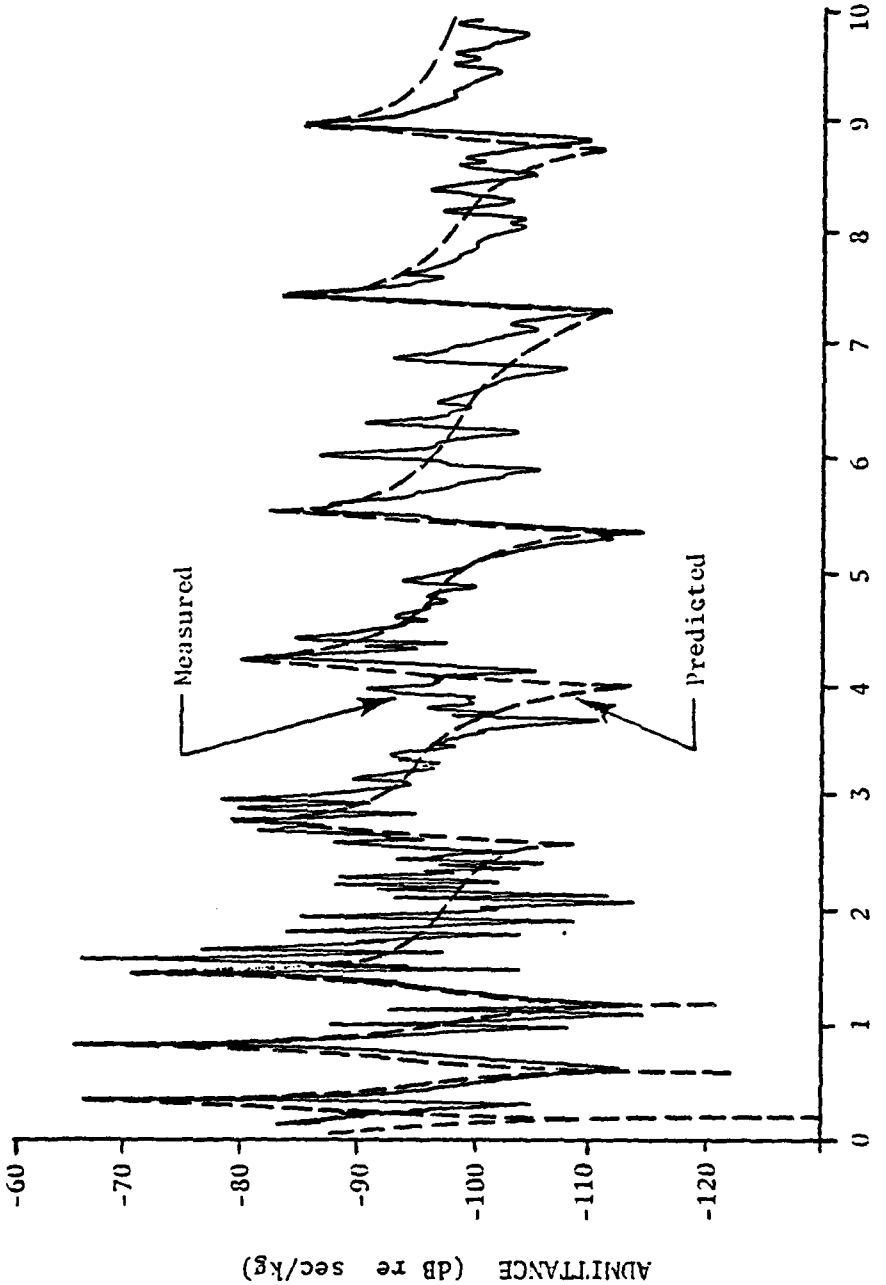

Figure 25 Hybrid Mode-Sum and Mean-Value Admittance Prediction Using the Measured Ring Resonance Frequencies and Loss Factors Compared with Measured Driving-Point Admittance of Ring-Stiffened Cylindrical Shell.

We can assume that most losses will occur in the shell; thus we let $\eta_u \simeq 0$. The shell circumferential loss factor, η_n, is assumed to be about 0.02. These crude approximations are adequate for our purpose, since we are concerned with the predicted mean-value response rather than the resonance peaks.

The mean-value driving-point admittance, predicted using the model in Figure 20, is presented along with the measured admittance in Figure 24. As shown in this figure, the hybrid mode-sum model is an excellent means of predicting the important details of the response curve. Figure 25 shows the driving-point admittance calculated using the measured ring resonance frequencies and loss factors. This figure clearly demonstrates the validity of the circuit representation of Figure 20.

By modeling the $\sigma \neq 0$ modes by their mean-value admittance and the $\sigma = 0$ modes by their individual admittances, the mode-sum computations are greatly simplified. There are only eight ring resonances within 0 - 10 kHz, and the summation need only be carried up to $\nu = 10$ for accurate results. In fact, because the ring resonances are well separated, excellent results can be obtained by combining the contributions of only the two closest modes.

4.2.2 Series Mean-Value Model

Returning to the general circuit illustrated in Figure 15, we see that the impedance of the ring-stiffened cylindrical shell, Z_T, may simply be represented as the mean value of the ring impedance, Z_r, in series with the mean value of the shell impedance, Z_s. The ring and shell impedances must, however, be modified to account for the modal coupling between ring and shell.

The primary effect of the shell on the ring is to mass load the ring, thereby shifting the ring resonance frequencies down by a factor of $\hat{\varepsilon}$ that is proportional to the square root of the added mode mass of the shell. The spacing between resonances is, therefore, modified by a factor of $\sqrt{\beta}$, and the ring impedance becomes:

$$Z_r = \frac{1}{\frac{\pi}{2\,\varepsilon_v M_v}(1-j)} = \frac{2\sqrt{\beta}}{\pi}\frac{\alpha_r}{r}\sqrt{\omega}\,M_r\,\frac{(1-j)}{2}$$

$$= 2\sqrt{\beta}\,m_r\,\alpha_r\sqrt{\omega}\,(1+j) \quad . \tag{4.23}$$

where m_r is the mass per unit circumferential length of the ring.

The primary effect of the ring on the shell is to stiffen the shell in the circumferential direction. By substituting the ring's bending stiffness for the shell's circumferential bending stiffness in the shell frequency equation, it has been shown that the spacing between resonance frequencies may be approximated by Equation (4.12). At high frequencies ($\omega > \omega_o$) the shell impedance then becomes:

$$Z_s = \frac{2(2\varepsilon_v)M_v}{\pi} = \frac{4\,\alpha_r\,\alpha_s\,M_s}{\pi\sqrt{ar}\,\ell}$$

$$= 8\sqrt{a/r}\,m_s\,\alpha_s\,\alpha_r \quad . \tag{4.24}$$

For most structures the ratio of a/r is approximately equal to 1. The high frequency shell impedance is the same as that of a plate whose bending stiffness constant is equivalent to the geometric mean of the ring and shell stiffness $\sqrt{\alpha_s\alpha_r}$. At low frequencies ($\omega < \omega_o$) the shell impedance becomes:

$$Z_s = \frac{1}{\frac{\pi}{2(2\varepsilon_\nu)\,\frac{1}{4}M_\nu}(1+j)} = \frac{4\sqrt{2}}{\pi}\frac{\alpha_r^2}{r\ell}\sqrt{\omega_o/\omega}\,M_s\frac{(1-j)}{2}$$

$$= 4\sqrt{2}\,(a/r)\,m_s\,\alpha_r^2\sqrt{\omega_o/\omega}\,(1-j) \quad . \qquad (4.25)$$

The low frequency shell impedance is primarily dictated by the ring-stiffened modes.

It should be noted that Equation (4.25) will become less accurate at very low frequencies, where the shell response is dominated by the virtual circumferential modes, whose mode masses are $\frac{M_s}{4}$, and whose resonance frequencies are the same as that of the ring: $\omega_\nu = \frac{\alpha_r^2}{r^2}\nu^2\beta$. These shell modes are shifted downward by the factor of β, which would make the shell impedance appear softer than predicted by Equation (4.25).

Combining the complex impedances in the proper manner, produces the expression for the mean-value driving-point admittance in the plane of the ring:

$$Y_T = \frac{1}{Z_T} = \frac{1}{Z_r + Z_s} \quad . \qquad (4.26)$$

Figure 26 presents the predicted mean value and the measured driving-point admittance of the ring-stiffened steel cylinder. The shell was heavily damped for this measurement. The agreement between the predictions and measurements is good, except for the very low frequencies.

The mean-value predictions can be improved at the very low frequencies by using the modified circuit representation illustrated in

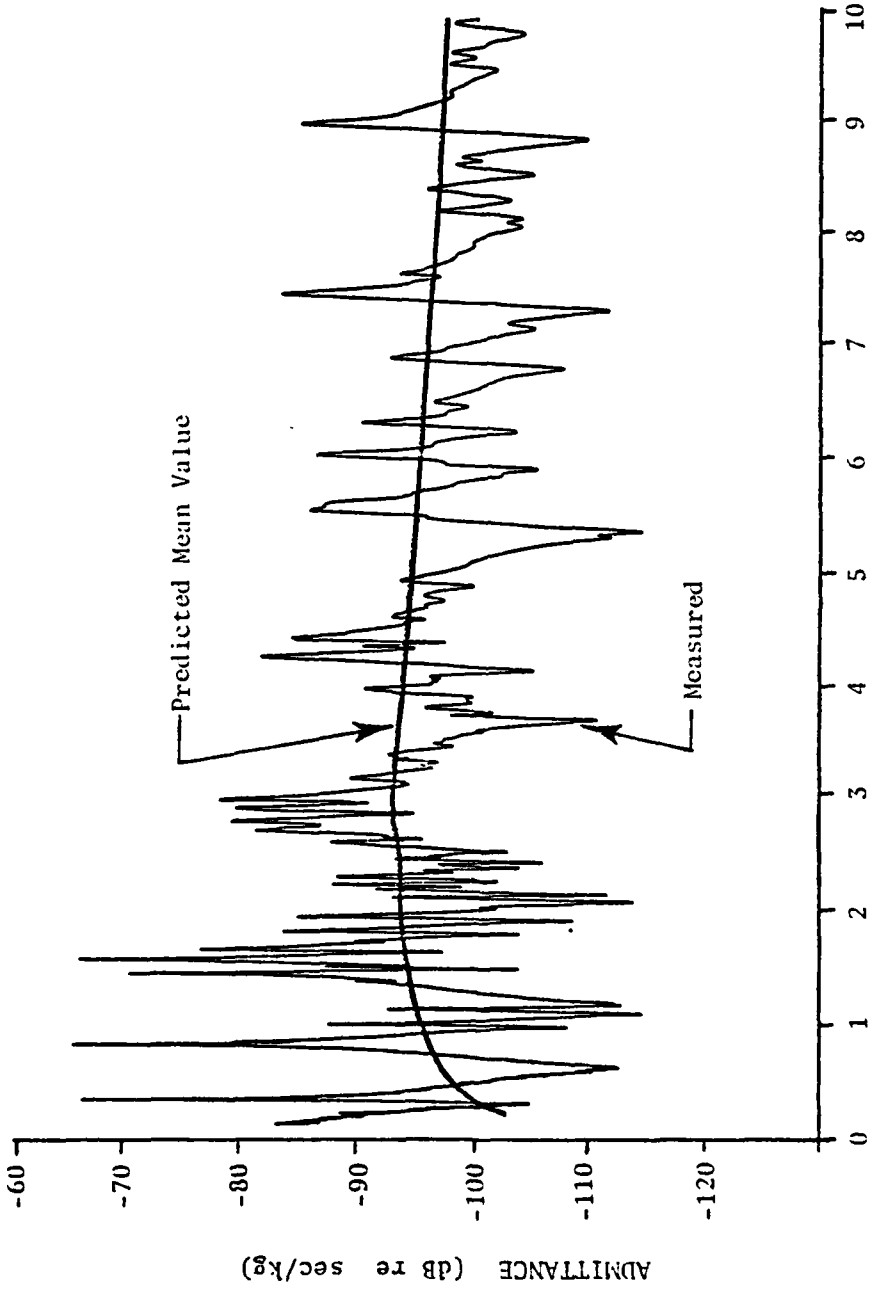

Figure 26 Series Mean-Value Prediction and Measured Driving-Point Admittance of Ring-Stiffened Cylindrical Shell.

Figure 27. To more accurately represent the low frequency ring-shell coupling, the shell impedance is represented by the parallel combination of the mean value of the circumferential mode impedances, Z_n, and the mean value of the noncircumferential mode impedances, Z_m.

Because the shell's bending pattern must match the ring's bending pattern at the driving point, for every ring mode there is a virtual shell circumferential mode. The impedance Z_n is, therefore, the mean value of the mode impedances whose mode masses are $\frac{M_s}{4}$ and whose frequency spacing is the same as that of the ring:

$$Z_n = \frac{1}{\frac{\pi}{2\varepsilon_v \frac{1}{4} M_s}(1+j)} = \frac{\sqrt{\beta}}{\pi}\frac{\alpha_r}{r}\sqrt{\omega}\, M_s \frac{(1+j)}{2}$$

$$= \sqrt{\beta}\,(a/r)\, m_s' \alpha_r \sqrt{\omega}\,(1+j) \quad . \qquad (4.27)$$

Here, m_s' is the mass per unit circumferential length of the shell.

The impedance of the noncircumferential modes, Z_m, may be approximated by Equations (4.24) and (4.25). By using these equations, we are assuming that there are many more noncircumferential modes ($\sigma \neq 0$) than there are circumferential modes ($\sigma = 0$). Thus, we can remove the $\sigma = 0$ modes to form Z_n without significantly changing Z_m. This approximation is valid except at very low frequencies. However, Z_m is large compared to Z_n at very low frequencies and can be neglected. The error in using Equations (4.24) and (4.25) for the impedance Z_m is, therefore, negligible.

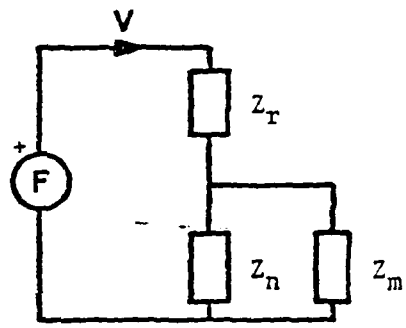

$$Z_T = Z_r + \frac{Z_n Z_m}{Z_n + Z_m}$$

Figure 27 Modified Series Circuit Representation of the Ring-Stiffened Cylindrical Shell for Radial Point Force in the Plane of the Ring.

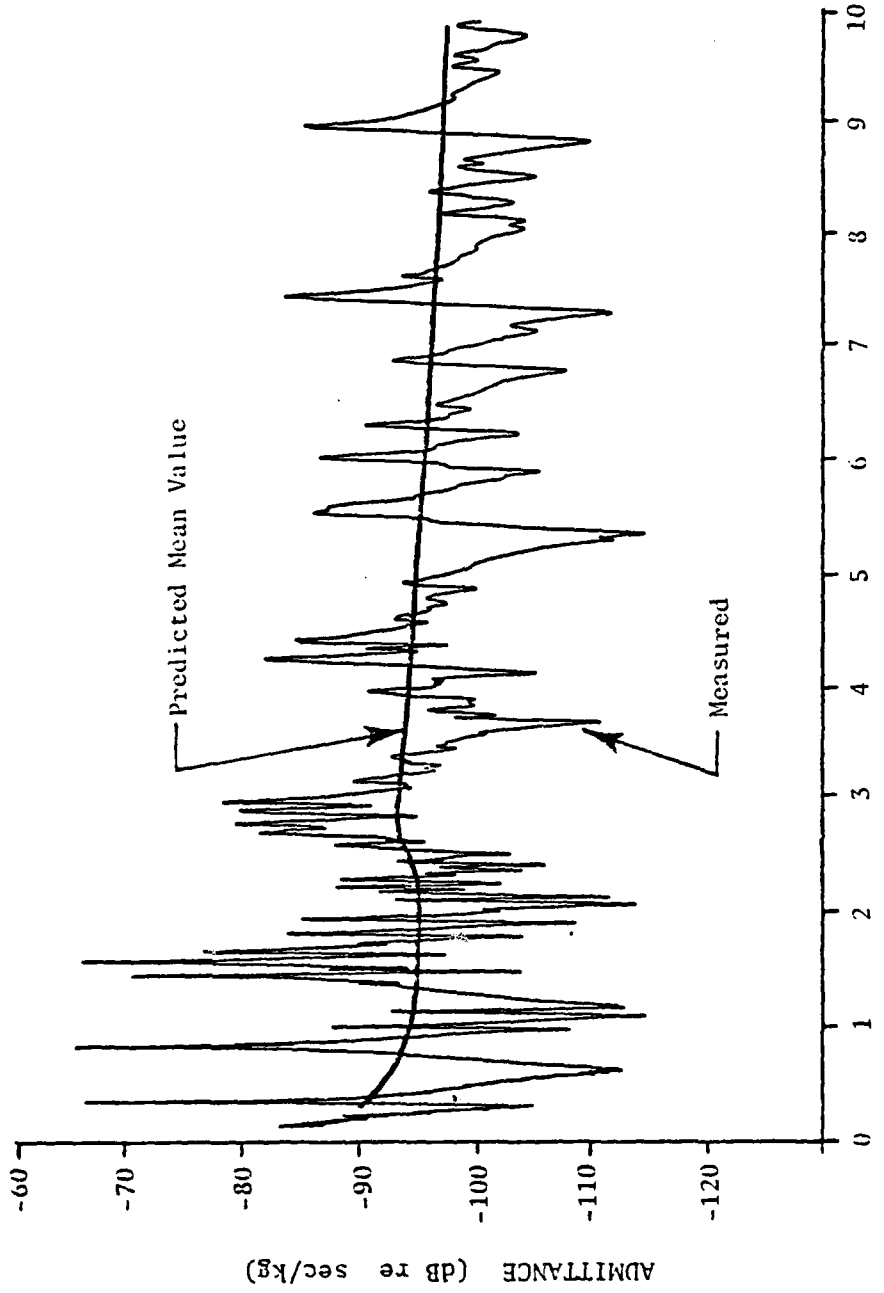

Figure 23 Modified Series Mean-Value Prediction and Measured Driving-Point Admittance of Ring-Stiffened Cylindrical Shell.

AD-A082 524 PENNSYLVANIA STATE UNIV UNIVERSITY PARK APPLIED RESE--ETC F/G 20/11
VIBRATION OF CYLINDRICAL SHELLS, WITH AND WITHOUT RING STIFFENI--ETC(U)
JAN 80 E C EICHELBERGER N00024-79-C-6043
UNCLASSIFIED ARL/PSU/TM-80-03 NL

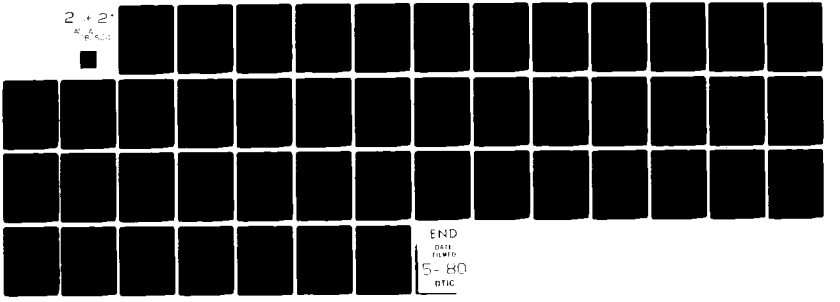

Combining the complex impedances in the proper manner produces the expression for the mean-value driving-point admittance in the plane of the ring:

$$Y_T = \frac{1}{Z_r + \frac{Z_n Z_m}{Z_n + Z_m}} \quad . \tag{4.28}$$

Figure 28 presents the predicted mean-value admittance computed using Equation (4.28) and the measured admittance of the ring-stiffened steel cylinder. The agreement between theory and measurements is good. The predicted mean value in Figure 28 is softer than the predicted mean value in Figure 26 at very low frequencies, and agrees better with the measurements.

4.2.3 High and Low Frequency Mean-Value Models

If one is interested in either the very high or very low frequency regions relative to the radial resonance frequency, the ring-stiffened cylindrical shell can be represented by very simple analytical models.

At low frequencies the response of the ring-stiffened shell is principally that of the ring with shell mass loading as shown in Figure 29. The resonance frequencies are the circumferential resonance frequencies of the combined ring-shell system as defined by Equation (4.15) and illustrated in Figure 17. If the ring is much stiffer than the shell:

$$\omega_\nu = \nu^2 \frac{\alpha_r^2}{r^2} \beta \quad , \tag{4.29}$$

and the frequency spacing between resonances is:

$$\epsilon_\nu = 2\sqrt{\beta} \frac{\alpha_r}{r} \sqrt{\omega} \quad . \tag{4.30}$$

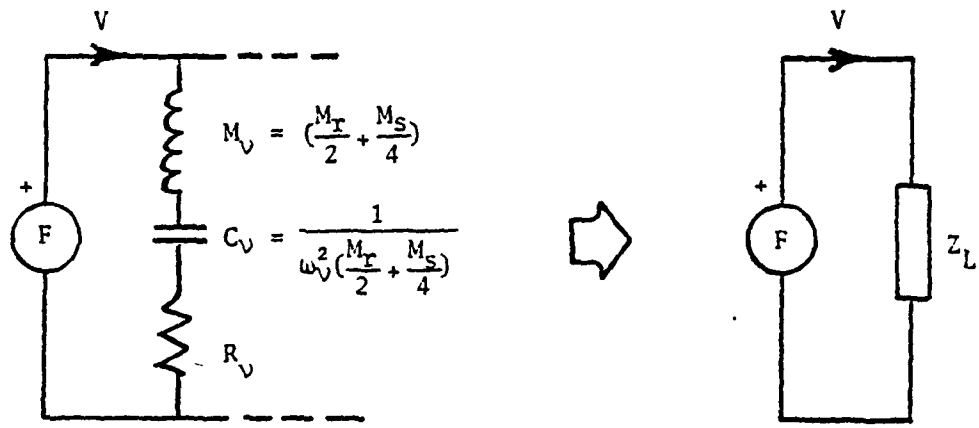

Figure 29. Low Frequency Circuit Representation of the Ring-Stiffened Cylindrical Shell for Radial Point Force in the Plane of the Ring.

The low frequency impedance is, therefore:

$$Z_L = \frac{1}{\frac{\pi}{2\,\varepsilon_\nu\,(\frac{M_r}{2} + \frac{M_s}{4})}\,(1 - j)} = \frac{\sqrt{\beta}}{2\pi}\,\frac{\alpha_r}{r}\,(2\,M_r + M_s)\,\sqrt{\omega}\,(1 + j)$$

$$= 2\sqrt{\beta}\,(m_r + \frac{a}{2r}\,m_s')\,\alpha_r\,\sqrt{\omega}\,(1 + j)$$

$$\simeq 2\sqrt{\beta}\,(m_r + \tfrac{1}{2}\,m_s')\,\alpha_r\,\sqrt{\omega}\,(1 + j) \quad . \qquad (4.31)$$

This is the same as the ring impedance, except for the factor of $\sqrt{\beta}$ and the added mass loading of the shell, which is approximately equal to half the shell mass per unit axial length.

At high frequencies, the ring-stiffened shell impedance is represented by the series mean-value model as presented in Section 4.2.2. The high frequency impedance is:

$$Z_H = Z_r + Z_s$$

$$\simeq 2\sqrt{\beta}\,m_r\,\alpha_r\,\sqrt{\omega}\,(1 + j) + 8\,m_s\,\alpha_s\,\alpha_r$$

$$= (8\,m_s\,\alpha_r\,\alpha_s + 2\sqrt{\beta}\,m_r\,\alpha_r.\sqrt{\omega}) + j(2\sqrt{\beta}\,m_r\,\alpha_r\,\sqrt{\omega}) \quad . \qquad (4.32)$$

Figure 30 presents the mean-value admittance using the high and low frequency models, and the measured driving-point admittance of the ring-stiffened shell. Despite the simplicity of these models, they provide a good estimate of the mean-value admittance. If the transition at the radial resonance frequency is smoothed, the resulting prediction would show very good agreement with the measurements. For most engineering applications, the high and low frequency models are all that are required for predicting the response of the ring-stiffened shell.

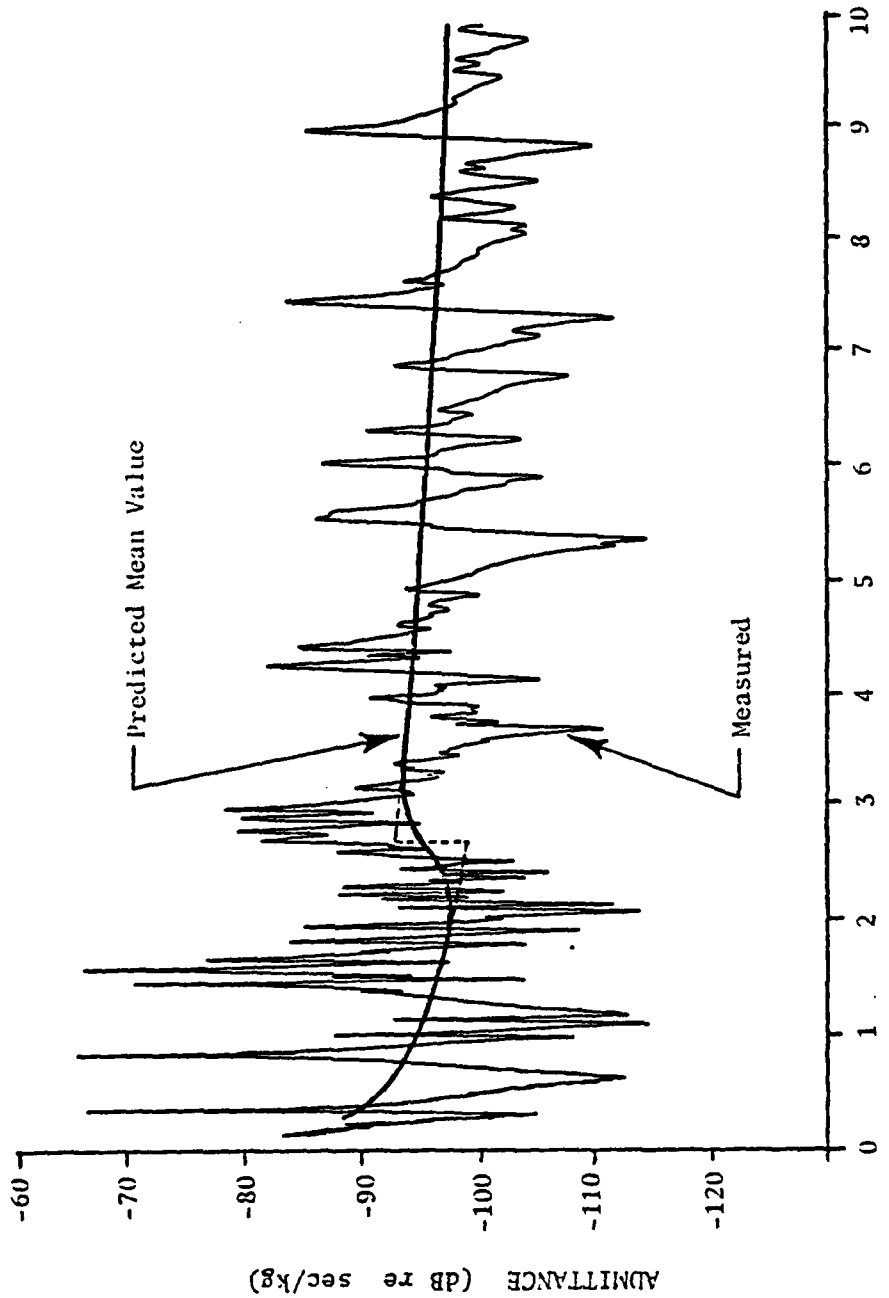

Figure 30 High and Low Frequency Mean-Valued Predictions and Measured Driving-Point Admittance of Ring-Stiffened Cylindrical Shell.

4.2.4 Ring Thickness Antiresonance Model

For thick rings, the high frequency model must be modified, as shown in Figure 31, to include the effect of the propagation of longitudinal nondispersive waves across the thickness of the ring. With the driver mounted on the inside of the ring, the velocity on the outside of the shell in-line with the driver is not equal to the velocity at the driven point. This phenomenon was observed during the experimental investigations, and is shown in Figure 32. At very high frequencies (10 kHz) the magnitude of the velocity on the shell is approximately 2½ dB higher than at the driving point. This slight rise is due to the first resonance (or more correctly, antiresonance) across the thickness of the ring.

The propatation of a nondispersive wave across the ring thickness can be modeled by a transmission line (or rod) of length h_r as shown in Figure 31 [11,14]. Here, the impedances are:

$$Z_1 = j Z_c \tan \frac{kh_r}{2} \tag{4.33}$$

and

$$Z_2 = -j \frac{Z_c}{\sin kh_r} \quad , \tag{4.34}$$

where the wavenumber, $k = \omega/c_{p\ell}$, and the characteristic impedance (of a nondispersive wave), $Z_c = \rho c_{p\ell} S$. The ring material may be considered infinite in one dimension; thus the velocity of sound is:

$$c_{p\ell} = \sqrt{E'/\rho} \quad . \tag{4.35}$$

As a crude approximation, the cross sectional area S may be taken as the square of the width of the ring, and the characteristic impedance is then:

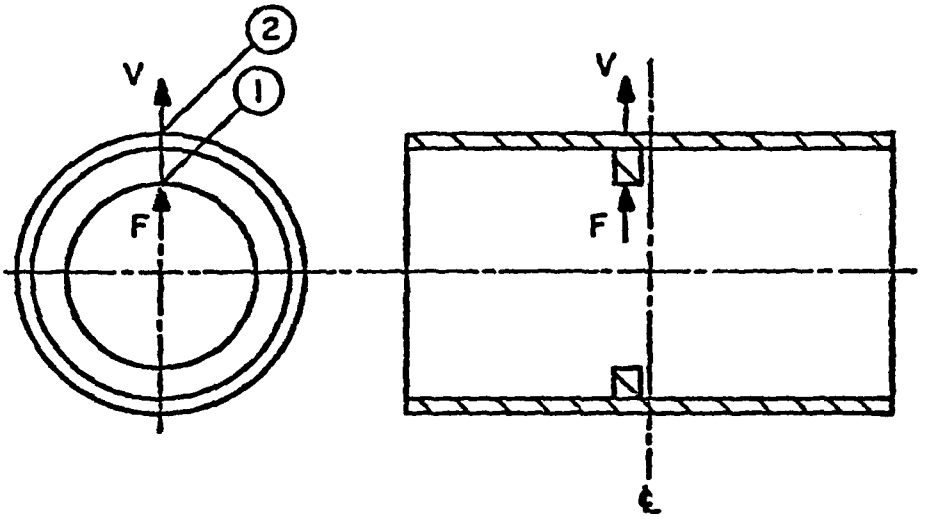

MECHANICAL SYSTEM

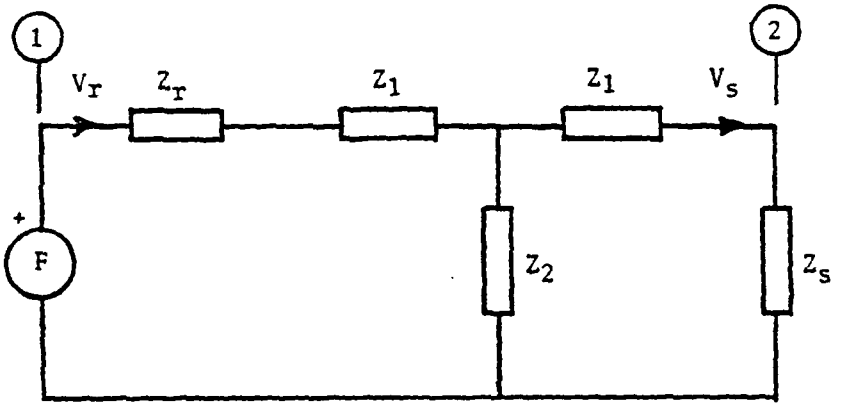

$$Z_T = \frac{V_r}{F} = (Z_r + Z_1) + \frac{Z_2 (Z_1 + Z_s)}{Z_2 + Z_1 + Z_s}$$

CIRCUIT REPRESENTATION

Figure 31 Circuit Representation of Ring-Stiffened Cylindrical Shell, Modified to Include the Effect of Nondispersive Waves Across the Ring Thickness.

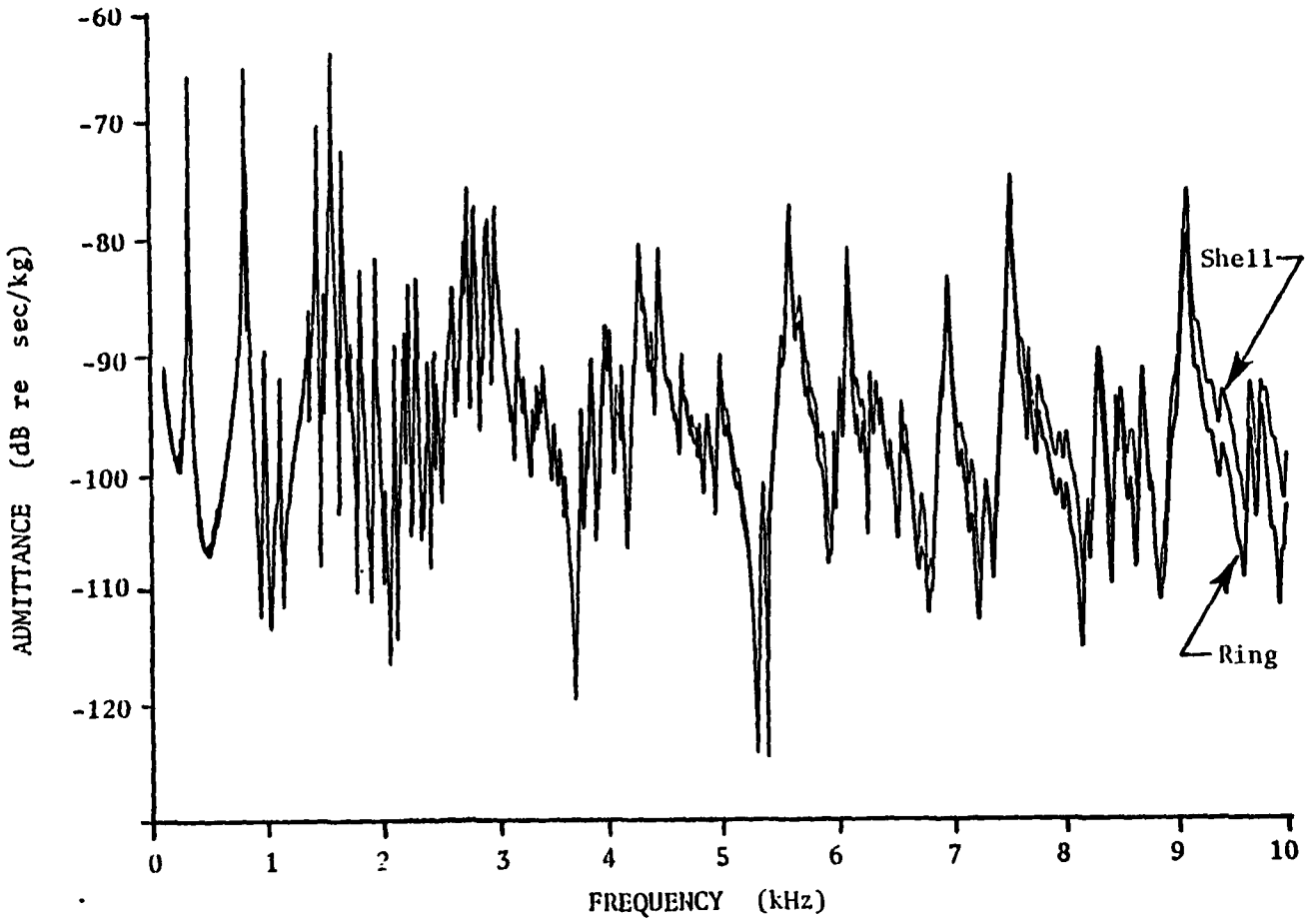

Figure 32 Measured Velocity on Inside of Ring and on Outside of Shell In-Line with Driving Point, Driver is Mounted on Inside of Ring.

$$Z_c = \rho c_{p\ell} b^2 \quad . \tag{4.36}$$

We are assuming that the wave propagation through the ring thickness is equivalent to the wave propagation in a rod of length h_r and cross sectional area of b^2.

From Figure 31 the ratio of the shell velocity over the ring velocity (at the driving point) is:

$$(Z_s + Z_1)\, v_s = \frac{Z_2\,(Z_s + Z_1)}{Z_2 + Z_s + Z_1}\, v_r \quad ,$$

$$\frac{v_s}{v_r} = \frac{Z_2}{Z_2 + Z_s + Z_1} = \frac{1}{\cos kh_r + j\,(Z_s/Z_c)\sin kh_r}$$

and

$$20 \log \left|\frac{v_s}{v_r}\right| = -10 \log \left[(\cos kh_r)^2 + \left(\frac{Z_s}{Z_c} \sin kh_r\right)^2 \right] \quad . \tag{4.37}$$

This function is plotted in Figure 33 for various values of Z_s/Z_c. The peak at $kh_r = \pi/2$ occurs when the ring thickness is in antiresonance at the driving point. As the shell impedance increases relative to the characteristic impedance of a longitudinal wave in the ring material, the antiresonance peak decreases. When $Z_s = Z_c$, the ring-shell interface will not reflect the incident wave, and $v_s = v_r$ for all frequencies.

For the experimental ring-stiffened cylindrical shell:

$$\frac{Z_s}{Z_c} \simeq \frac{8\, m_s \alpha_s \alpha_r}{\rho c_{p\ell} b^2} = 0.3$$

and

$$kh_r = 0.076\, f \quad (\text{in kHz}) \quad .$$

At 10 kHz, $kh_r = 0.76$ and the shell velocity is about 2½ dB higher than the ring velocity. This is in good agreement with the measurements

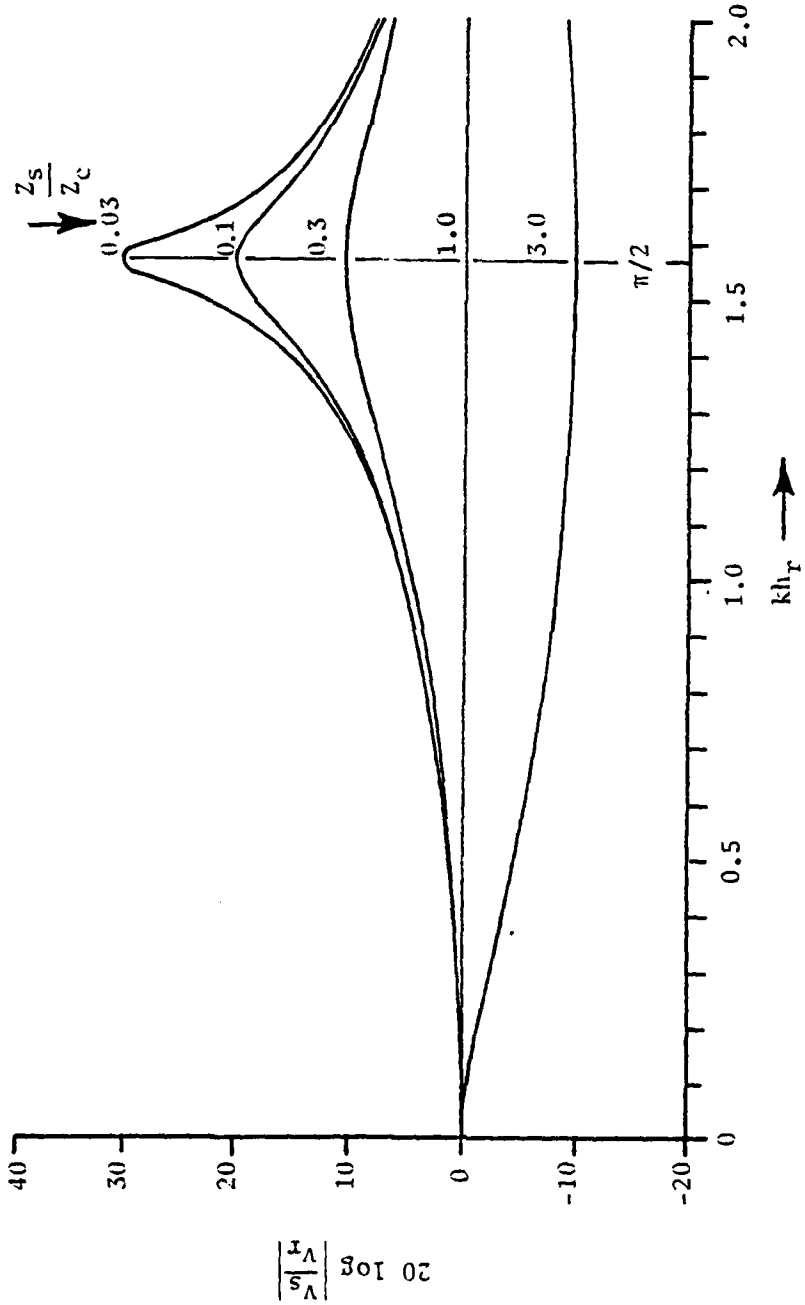

Figure 33 Calculated Ratio of Shell to Ring Velocity, Inline with the Driving Point.

presented in Figure 32.

From the equivalent circuit in Figure 31:

$$Z_T = (Z_r + Z_1) + \frac{Z_2(Z_s + Z_1)}{Z_2 + Z_s + Z_1} \quad . \tag{4.38}$$

Substituting the relationships for Z_1 and Z_2, the expression for the high frequency driving-point admittance becomes:

$$Z_H = Z_r + Z_s \left[\frac{(Z_c/Z_s) - j \cot kh_r}{(Z_s/Z_c) - j \cot kh_r} \right] \quad . \tag{4.39}$$

Note that if kh_r is very small, this expression reduces to: $Z_H = Z_r + Z_s$.

4.3 Velocity Insertion-Loss of Ring

Quite often a ring is added to a cylindrical shell to stiffen the shell at the point of excitation, thereby reducing the vibrational energy that is transmitted to the shell. A practical application is the mounting of a motor inside a cylinder. For a rotating imbalance, the motor may be considered a constant force generator, and we are interested in reducing the velocity at the motor mountings by the insertion of the ring. Defining the insertion loss as the difference in decibels between the shell velocities before and after insertion of the ring, we have:

$$IL = 10 \log \left| \frac{v_2^2}{v_1^2} \right| = 20 \log \left| \frac{Z_1}{Z_2} \right| \quad \text{dB} \quad . \tag{4.40}$$

Here, the 1 and 2 subscripts refer to before and after insertion of the ring, respectively.

At low frequencies ($\omega < \omega_0$) the impedances above are:

$$Z_1 = \frac{1}{\frac{\sqrt{\Omega/2}}{8\, m_s\, \alpha_s^2}(1+j)} = 4\sqrt{2}\; m_s\, \alpha_s^2 \sqrt{\omega_o/\omega}\; (1-j) \qquad (4.41)$$

and

$$Z_2 = 2\sqrt{\beta}\; (m_r + \tfrac{1}{2} m_s')\, \alpha_r \sqrt{\omega}\; (1+j) \quad . \qquad (4.42)$$

By combining these complex impedances in the proper manner and taking the magnitude, the insertion loss is:

$$IL = 20 \log \left[\frac{4\, m_s\, \alpha_s^2 \sqrt{\omega_o}}{\sqrt{\beta}\; (m_r + \tfrac{1}{2} m_s')\, \alpha_r} \right] - 20 \log \omega \quad . \qquad (4.43)$$

At high frequencies ($\omega > \omega_o$) the before and after impedances are:

$$Z_1 = 8\, m_s\, \alpha_s^2 \qquad (4.44)$$

and

$$Z_2 = 8\, m_s\, \alpha_s\, \alpha_r + 2\sqrt{\beta}\; m_r\, \alpha_r \sqrt{\omega}\; (1+j) \quad . \qquad (4.45)$$

The insertion loss is, therefore:

$$IL = 20 \log \frac{1}{(A+B) + jA} = -10 \log[(A+B)^2 + A^2] \;, \qquad (4.46)$$

where:

$$A = \frac{\sqrt{\beta}\, m_r\, \alpha_r}{4\, m_s\, \alpha_s^2} \sqrt{\omega} \qquad (4.47)$$

and

$$B = \alpha_r/\alpha_s \quad . \qquad (4.48)$$

Figure 34 shows the mean-value insertion loss computed for the ring-stiffened steel cylinder. The measured driving-point admittance of the damped shell, with and without the stiffening ring, is shown in

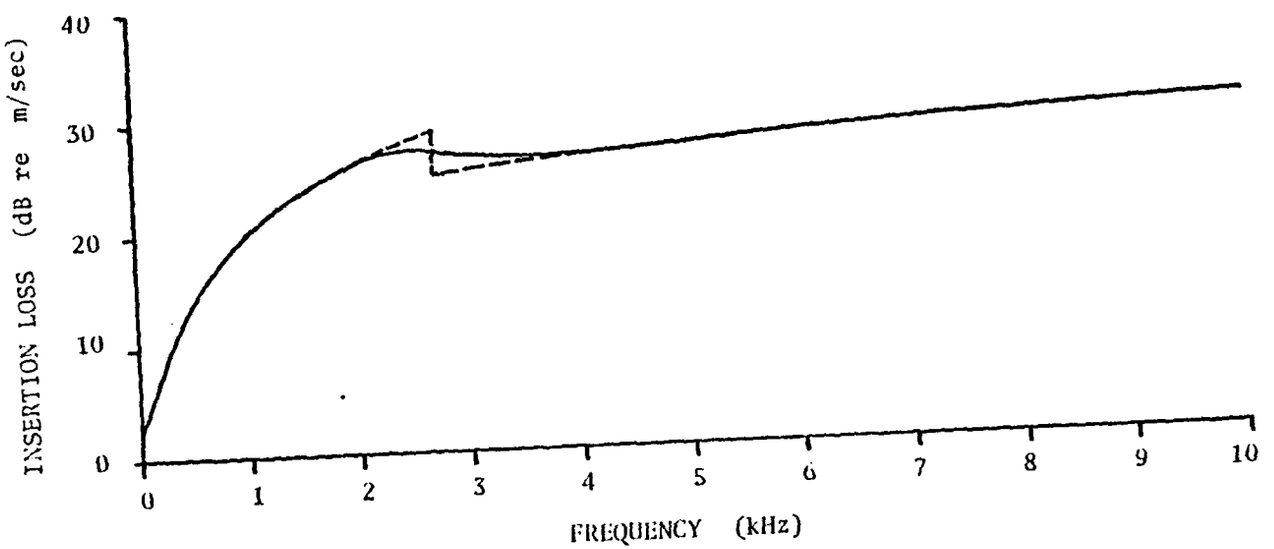

Figure 34 Calculated Velocity Insertion-Loss of Stiffening Ring.

Figure 35. The difference between these curves is the velocity insertion loss. The upper curve was measured at the edge of the shell and was shifted downward 6 dB to represent an interior point. The lower mean-value curve in Figure 35 was computed by subtracting the insertion loss from the upper mean-value curve.

Above the radial resonance frequency, the ring is very effective in reducing the velocity transmitted to the shell. At lower frequencies, the shell is inherently stiff and the addition of the ring is not as effective. If the shell was prestressed, for example, by exterior fluid pressure, the shell would become stiffer and the insertion loss of the ring would be less effective.

By substituting $m_r = \rho b h_r$ and $\alpha_r^2 = c_E h_r / \sqrt{12}$ into Equation (4.46), one can show that the improvement in insertion loss with an increase in ring thickness and ring width is approximately:

$$\Delta IL \approx -30 \log \Delta h_r - 20 \log \Delta b \quad . \qquad (4.49)$$

There is a significant improvement in the insertion loss with an increase in ring thickness. However, with the trend toward lightweight structures, we usually cannot afford the luxury of increasing the cross-sectional area or mass of the ring. Besides the added mass, there is another practical limit on how much the thickness can be increased. As the ring thickness increases, the thickness antiresonance will decrease toward the frequency region of interest, thereby increasing the shell velocity relative to the driving-point velocity. For example, if the thickness of our ring were increased by 30 percent, Equation (4.49) gives a 3½ dB increase in insertion loss. In Figure 33, kh_r at 10 kHz, is now

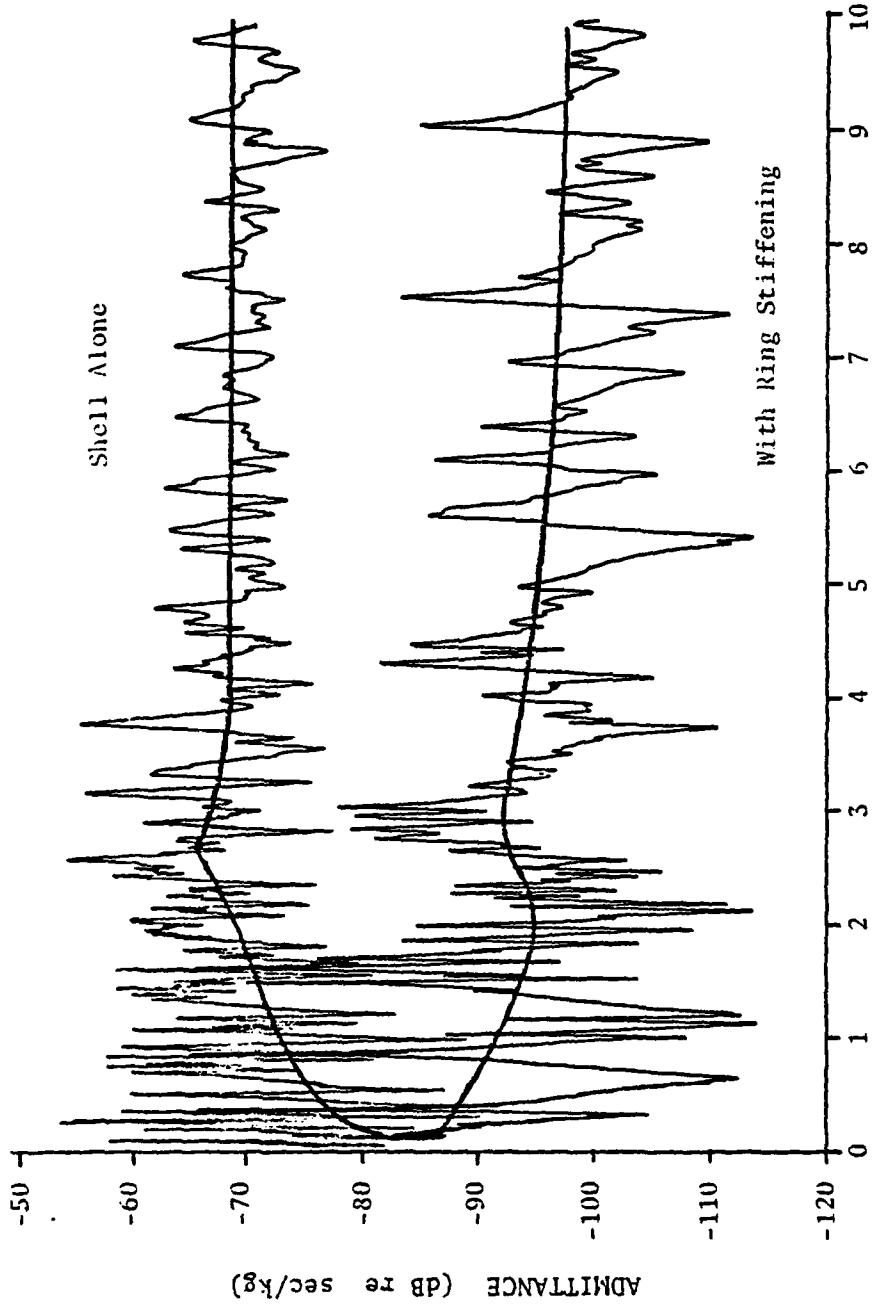

Figure 35 Measured Driving-Point Admittance of Cylindrical Shell With and Without Stiffening Ring.

0.76 x 1.3 = 1.0, and we see that the increase in shell velocity versus the driving-point velocity is 3½ dB. Thus, at 10 kHz, the benefit of increasing the ring thickness by 30 percent would be completely negated by the effect of the thickness antiresonance.

4.4 Transfer Admittance in the Plane of the Ring

It is not the intent of this thesis to provide an exhaustive treatment of transfer admittances. However, the hybrid model presented in Section 4.2.1 lends itself so well to the prediction of transfer admittances in the plane of the ring, that it would be wrong to pass over this subject without some discussion.

We can assume that the amplitude of the radial displacement in the plane of the ring is reasonably constant as the receiver is moved around the circumference away from the driving point because: (1) the losses in the ring are negligible, (2) there is no dispersion of the vibrational energy outward from the driving point as occurs in a two-dimensional vibrator, and (3) there is no edge distortion as occurs in a finite beam. With receiver and driving point separate, but both in the plane of the ring, the mode masses as shown in Figure 20 become:

$$M_u = \frac{M_r \langle \xi_u^2 \rangle}{\xi_u(F)\, \xi_u(A)} = \frac{M_r}{2} \frac{1}{\cos u\phi_A} \tag{4.50}$$

and

$$M_n = \frac{M_s \langle \xi_{m,n}^2 \rangle}{\xi_{m,n}(F)\, \xi_{m,n}(A)} = \frac{M_s}{4} \frac{1}{\cos n\phi_A} \quad , \tag{4.51}$$

where ϕ_A is the location of the receiver, and where $\nu = u = n$. The mode masses can now be negative if the point of observation in in antiphase with the driving point. Using Equations (4.50) and (4.51) in the Hybrid Mode-Sum and Mean-Value Model, Figure 20, we can predict the mean-value transfer admittance of the ring-stiffened cylindrical shell for any location in the plane of the ring.

The measured transfer admittance, along with the predicted mean value, is presented in Figures 36 and 37 for two separate receiver locations. The measured ring resonances and loss factors were used in these predictions. Figure 36 is with the receiver and driver separated by one-half the circumference ($\phi_A = 2\pi/2$). With the receiver in this position, $\cos \nu\phi_A = +1, -1, +1, \ldots$, and the circumferential mode masses alternate in sign, producing shallow troughs between the ring resonance frequencies. Figure 37 is with the receiver and driver separated by one-quarter the circumference ($\phi_A = 2\pi/4$); thus, $\cos \nu\phi_A = +1, 0, -1, 0, \ldots$ The odd ordered mode masses becomes infinite, and the admittance is zero. The response is, therefore, determined by only the even ordered modes, whose mode masses alternate in sign, producing shallow troughs between their resonance frequencies. This simply means that for the odd-ordered modes the receiver is located on a node (with respect to the radial displacement). Note, however, that below the radial resonance frequency the first and third circumferential modal responses are not significantly suppressed. The radial nodes associated with these modes possess a large tangental motion. The measured response is likely due to the transverse sensitivity of the accelerometer.

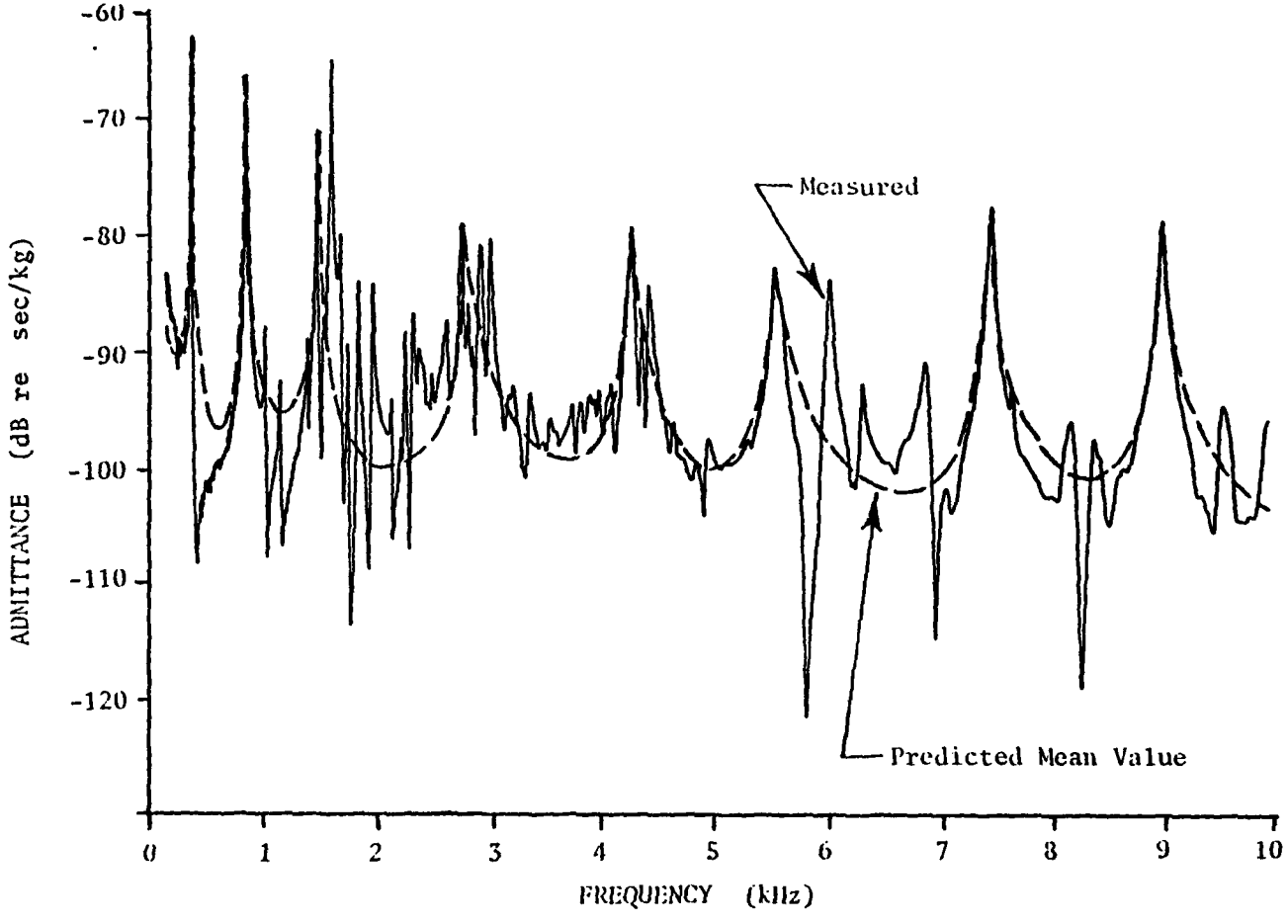

Figure 36 Predicted and Measured Transfer Admittance of Ring-Stiffened Cylindrical Shell with Receiver and Driver ½ Circumference Apart in the Plane of the Ring.

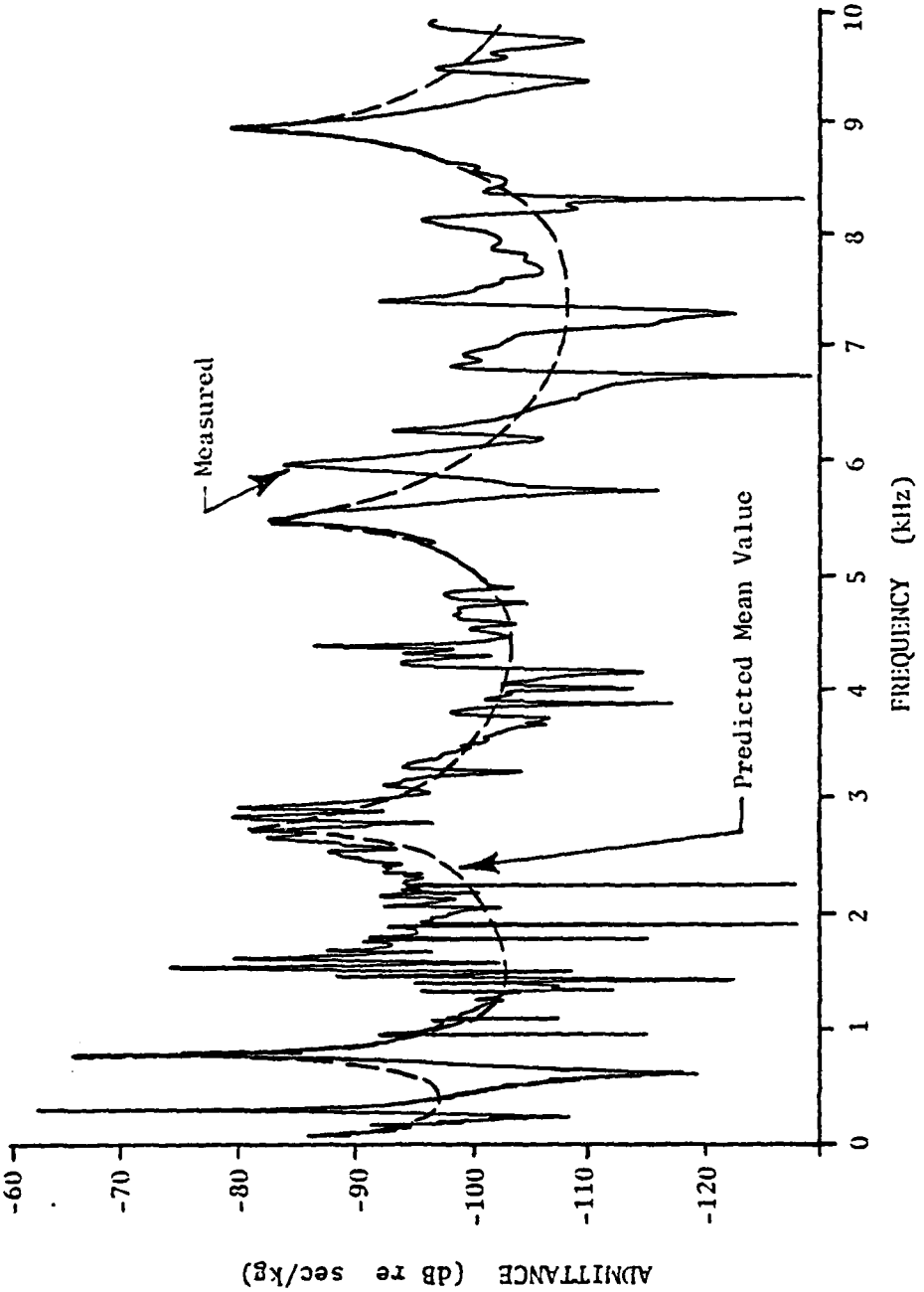

Figure 37 Predicted and Measured Transfer Admittance of Ring-Stiffened Cylindrical Shell with Receiver and Driver ¼ Circumference Apart in the Plane of the Ring.

It is significant to note that the predicted transfer admittances in Figures 36 and 37 were computed using $\omega_n = \frac{\alpha_r^2}{r^2} n^2 \beta \simeq \omega_\nu$ in Equation (4.11) rather than $\omega_n = \frac{\alpha_r^2}{r^2} n^2 \simeq \omega_\nu / \beta$, as was used in computing the driving-point admittance. The measured response is much softer than that predicted without using the shift factor of β. One may speculate that for the transfer admittance in the plane of the ring the shell's response is primarily dictated by circumferential modes which must match the ring modes. It is not clear, however, why this does not seem to be the case for the driving-point admittance.

CHAPTER V

SUMMARY AND RECOMMENDATIONS

5.1 Summary of Results

Using the mean-value admittance method [4], practical means have been demonstrated for predicting the driving-point admittance of cylindrical shells, both with and without ring-stiffening. The method predicts the geometric mean of the response of a vibrator with respect to frequency, and in contrast to other methods, is applicable at low as well as high frequencies. The basic computations involve the mode mass and the mode density. The results obtained provide a good first approximation with which to evaluate the design of many complex structures consisting of the fundamental components of plates, shells, beams and rings. Where the mode densities are small, the mean-value method can be improved by hybrid mode-sum representations.

The task of determining the driving-point admittance of the cylindrical shell essentially reduces to that of determining the density of resonances. The derivation of the density of resonances was generalized to the case of orthotropy, where the bending stiffnesses are not equal along the principal axes of the shell. The orthotropic shell is a useful model of a cylinder with stiffening rings or stringers. The results of the analytical development clearly demonstrated that:

1. At frequencies above the radial resonance frequency, the effective bending stiffness of an orthotropic shell is equal to the geometric mean of the bending

stiffnesses in the circumferential and axial directions.

2. At frequencies below the radial resonance frequency, the effective bending stiffness of an orthotropic shell is principally that of the circumferential bending stiffness. This result has certain practical limitations. It is, of course, valid for an isotropic shell and for a shell with greater circumferential than axial stiffness. However, if the axial stiffness is much greater than the circumferential stiffness, this result is valid at only the very low frequencies.

The analytical results showed excellent agreement with experimental measurements on an orthotropic shell.

Particular attention was placed on the use of ring-stiffening to provide velocity insertion loss at the driving-point. Several analytical models were developed that describe in a simplified manner the coupling between ring and shell modes, while retaining the important features of the vibrational response. Each model varies in its complexity and its accuracy in predicting the driving-point admittance in the plane of the ring. The selection of which model to use in an application depends on what details of the frequency response that the designer is interested in.

The fundamental results of the experimental and analytical investigations of the ring-stiffened cylindrical shell for point excitation in the plane of the ring are:

1. The primary effect of the shell on the ring is to mass load the ring, thereby shifting the ring resonance frequencies downward by a factor that is proportional to the square root of the added mode mass of the shell.

2. The primary effect of the ring on the shell is to stiffen the shell in the circumferential direction. By acting indirectly as a driver, the ring excites only those shell modes that closely match its bending wavelength. All other shell modes will be weakly excited. This phenomenon can be interpreted analytically as an effective increase in the shells circumferential stiffness, and the general expressions derived for the orthotropic shell apply.

The most significant contribution of this investigation is a simplified approach toward analyzing the modal coupling between a one-dimensional and a two-dimensional vibrator (Section 4.2.1). This approach uses the canonic circuit representation of a homogeneous vibrator. By matching the mode numbers of the two component vibrators, the mode parameters of each vibrator can be combined by simple electrical network theorems to produce effective mode parameters of the combined system.

The most important analytical results of this investigation are summarized in Table II.

5.2 Suggested Future Research

The principal shortcoming of the experimental investigations

Table II

Summary of Mode Parameters and Impedance/Admittance of Cylindrical Shell, With and Without Ring Stiffening

		FREQUENCY EQUATION	FREQUENCY SPACING BETWEEN RESONANCES, ϵ_ν *	POINT MODE MASS, M_ν **	DRIVING POINT IMPEDANCE *** $Z_c = 1/Y_c$
CYLINDRICAL SHELL length ℓ, radius a, thickness h_s, surface mass $m_s = \rho h_s$, thickness/radius parameter $\gamma_s = \frac{h_s}{\sqrt{12}\,a}$, stiffness constant $\alpha_s^2 = \frac{c_{p\ell}\,h_s}{\sqrt{12}}$, $c_{p\ell}$ is longitudinal velocity in a plate	ORTHOTROPIC Subscripts: 1 - circumferential direction 2 - axial direction	$\Omega^2 = \frac{\sigma^4}{(n^2+\sigma^2)^2} + (\gamma_1 n^2 + \gamma_2 \sigma^2)^2$ where: $\Omega = \omega/\omega_o$	$\epsilon_\nu = \begin{cases} \frac{4\alpha_1\alpha_2}{a\ell}, & \omega>\omega_o \\ \frac{4\sqrt{2}\,\alpha_1^2}{a\ell\sqrt{\Omega}}, & \omega<\omega_o \end{cases}$	$\frac{M_s}{4}$	$Z_s = \begin{cases} 8 m_s \alpha_1\alpha_2, & \omega>\omega_o \\ \frac{8 m_s \alpha_1^2}{\sqrt{\Omega/2}}(1-j), & \omega<\omega_o \end{cases}$
	ISOTROPIC $\gamma_1 = \gamma_2 = \gamma_s$ $\alpha_1 = \alpha_2 = \alpha_s$	$\Omega^2 = \frac{\sigma^4}{(n^2+\sigma^2)^2} + \gamma_s^2 (n^2+\sigma^2)^2$	$\epsilon_\nu = \begin{cases} \frac{4\alpha_s^2}{a\ell}, & \omega>\omega_o \\ \frac{4\sqrt{2}\,\alpha_s^2}{a\ell\sqrt{\Omega}}, & \omega<\omega_o \end{cases}$	$\frac{M_s}{4}$	$Z_s = \begin{cases} 8 m_s \alpha_s^2, & \omega>\omega_o \\ \frac{8 m_s \alpha_s^2}{\sqrt{\Omega/2}}(1-j), & \omega<\omega_o \end{cases}$
RING STIFFENED CYLINDRICAL SHELL ring thickness h_r, ring radius r, ring width b, ring stiffness constant $\alpha_r^2 = \frac{c_E\,h_r}{\sqrt{12}}$, c_E is longitudinal velocity in a rod, shell mass per unit circumferential length $m_s' = \rho h_s \ell$	RING WITH SHELL MASS LOADING	$\omega_u = \frac{(u+1)\left((u+1)^2-1\right)}{\sqrt{(u+1)^2+1}} \frac{\alpha_r^2}{r^2}\beta = u^2 \frac{\alpha_r^2}{r^2}\beta$ where: $\beta = \left(\frac{1}{2}M_r / \left(\frac{1}{2}M_r + \frac{1}{4}M_s\right)\right)^{\frac{1}{2}}$	$\epsilon_\nu = 2\sqrt{\beta}\,\frac{\alpha_r}{r}\sqrt{\omega}$	$\frac{M_r}{2}$	$Z_r = 2\sqrt{\beta}\, m_r \alpha_r \sqrt{\omega}\,(1+j)$
	SHELL WITH RING-STIFFENING	$\omega_{m,n}^2 = \frac{\omega_o^2\sigma^4}{(n^2+\sigma^2)^2} + \left(\frac{\alpha_r^2}{r^2}n^2 + \frac{\alpha_s^2}{a^2}\sigma^2\right)^2$	$\epsilon_\nu = \begin{cases} \frac{4\alpha_r\alpha_s}{\sqrt{ar}\,\ell}, & \omega>\omega_o \\ \frac{4\sqrt{2}\,\alpha_r^2}{r\ell\sqrt{\Omega}}, & \omega<\omega_o \end{cases}$	$\frac{M_s}{4}$	$Z_s = \begin{cases} 8\sqrt{a/r}\, m_s \alpha_r\alpha_s, & \omega>\omega_o \\ \frac{8\sqrt{a/r}\, m_s \alpha_r^2}{\sqrt{\Omega/2}}(1-j), & \omega<\omega_o \end{cases}$
	COMBINED SYSTEM	Shell equation with n = u	(See section 4.2)	$\frac{M_r}{2} + \frac{M_s}{4}$	$Z_L = Z_r + Z_s$ $= 2\sqrt{\beta}\, m_r \alpha_r \sqrt{\omega}\,(1+j) + 8 m_s \alpha_r\alpha_s$, $\omega>\omega_o$ $Z_L = 2\sqrt{\beta}\,(m_r + \frac{1}{2}m_s')\,\alpha_r\sqrt{\omega}\,(1+j)$, $\omega<\omega_o$

(Note: See section 4.2 for more accurate analytical models)

* Inverse of the mode density.

** See section 2.1 for the general expression.

*** In general: $Y_c = G_c + jB_c = \frac{\pi}{2\epsilon_\nu M_\nu} + jB_c$, where: $B_c = \begin{cases} -G_c, & \text{if } \epsilon_\nu M_\nu \text{ varies as } \sqrt{\omega} \\ 0, & \text{if } \epsilon_\nu M_\nu \text{ is constant} \\ +G_c, & \text{if } \epsilon_\nu M_\nu \text{ varies as } 1/\sqrt{\omega} \end{cases}$

was that the ring-stiffened shell was constructed with too thick a ring. Consequently, the ring impedance was very large compared with the shell impedance. Considering the accuracy of the driving-point measurements, it was difficult to observe the shell impedance which is in series with the ring impedance. More importantly, it would have been desirable to verify in more detail the modal coupling analysis presented in Section 4.2.1. The fundamental result of this section was the shift in ring resonance frequencies with the addition of the shell:

$$\omega_\nu = \nu^2 \left[\frac{\frac{\alpha_r^4}{r^4}\frac{M_r}{2} + \frac{\alpha_s^4}{a^4}\frac{M_s}{4}}{\frac{M_r}{2} + \frac{M_s}{4}} \right]^{\frac{1}{2}} \approx \nu^2 \frac{\alpha_r^2}{r^2}\beta \quad . \qquad (5.1)$$

Unfortunately, the α_r^4/r^4 term is 140 times larger than the α_s^4/a^4 term, and the frequency shift factor β is principally that of the added mode mass of the shell. In order to verify Equation (5.1) beyond a reasonable doubt, it would be desirable to test a structure where the stiffness of the two-dimensinal vibrator could be observed in the frequency shift. Such a structure could most simply be a rib-stiffened plate. Several plates with varying rib stiffeners could be tested to verify the shift in rib resonance frequencies as prediced by Equation (5.1) for various ratios of rib to plate stiffnesses. The case where α(rib) = α(plate) would be of particular interest, because a mode mass of $\frac{M_{pl}}{2}$ would probably have to be substituted for $\frac{M_{pl}}{4}$ in the frequency equation. Dispite this shortcoming, the experimental measurements did provide strong evidence to support the modal coupling analysis in Section 4.2.1.

This is evident in the Hybrid Mode-Sum and Mean-Value Model where the magnitude of the shell impedance can be observed between the widely spaced ring resonances.

As alluded to in Section 4.3, a practical topic for investigation would be to study the effect of various ring or rib cross sectional geometries on the velocity insertion loss. The objective would be to devise various methods of stiffening shells or plates to obtain an optimum insertion loss. Some examples of practical applications are lightweight aircraft and surface vehicle structures, or inexpensive building partitions.

The next analytical step from this investigation is to develop a simplified method for the prediction of the transfer admittance of cylindrical shells. The transfer admittance can *always, in concept,* be predicted using the mode-sum procedure. This procedure was used in Section 4.4 to compute the transfer admittance in the plane of the ring using the Hybrid Mode-Sum and Mean-Value Model. Here, there were only eight ring resonances which needed to be accounted for in the calculations. Unfortunately, the mode functions and resonance frequencies are usually too difficult to predict or are too numerous such that the mode sum calculation becomes tedious. Furthermore, for most practical systems with numerous resonance frequencies, we are usually interested in the gross response of the system over some frequency interval, rather than the numerous and sometimes misleading details of the response provided by a mode-sum calculation. There is a need for a simplified method of predicting the transfer admittance, where we are not interested in the individual modal responses, but rather the mean-value of these

responses over some frequency interval. Such a procedure was presented by Williams [15] for vibrating plates. Williams accounts for the spreading of the vibrational energy into two-dimensional space and for the losses which determine a background or reverberant field. The results presented by Williams for plates would, of course, be valid for cylindrical shells above the radial resonance frequency. The low frequency transfer admittance, however, needs further study.

Another analytical step from this investigation is to consider line or area excitation, such as an acoustical pressure. Again, the mode-sum procedure can be used by expanding the excitation in terms of the vibrational modes of the shell, and by computing a separate excitation constant and mode mass for each shell mode. Walter [20] has shown that the coincidence of spinning acoustic modes with shell vibrational modes is a major, if not controlling, factor in the response of a pipe to internal propagating sound. Walter qualitatively predicted the response of a pipe wall to a spinning acoustic mode by computing the excitation constant and substituting into the mean-value admittance expressions. His results, however, included an effective length over which the acoustic field drives the shell. It is the author's opinion that a relationship can be found using the mean-value theory that is independent if an effective length of excitation. All of the analytical expressions derived in this thesis are independent of shell length. The mean-value frequency response represents a characteristic wave that is independent of shell length or, in other words, it represents a progressive wave in the axial direction. Spinning acoustic waves are also progressive in the axial direction. One should be able to evaluate the matching between these waves on the basis of a unit axial wavelength which for a

progressive wave is a function of frequency and the characteristic velocity of sound in the material. The results of such a study would be of great value in designing pipes with high transmission loss.

LIST OF REFERENCES

1. Junger, M. C. and Feit, D. C., Sound, Structures, and Their Interaction, M.I.T. Press; Cambridge, Mass. (1972).

2. Kalnins, A. and Dym, C., Vibration of Beams, Plates, and Shells, Benchmark Papers in Acoustics/8; Dowden, Hutchinson & Ross, Inc., Stroudsburg, PA (1976).

3. Arnold, R. and Warburton, G., "Flexural Vibrations of the Walls of Thin Cylindrical Shells Having Freely Supported Ends," Proc. Roy. Soc. London, A197, 238-256 (1949).

4. Greenspon, J. E., "Vibrations of a Thick-Walled Cylindrical Shell - Comparison of the Exact Theory and Approximate Theories," J. Acoust. Soc. Am. 32, 571-578 (1960).

5. Leissa, A. W., Vibration of Shells, NASA SP-288 (1973). Available from NTIS No. N73-26924.

6. Franken, P. A., "Input Impedances of Simple Cylindrical Structures," J. Acoust. Soc. Am. 32, 473-477 (1960).

7. Heckl, M., "Vibrations of Point-Driven Cylindrical Shells," J. Acoust. Soc. Am. 34, 1553-1557 (1962).

8. Palladino, J. L. and Neubert, V. H., "Mobility of a Long Cylindrical Shell," J. Acoust. Soc. Am. 42, 403-411 (1966).

9. Skudrzyk, E., "The Mean-Value Method of Predicting the Dynamic Response of Complex Vibrators," to be published in the J. Acoust. Soc. Am. (Submitted December 1979).

10. Skudrzyk, E., "Mean-Value Characteristic-Impedance Method of Predicting Vibration and Sound Radiation," paper 32, presented at the 82nd Meeting of the Acoustical Society of America, Denver, 19-22, October 1971. Abstract in J. Acoust. Soc. Am. 51, 98 (1972).

11. Skudrzyk, E., Simple and Complex Vibratory Systems, Pennsylvania State University Press (1968).

12. Hanon, R., "Vibration and Sound Radiation of a Plate," Ph.D. Thesis The Pennsylvania State University (1975).

13. Timoshenko, S., Vibration Problems in Engineering, D. Van Nostrand Co., New York (1955).

14. Mason, W. P., Electromechanical Transducers and Wave Filters, D. Van Nostrand Co., Princeton, N.J. (1942), p. 202.

15. Williams, E., "Vibrations of Plates of Various Geometries," Ph.D. Thesis, Physics Department, The Pennsylvania State University (1979).

16. Wilcoxon Research, "Attachment of the Impedance Head to the Test Specimen," Bulletin No. 2, Bethesda, Maryland.

17. Wilcoxon Research, "Inherent Limitation of Measureable Impedances," Bulletin No. 4, Bethesda, Maryland.

18. Wilcoxon Research, "Weight Limitations of Accelerometers for High Frequency Vibration Measurements," Bulletin No. 1, Bethesda, Maryland.

19. Creamer, L. and Heckl, M., Structure-Born Sound, translated by E. Ungar, Springer-Verlag, New York, (1973).

20. Walter, J., "Coincidence of Higher-Order Modes - a Mechanism of the Excitation of Cylindrical Shell Vibrations via Internal Sound," Ph.D. Thesis, Department of Mechanical Engineering, The Pennsylvania State University (1979).

APPENDIX A

EXPERIMENTAL INVESTIGATIONS

A.1 Test Specimens

Various driving-point and transfer admittances were measured on two circular cylindrical shells, one with and one without ring stiffening. The fundamental dimensions and physical properties of these two shells are listed in Table III.

Table III

Dimensions and Physical Properties of the Cylindrical Shell Test Specimens

		Aluminum Cylindrical Shell	Steel Cylindrical Shell With Ring-Stiffener
Shell			
length	ℓ	0.724 m	1.00 m
nominal radius	a	0.262 m	0.310 m
thickness	h_s	0.008 m	0.005 m
Young's elastic modulus	E	7.1×10^{10} nt/m^2	1.95×10^{11} nt/m^2
density	ρ	2700 kg/m^3	7700 kg/m^3
Poisson's ratio	μ	0.33	0.28
Ring			
width	b		0.0254 m
nominal radius	r		0.273 m
thickness	h_r		0.0635 m
Young's elastic modulus	E		1.95×10^{11} nt/m^2
density	ρ		7700 kg/m^3
Poisson's ratio	μ		0.28

The aluminum cylindrical shell was originally fabricated for an underwater experiment, and the ends of the shell were fitted with tongue-and-grooved rings for the attachment of waterproof caps. These end rings present a mass-like loading on the shell ends, which makes the length of the shell appear slightly shorter. As long as the driver is located at an internal point, the effective length of the shell has little influence on the driving-point admittance. The end rings, therefore, will not affect our measurements.

Both the ring and shell of the ring-stiffened shell were fabricated from steel, and were attached by a continuous weld. The ring was located just off center of the shell, so that the ring would excite all of the shell's axial modes.

A.2 Method of Support

Both of the cylindrical shells were supported by approximately six inches of foam rubber. This method of support was investigated by Williams in his thesis [15]. Williams demonstrated that the vibration patterns and natural frequencies of a plate were not altered by the foam support. The foam support does, however, reduce the resonance peak heights if the vibrator is lightly damped. This is of no importance, since we are primarily concerned with the behavior of the shell as damping is increased.

The use of foam rubber is an excellent method of supporting test specimens where the objective is to simulate free-boundary conditions. The impedance of the foam, although extremely small, is similar to a pure radiation resistance. The loss of vibrational energy to the foam support is, therefore, predictable and constant for all of the

test specimen's vibrational modes.

A.3 Method of Damping

Measurements on both shells were performed with and without damping. A commercially available compound was used to dampen the shells. This material is troweled on and cures to a hard consistency similar to plaster. The elastic modulus and density of the damping compound are:

$$E_d = 4 \times 10^9 \text{ nt/m}^2$$

and

$$\rho_d = 1600 \text{ kg/m}^3 \quad .$$

In order to compare the damped with the undamped frequency response curves, we must predict the change in characteristic admittance of the test specimens with the addition of the damping compound. The method used in Section 4.2.1 is used here to estimate the influence of the damping.

For convenience, consider a square, freely supported panel of thickness h_p and length ℓ of both sides, on which is applied a layer of damping compound of thickness h_d. With the application of the damping layer, the mode parameters of the panel will change as illustrated in Figure 38. The mode parameters with the 1, 2, and 3 subscripts are that of the panel alone, the damping layer alone, and the combined panel with damping, respectively. The compliance of the combined system is:

$$C_3 = \frac{1}{\frac{1}{C_1} + \frac{1}{C_2}} \tag{A.1}$$

and

$$\frac{1}{\omega_{\nu 3}^2 \left(\frac{M_p}{4} + \frac{M_d}{4}\right)} = \frac{1}{\omega_{\nu 1}^2 \frac{M_p}{4} + \omega_{\nu 2}^2 \frac{M_d}{4}} \quad ,$$

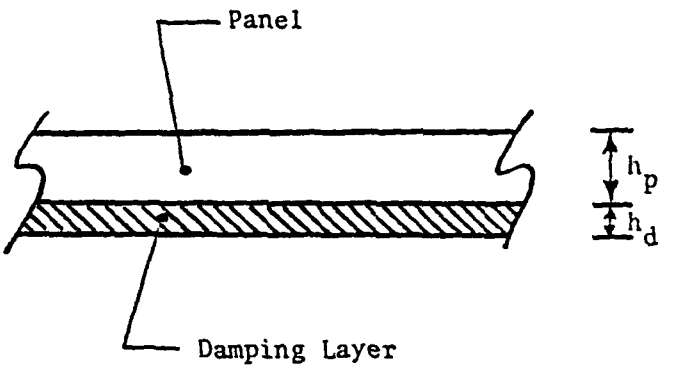

MECHANICAL SYSTEM

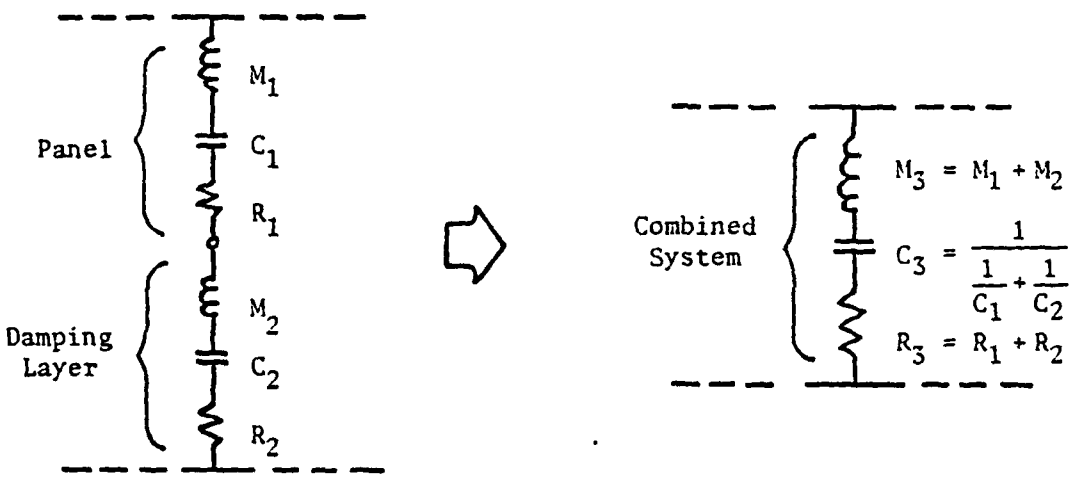

CIRCUIT REPRESENTATION

Figure 38 Circuit Representation of Panel with Damping Layer.

and the resonance frequencies, $\omega_{\nu 3}$, of the combined panel with damping is:

$$\omega_{\nu 3}^2 = \frac{\pi^4 \frac{\alpha_p^2}{\ell^4} (m_1^2 + n_1^2) M_p + \pi^4 \frac{\alpha_d^2}{\ell^4} (m_2^2 + n_2^2) M_d}{M_p + M_d} \quad . \qquad (A.2)$$

Here, α_p is the plate stiffness constant, and α_d is the stiffness constant of the damping layer. Because the modal shape of the damping layer must match the modal shape of the panel,

$$m_2 = m_1 \quad , \quad n_2 = n_1 \qquad (A.3)$$

and

$$\omega_{\nu 3}^2 = \frac{\pi^4}{\ell^4} (m_1^2 + n_1^2) \left[\frac{\alpha_p^4 M_p + \alpha_d^4 M_d}{M_p + M_d} \right]$$

$$= \omega_{\nu 1}^2 \left[\frac{1 + \frac{\alpha_d^4}{\alpha_p^4} \frac{M_d}{M_p}}{1 + \frac{M_d}{M_p}} \right] \quad . \qquad (A.4)$$

The change in the resonance frequencies of the panel with the added damping layer is, therefore:

$$\delta_\omega = \sqrt{\frac{1 + \delta_s}{1 + \delta_m}} \quad , \qquad (A.5)$$

where:

$$\left.\begin{aligned} \delta_s &= \frac{\alpha_d^4}{\alpha_p^4} \frac{M_d}{M_p} = \frac{E_d h_d^3}{E_p h_p^3} \\ \text{and} \\ \delta_m &= \frac{M_d}{M_p} = \frac{\rho_d h_d}{\rho_p h_p} \end{aligned}\right\} \quad . \qquad (A.6)$$

The E_p and E_d are the respective elastic moduli of the panel and damping compound; and the ρ_p and ρ_d are the respective densities. The δ_s represents the effective change in bending stiffness, and δ_m represents the effective change in mass.

Given the shift δ_ω in the resonance frequencies of the panel, the change in frequency spacing between successive resonances is $\sqrt{\delta_\omega}$. The change in the mode mass is:

$$\frac{\frac{1}{4}M_p + \frac{1}{4}M_d}{\frac{1}{4}M_p} = 1 + \delta_m \quad . \tag{A.7}$$

From the general expression of the mean-value driving-point admittance, Equation (2.9), the change in admittance is therefore:

$$\Delta Y_o = \frac{1}{\sqrt{\delta_\omega}\ (1 + \delta_m)} = (1 + \delta_s)^{-\frac{1}{4}}\ (1 + \delta_m)^{-\frac{3}{4}} \quad . \tag{A.8}$$

The aluminum cylindrical shell was coated with approximately a 0.25 cm thickness of damping compound. Using the shell data in Table III. the change in effective stiffness and effective mass is:

$$\delta_s = 0.0016$$

and

$$\delta_m = 0.18 \quad ,$$

and the change in the characteristic admittance is:

$$20 \log \Delta Y_o = -1 \text{ dB re sec/kg} \quad .$$

This small change was added to the predictions in Section 3.2.

The ring-stiffened cylindrical shell was coated twice with damping compound. The first layer was approximately 0.15 cm thick, and with the added layer, the final thickness was approximately 0.3 cm thick. The effect of the first coat is:

$$\delta_s = 0.00044 \quad ,$$

$$\delta_m = 0.058$$

and

$$20 \log \Delta Y_o = -\tfrac{1}{2} \text{ dB re sec/kg} \quad .$$

and the effect of the final coat is:

$$\delta_s = 0.0039 \quad ,$$

$$\delta_m = 0.12$$

and

$$20 \log \Delta Y_o = -\tfrac{3}{4} \text{ dB re sec/kg} \quad .$$

Considering that the ring-stiffened shell impedance is dominated by the ring impedance, these small changes in the shell admittance were neglected.

Strictly speaking, the estimates above are only valid for frequencies above the radial resonance frequencies where the shell behaves as a plate. At frequencies below the radial resonance frequency, membrane forces predominate and the change in bending stiffness can be neglected, leaving only the change in effective mass. However, the calculations above demonstrate that mass loading predominates at high frequencies as well as at low frequencies for these particular shells. Therefore, the estimates are valid below as well as above the radial resonance frequencies.

A.4 Measurement Apparatus

The experimental measurements were condicted with the system illustrated in Figure 39. The measurement system was originally assembled by Hannon [12] and later improved by Williams [15]. The basic principal of the system is to maintain a constant driving force via a feedback loop, while harmonically sweeping through the frequency spectra.

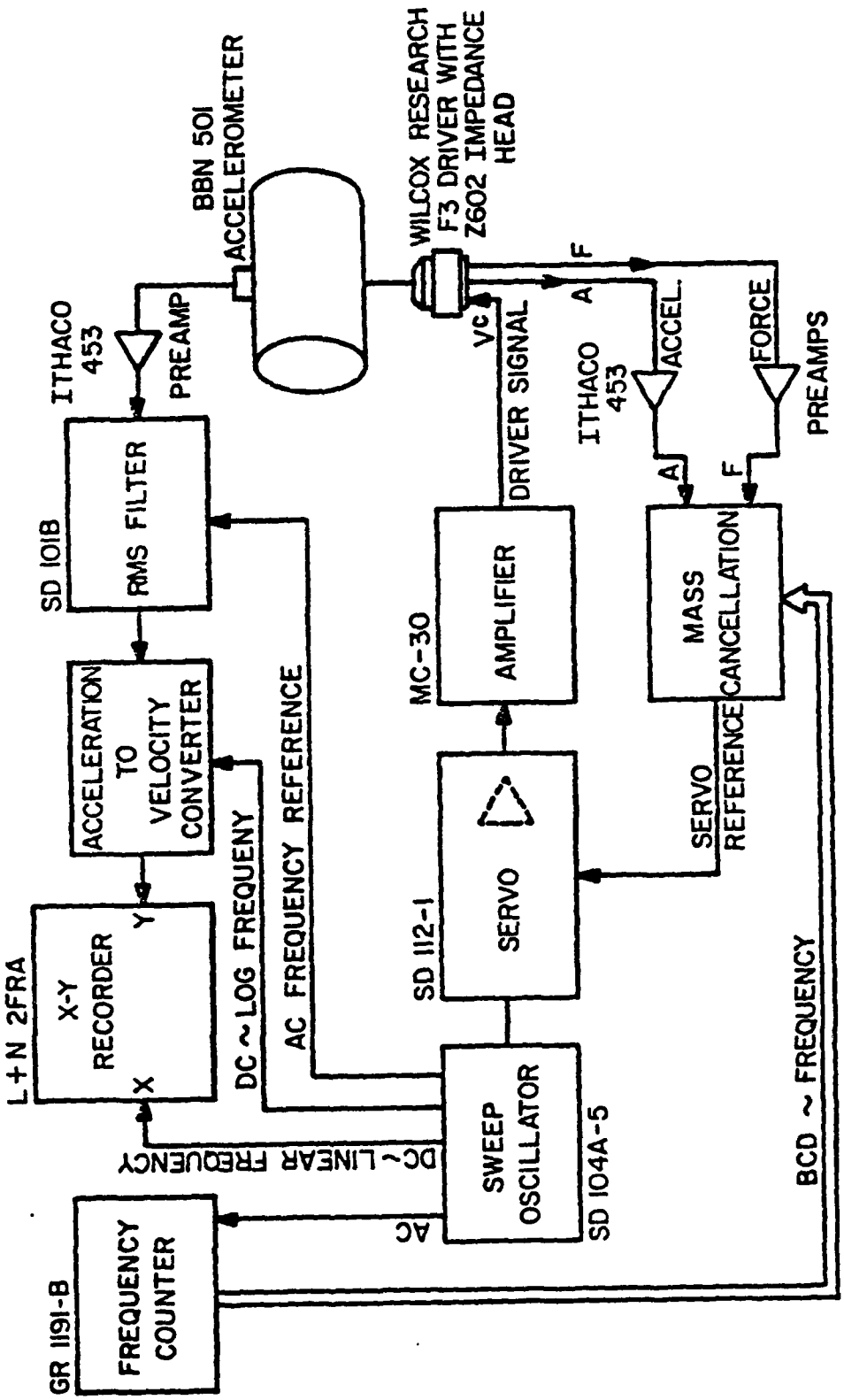

Figure 39 Functional Diagram of the Measurement System.

For a constant driving force, the measured velocity is directly proportional to the admittance.

The sweep oscillator (Spectral Dynamics SD104A-5) generates a harmonic signal that automatically sweeps through a preset frequency range. The output of the oscillator is fed into an amplitude servo/monitor (Spectral Dynamics SD112-1) which maintains a constant force at the driving-point through a feedback loop. The servo output is amplified by a McIntosh MC-30 Amplifier which drives the voice coil of the Wilcoxon Research F3 Driver. A Wilcoxon Research Z602 Impedance Head containing a force gauge and accelerometer is mounted with the driver. The force and acceleration signals from the impedance head are amplified by Ithaco 453 Preamps, and are used by the mass cancellation unit to provide a reference signal to the servo that is proportional to the force at the driving-point.

The mass cancellation unit was designed and built by Williams and the circuitry is described in his thesis. To understand the purpose of this component we refer to part (b) of Figure 40. Here, a_h is the acceleration, F_h is the force measured by the impedance head, M_h is the mass of the mounting head, F_s is the actual force at the driving point, and Z_s is the impedance of the test specimen. The acceleration at the driving point is the same as the measured acceleration; however, the actual force at the driving point is related to the measured force by:

$$F_s = F_h - M_h a_h \quad . \tag{A.9}$$

This subtraction is carried out by an operational amplifier in the mass cancellation unit. The slight change in the accelerometer's sensitivity

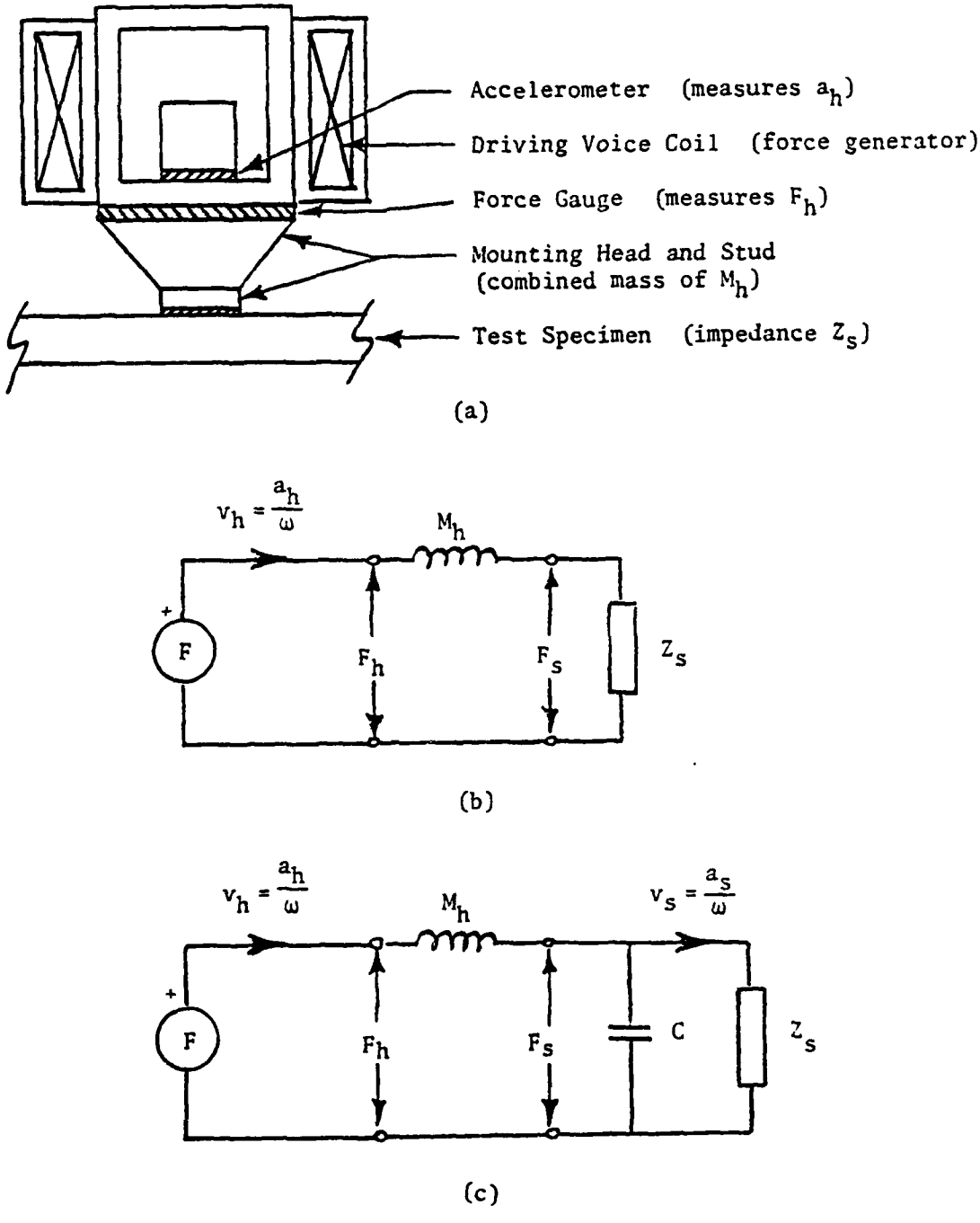

Figure 40 Impedance Head: (a) Mechanical System, (b) Circuit Representation, and (c) Circuit Representation with Mounting Compliance.

with frequency is also compensated for by programmable gains in the operational amplifier.

The vibrations of the cylinder are measured using a 1.8 gram BBN Model 501 Accelerometer. The accelerometer signal is amplified, then processed by a Spectral Dynamics SD101 Dynamic Analyzer using a 10 Hz bandwidth filter and RMS circuitry. The output of the RMS filter is converted from acceleration in decibels to velocity in decibels by subtracting a DC proportional to log frequency signal as follows:

$$20 \log v_s = 20 \log a_s - 20 \log f - \text{constant} \quad . \qquad (A.10)$$

The acceleration to velocity conversion is implemented by a simple voltage divider network as shown in Figure 41. This circuit was designed and built by Williams.

The dynamic range of the measurement system is approximately 60 dB . The adjustment of the system dynamic range involves a tradeoff between clipping the resonance peaks and losing the antiresonances in the low frequency noise floor. Since we are seldom interested in the low frequency antiresonances, the system was always set up to provide a true plot of the resonance peaks. For some measurements, this means that the low frequency antiresonances are lost in the noise floor of the system. Because we are using an accelerometer to measure vibration, the noise floor is proportional to acceleration, and when plotted on a velocity scale, will be inversely proportional to frequency. Where applicable, the system noise floor is indicated on the measurements.

Two methods were used to attach the driver to the test specimen. For the ring stiffened shell, the driver was attached to the ring

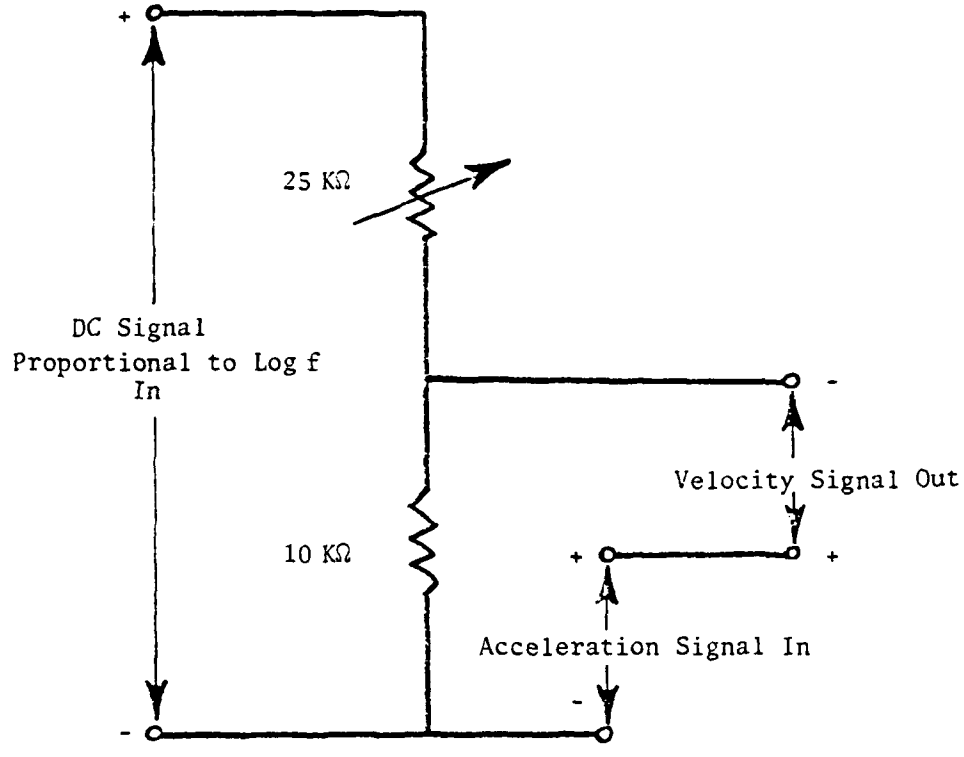

Figure 41 Electrical Circuit for the Conversion of the Acceleration Signal to a Velocity Signal.

by a stud which was screwed into the impedance head and ring. For all of the other measurements, the driver was attached to the test specimen by a flat mounting stud which was glued to the shell and screwed into the driver.

Any method of attachment will produce a small compliance between the impedance head and the test specimen [16]. Even if the impedance head were ideally attached to the test specimen, local deformation of the test specimen material or deformation of the impedance head itself would produce a compliant effect at high frequencies [17]. For the Z602 impedance head this compliance is on the order of 1×10^{-9} m/nt. This compliance can usually be neglected compared to the compliance of a glue layer or other method of attachment. The effect of a compliance between the impedance head and test specimen is illustrated by the equivalent circuit in part (c) of Figure 40. In this figure, C is the compliance due to the attachment method, and v_s is the actual velocity of the test specimen at the point of attachment. From Figure 40:

$$F_s = Z_s v_s = \frac{Z_s \frac{1}{j\omega C}}{Z_s + \frac{1}{j\omega C}} v_h \quad ,$$

$$\frac{v_h}{v_s} = \frac{a_h}{a_s} = \frac{Z_s + \frac{1}{j\omega C}}{\frac{1}{j\omega C}} = 1 + j\omega C Z_s$$

and

$$20 \log \left|\frac{a_h}{a_s}\right| = 20 \log \left|1 + j\omega C Z_s\right| \quad . \qquad (A.11)$$

At high frequencies the compliance short circuits the driving velocity, thereby reducing the velocity of the test specimen. If Z_s is large, the measured acceleration (a_h) will be greater than the actual acceleration (a_s) of the test specimen.

The compliance of both methods of attachment were measured by Williams. The combined compliance of the glue layer and flat mounting stud was found to be approximately 1×10^{-8} m/nt, and the compliance of the stud screwed into both the head and test specimen was approximately 7×10^{-9} m/nt. The largest impedance measured with the glued mounting was approximately 95 dB ($Z_s = 5.6 \times 10^{4}$ kg/sec). Thus, the difference between a_h and a_s at 10 kHz is approximately:

$$20 \log \left|\frac{a_h}{a_s}\right| = 31 \text{ dB} \quad .$$

The largest impedance measured with the stud screwed into both the head and test specimen was approximately 120 dB ($Z_s = 1 \times 10^{6}$ kg/sec), and the difference between a_h and a_s at 10 kHz is approximately 53 dB. In summary, at high frequencies and for large test specimen impedances, the acceleration measured by the impedance head (a_h) is grossly in error of the true acceleration of the test specimen (a_s).

The problem of the mounting compliance was avoided by using a separate accelerometer to measure the response of the cylindrical shells. The impedance head acceleration signal was, however, used by the mass cancellation unit because it correctly represents the acceleration of the head mass (M_h).

The attachment of the accelerometer to the test specimen can influence the measurement in two ways. First, if the mass impedance of

the accelerometer approaches the impedance of the test specimen, the added mass of the accelerometer will reduce the response of the test specimen at the point of attachment. Problems with transducer mass loading are well known and are discussed throughout the literature [18,19]. Second, any method of attachment will result in a small compliance between the accelerometer and test specimen, and the mass of the accelerometer will vibrate in antiresonance with the compliance at the point of attachment. Both of these effects are illustrated by the equivalent circuit in Figure 42.

From Figure 42, we see that:

$$v_o = \frac{Z_s + Z_1}{Z_s} v_1 \qquad (A.12)$$

and

$$v_1 = \frac{j\omega M}{Z_1} v_2 \quad , \qquad (A.13)$$

where:

$$Z_1 = \frac{j\omega M \ \frac{1}{j\omega C}}{j\omega M + \frac{1}{j\omega C}} = \frac{j\omega M}{1 - \omega^2 M C} \quad . \qquad (A.14)$$

The difference in decibels between the measured velocity (v_2) and the actual velocity (v_o) of the test specimen without the accelerometer mass loading is, therefore:

$$20 \log \left| \frac{v_2}{v_o} \right| = -20 \log \left| 1 - \frac{\omega^2}{\omega_o^2} + j \frac{\omega M}{Z_s} \right| \quad . \qquad (A.15)$$

The ω^2/ω_o^2 term represents the effect of the antiresonance between the mass of the accelerometer and the compliance at the point of attachment. The antiresonance frequency is defined as $\omega_o^2 = 1/MC$. The $j\omega M/Z_s$ term represents the effect of the accelerometer mass loading on the test

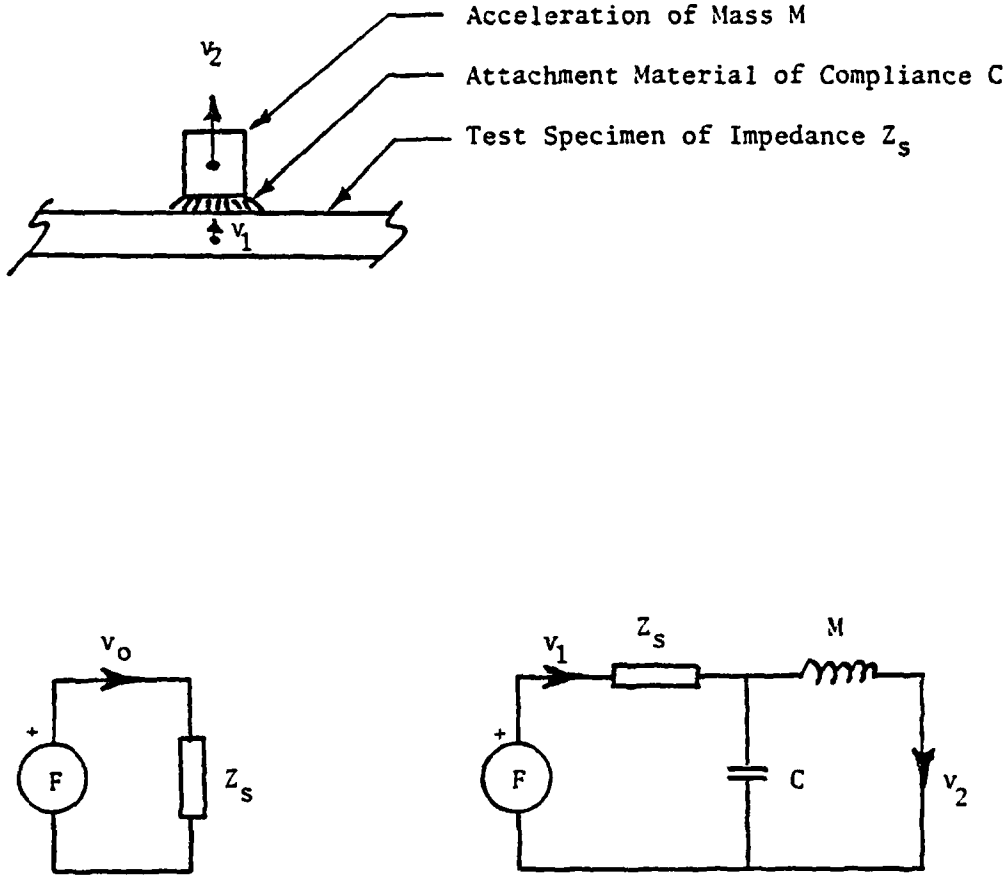

Figure 42 Circuit Representation of Accelerometer Attached to Test Specimen.

specimen. The effect of the mass loading reduces the measured velocity, while the effect of the antiresonance between M and C increases the measured velocity, Because of their frequency dependence, both these effects are only important at high frequencies.

The accelerometer was attached to the cylindrical shells by means of a sticky putty, known commercially as Duxseal. The compliance of a small layer of putty was measured by Williams, and was found to be approximately 2×10^{-8} m/nt. The mass of the accelerometer is 1.8 grams. The effect of the antiresonance between M and C at the highest frequency of interest, 10 kHz, is then $\omega^2/\omega_o^2 = 0.14$, which may be neglected compared to 1 in Equation (A.15). At 10 kHz, the magnitude of $j\omega M/Z_s$ should be less than 0.25 for its contribution to be neglected in Equation (A.15). This means that Z_s should be greater than 452 kg/sec (53 dB) or that Y_s should be less than -53 dB. The measured resonance peaks of the undamped, unstiffened shell exceed an admittance of -53 dB and are slightly compressed by the accelerometer mass loading. Fortunately, we are not as concerned about the resonance peaks of the undamped measurements as those of the damped measurements. The damped, unstiffened shell and all of the ring stiffened shell measurements do not exceed the limiting value of -53 dB and are not affected by the accelerometer mass loading.

DISTRIBUTION

Commander (NSEA 09G32)
Naval Sea Systems Command
Department of the Navy
Washington, DC 20362 — Copies 1 and 2

Commander (NSEA 0342)
Naval Sea Systems Command
Department of the Navy
Washington, DC 20362 — Copies 3 and 4

Defense Technical Information Center
5040 Duke Street
Cameron Station
Alexandria, VA 22314 — Copies 5 through 16